

WIND INDUCED HEAT LOSSES FROM SOLAR DISH-RECEIVER SYSTEMS

Muhammad Uzair

A thesis submitted to

Auckland University of Technology

in fulfilment of the requirements for the degree of

Doctor of Philosophy (PhD)

2018

School of Engineering, Computer and Mathematical Sciences

ABSTRACT

Parabolic dish-receiver concentrating solar power (CSP) plants are a promising technology for the generation of renewable electricity. However, the high operating temperatures of the cavity receivers mean the performance of these CSP systems is very sensitive to heat losses, in particular by wind.

A comprehensive literature review revealed a lack of work undertaken on wind flow around parabolic dish CSP systems and its impact on the heat loss from them. Previous studies investigating the effect of convective heat loss treated the receiver as an isolated entity, decoupled from the dish/reflector structure. Hence, the effect of the dish on the airflow around the receiver had not previously been considered.

This gap in the literature indicated a need to understand the effect of the dish in order to develop realistic heat loss models for the design of parabolic dish CSP systems. Hence, the research focused on the interaction between the wind and the dish structure causing local effects of air motion at the cavity inlet and the resulting in convective heat loss.

To verify the assertion that the dish would affect the flow of air around the receiver, and hence the heat loss, wind tunnel testing was performed on a scale model of a parabolic dish reflector. This study showed a significant disturbance to the flow field both qualitatively and quantitatively near where the receiver would be located. On this basis, a computational fluid dynamics (CFD) model of the airflow around a scaled dish and receiver was developed. These simulations showed good agreement with the quantitative measurements and qualitative visualization undertaken in the wind tunnel, thus validating the computational approach.

Having validated the simulation scheme, a detailed CFD study was undertaken to determine the heat loss from a 20m² parabolic dish and receiver system, developed by the

Australian National University for a range of dish orientations, wind speeds and incidence angles.

The CFD simulations confirmed that the dish's presence had a significant impact on the convective heat loss experienced by the system. With the flow around the dish structure being considered, the heat loss experienced by the receiver was markedly different, and in some cases lower (up to 40%), than when it was assumed the receiver acted in isolation. Furthermore, it was found that for dish tilt angles and wind incidence angles between +/- 30° and 0°, the heat loss significantly increased. This can be attributed to the receiver moving into the free stream and being subject to stronger forced flow than experienced in the dish's wake.

In summary, the results delivered quantitative data as to the effect of the dish's orientation, wind speed and wind incidence angle on heat loss. Using this information, a series of correlations were established to allow designers of parabolic dish CSP systems to incorporate the impact of the dish on the convective heat loss from the receiver. More broadly, the work demonstrated the importance of considering the influence of the dish when determining the heat loss from a parabolic dish receiver to avoid designing overly conservative, and hence costly, CSP systems.

ACKNOWLEDGMENTS

I am extremely grateful to **Almighty ALLAH** for providing me with the ability and understanding to carry out this research.

This thesis would not have been possible without the generous support of the wonderful people around me, particularly the help, support and patience of my Supervisor **Dr. Timothy Anderson** throughout these four years. The good advice and support of my second supervisor **Dr. Roy Nates** has been invaluable for which I am extremely grateful. The knowledge, skills and encouragement I have received from both supervisors have been of enormous value and I attribute the completion of my thesis to their influence.

I extend my gratitude to the **Auckland University of Technology (AUT)** and the **School of Engineering, Computer and Mathematical Sciences** for providing me with the comfortable working space and facilities to conduct this research. I am also grateful to Jim Crossen and Tim Luton from the workshop for their efforts and help during my whole experimental setup.

I would also like to acknowledge the **NED University of Engineering and Technology** for offering me the PhD Scholarship, which enabled me to pursue my advanced study at the Auckland University of Technology.

I am also very thankful to my research colleagues Noman Uddin Yousuf, Piratheepan, Reza, Aziz, Etienne, Riaz Uddin and Naveed ur Rehman for their valuable suggestions throughout the research.

I would like to thank to my parents, **Sabir Hussain** and **Rukhsana Sabir**, and all my brother and sisters, who always supported and encouraged me during my difficult times.

Finally, my heartfelt thanks to my wife **Iram Uzair** and **my children (Umer, Junaid and Hamna)**, for patiently putting up with me during the hardship of these four years.

LIST OF PUBLICATIONS

The following papers have been published over the course of this research.

Journal paper:

- 1) Uzair, M., Anderson, T.N., and Nates, R.J., 2017, “The impact of the parabolic dish concentrator on the wind induced heat loss from its receiver”, *Solar Energy*, Vol. 151, pp. 95-101

Conference papers:

- 1) Uzair, M., Anderson, T., and Nates, R., 2017, “Convective heat loss investigation from a couple parabolic dish receiver system”, *Proceedings of the 10th Australasian Natural Convection workshop (10ANCW)*, Auckland, New Zealand.
- 2) Uzair, M., Anderson, T., and Nates, R., 2016, “Impact of dish structure on the convective heat loss from a parabolic dish solar cavity receiver”, *Proceedings of the Asia-Pacific Solar Research Conference*, Canberra, Australia.
- 3) Uzair, M., Anderson, T., Nates, R., and Etienne, J., 2015, “A validated simulation of wind flow around a parabolic dish”, *Proceedings of the Asia-Pacific Solar Research Conference*, Brisbane, Australia.
- 4) Uzair, M., Anderson, T., and Nates, R., 2014, “Wind Flow around a Parabolic Dish Solar Concentrator”, *Proceedings of the Asia-Pacific Solar Research Conference*, Sydney, Australia.

CONTENTS

ABSTRACT	i
ACKNOWLEDGMENTS	iii
LIST OF PUBLICATIONS	iv
LIST OF FIGURES	viii
LIST OF TABLES	xii
ATTESTION OF AUTHORSHIP	xiii
Chapter 1: Introduction	1
1.1 Line concentrating systems.....	3
1.2 Point concentrating systems.....	5
1.3 Heat loss from parabolic dish concentrators.....	8
1.4 Research objective	11
Chapter 2: Flow behaviour around a coupled dish-receiver system	12
2.1 Numerical setup	13
2.2 Experimental setup	16
2.3 Comparison between wind tunnel tests and numerical model.....	18
2.4 Validation with available data of drag and lift coefficients.....	24
2.5 Velocity profile in wake region of the dish	27
2.6 Effect of dish shape and focal length on flow field	29
2.7 Significance of inclusion of the dish.....	31
2.7.1 Flow behavior with and without the presence of the dish.....	32

2.8	Chapter Summary	42
Chapter 3: Investigation into the presence of the dish on heat loss from the cavity receiver		
.....		43
3.1	Natural convection from the receiver	44
3.1.1	Numerical setup.....	44
3.1.2	Validation	45
3.2	Forced convection heat loss from receiver with and without the dish.....	49
3.3	Effect of dish shape on convective heat loss from the receiver.....	53
3.4	Chapter Summary	57
Chapter 4: Effect of wind and dish orientation on convective heat loss.....		58
4.1	Convective heat loss from cavity receiver.....	58
4.2	Effect of wind incidence on heat loss:.....	60
4.2.1	Wind flow parallel to the aperture plane (zero incidence angle).....	60
4.2.2	Wind flow from the front of the dish (positive incidence angles).....	61
4.2.3	Wind flow from the back of the dish (negative incidence angles).....	64
4.3	Effect of tilt on heat loss	67
4.4	Effect of wind incidence on heat loss	75
4.5	Heat loss correlation for coupled dish-receiver system.....	84
4.5.1	No-wind condition, heat transfer correlation	86
4.5.2	Forced convection heat transfer correlation	86
4.6	Chapter Summary	89
Chapter 5: Conclusion and Recommendations		91

5.1 Recommendations for future work	92
References	94
Appendix A: Mesh sensitivity analysis and domain selection.....	104
Appendix B: Wind tunnel testing results	108
Appendix C: Step to establish the Nusselt number correlation.....	111

LIST OF FIGURES

Figure 1: Solar energy conversion techniques	2
Figure 2: Schematic of parabolic trough system.....	3
Figure 3: Schematic of linear Fresnel collector	4
Figure 4: Schematic of solar power tower	6
Figure 5: Schematic of parabolic dish system	7
Figure 7: (a) Schematic of parabolic dish system (b) Orientation of dish with respect to different tilt angles	14
Figure 8: Simulation domain around dish cavity system.....	16
Figure 9: Schematic representation of the wind tunnel experiment.....	17
Figure 10: Cross section view at section AA'	18
Figure 11: CFD streamlines and flow visualization for 90° tilt angle	20
Figure 12: CFD streamlines and flow visualization for 60° tilt angle	20
Figure 13: CFD streamlines and flow visualization for 45° tilt angle	20
Figure 14: CFD streamlines and flow visualization for 30° tilt angle	21
Figure 15: CFD streamlines and flow visualization for 0° tilt angle	21
Figure 16: CFD streamlines and flow visualization for -30° tilt angle.....	22
Figure 17: CFD streamlines and flow visualization for -45° tilt angle.....	22
Figure 18: CFD streamlines and flow visualization for -60° tilt angle.....	23
Figure 19: CFD streamlines and flow visualization for -90° tilt angle.....	23
Figure 20: Comparison of drag coefficient at different tilt angles.....	26
Figure 21: Comparison of lift coefficient at different tilt angles	27
Figure 22: Sketched of dishes of different shape showing the focal length for same diameter.....	30
Figure 23: Drag coefficients at different tilt angles for the selected dish geometries.....	31

Figure 24: Flow at 90° (a) with dish (b) without dish structure.....	33
Figure 25: Flow at -90° (a) with dish (b) without dish structure	34
Figure 26: Flow at 60° (a) with dish (b) without dish structure.....	35
Figure 27: Flow at -60° (a) with dish (b) without dish structure	36
Figure 28: Flow at 45° (a) with dish (b) without dish structure.....	37
Figure 29: Flow at -45° (a) with dish (b) without dish structure	38
Figure 30: Flow at 30° (a) with dish (b) without dish structure.....	39
Figure 31: Flow at -30° (a) with dish (b) without dish structure	40
Figure 32: Flow at 0° (a) with dish (b) without dish structure.....	41
Figure 33: Boundary conditions.....	45
Figure 34: Validation of numerical simulation with other correlations.....	46
Figure 35: Temperature and velocity contours at 0°	47
Figure 36: Temperature and velocity contours at 30°	47
Figure 37: Temperature and velocity contours at 45°	47
Figure 38: Temperature and velocity contours at 60°	48
Figure 39: Temperature and velocity contours at 90°	48
Figure 40: Validation of heat loss from the receiver without the dish structure.....	50
Figure 41: Convective heat loss at various tilt angles with a wind velocity of 5 m/s.....	50
Figure 42: Location of the receiver at 0° tilt angle	52
Figure 43: Location of the receiver at 30° tilt angle	52
Figure 44: Location of the receiver at -30° tilt angle.....	53
Figure 45: Sketched of dishes of different shape showing the focal length for same diameter.....	54
Figure 46: Convective heat loss from the cavity receiver with different focal lengths ..	54
Figure 47: Velocity contour around different dishes at 90° tilt angle.....	56
Figure 48: Definition of tilt angle (θ).....	59

Figure 49: Orientation of dish-receiver system.....	59
Figure 50: Parallel flow to the cavity aperture plane ($\varphi = 0^\circ$)	61
Figure 51: Flow impinging directly on the reflective (front) surface of the dish	62
Figure 52: Effect of the dish on the velocities near the receiver at 5 m/s.....	63
Figure 53: Temperature profile at 45° tilt angle at different wind speeds	64
Figure 54: Velocity vectors at receiver aperture for 0° tilt angle.....	64
Figure 55: Flow impinging on the rear of the dish ($\varphi = -90^\circ$)	65
Figure 56: Effect of the dish on the velocities near the receiver at 5 m/s.....	66
Figure 57: Convective heat loss as a function of tilt angle at $V=1$ m/s	67
Figure 58: Temperature contours at different wind incidence angles with a wind velocity of 1 m/s at 90° tilt angle	68
Figure 59: Temperature contours at different tilt angles with a wind velocity of 1 m/s at 0° wind incidence angle	68
Figure 60: Convective heat loss as a function of tilt angle at $V=3$ m/s	69
Figure 61: Streamlines showing the recirculation provided by the dish at $\varphi=-60^\circ$	70
Figure 62: Convective heat loss as a function of tilt angle at $V=5$ m/s	71
Figure 63: Convective heat loss as a function of tilt angle at $V=10$ m/s	72
Figure 64: Normal and parallel velocity contour at receiver aperture at 10 m/s.....	72
Figure 65: Convective heat loss as a function of tilt angle at $V=20$ m/s	73
Figure 66: Temperature contours inside receiver at 20 m/s with positive wind incidence angle	74
Figure 67: Convective heat loss as a function of wind incidence angle at $V= 1$ m/s	76
Figure 68: Temperature contours at receiver aperture with $V= 1$ m/s	76
Figure 69: Velocity vector at receiver aperture with $V= 1$ m/s	77
Figure 70: Convective heat loss as a function of wind incidence angle at $V= 3$ m/s	77
Figure 71: Velocity contours at 30° wind incidence angle with $V=3$ m/s	79

Figure 72: Velocity contour at 0° wind incidence angle with V= 3 m/s.....	79
Figure 73: Convective heat loss as a function of wind incidence angle at V= 5 m/s	80
Figure 74: Top view of velocity contour at 45° wind incidence angle with V= 5 m/s ...	81
Figure 75: Convective heat loss as a function of wind incidence angle at V= 10 m/s ...	82
Figure 76: Convective heat loss as a function of wind incidence angle at V= 20 m/s ...	83
Figure 77: Velocity vectors for $\phi = -90^\circ$ tilt angle with the dish structure	83
Figure 78: Comparison of Nusselt number obtained from correlation and numerical results	89
Figure 79: Grid independency test	105
Figure 80: Mesh around the dish and receiver	105
Figure 81: Variation of drag force v/s domain size.....	106
Figure 82: Simulation domain around dish cavity system.....	107
Figure 83: Surface plot of velocity profile with 100% open fan.....	109
Figure 84: Surface plot of velocity profile with 75% open fan.....	109
Figure 85: Surface plot of velocity profile with 50% open fan.....	110

LIST OF TABLES

Table 1: Experimental and simulation velocities values at selected plane with 90° tilt angle	28
Table 2: Values of coefficients used in Nusselt correlation (Eq.9).....	88
Table 3: Wind velocity data in empty tunnel	108
Table 4: Values of coefficients used in Nusselt correlation (Eq.9).....	112

ATTESTION OF AUTHORSHIP

I hereby declare that this submission is my own work and that, to the best of my knowledge and belief, it contains no material previously published or written by another person (except where explicitly defined in the acknowledgments), nor material which to a substantial extent has been submitted for the award of any other degree or diploma of a university or other institution of higher learning.

Auckland

Signature _____

Muhammad Uzair

Chapter 1: Introduction

The Sun is the major source of energy and every hour provides more than the annual collective energy consumption of the earth. Due to the increase in the global energy demand and high depletion rate of conventional energy resources, there is a need to look toward solar energy. The estimated rate of energy produced by the Sun is 3.8×10^{23} kW while only a fraction (1.8×10^{14} kW) reaches earth (Philibert, 2011). The amount of solar energy striking the earth every hour (4.3×10^{20} J) would be enough to power the whole planet for a year, as the current usage is 4.1×10^{20} J (Foster et al., 2010). Nowadays, solar power technologies are growing faster than any other renewable technology. According to a forecast, solar energy power generation systems should be able to provide up to one-third of the world's total energy demand after 2060 (Philibert, 2011). The solar energy received in one year can cover the total energy consumption of 6,000 years, while proven fossil reserves represent 46 years (oil), 58 years (natural gas) and almost 150 years (coal) of consumption at current rates (Philibert, 2014). The incoming solar radiation can be utilized to produce useful electricity either by direct conversion in photovoltaic systems or indirect generation of thermal energy by solar thermal systems. Existing solar energy conversion techniques are summarized in Figure 1.

In solar photovoltaic (PV) systems a semiconductor is used to convert direct and diffused sun light directly into electricity with 10-15 percent overall system efficiency (Goswami et al., 2000). In solar thermal systems, the solar radiation is absorbed by a material or fluid and this heat is used to drive a thermal power plant to produce electricity. Solar thermal energy conversion is considered to be the most promising available technique due to higher efficiency of up to 35 percent with combined cycle turbine and relatively low cost per unit produced energy (Wu et al., 2010). Solar thermal systems can be classified as concentrating and non-concentrating collectors. Non-concentrated solar

collectors are generally used for domestic use and some industrial applications with maximum temperature of 200°C. Concentrating solar power (CSP) systems concentrate the direct solar irradiation, using various arrangements of mirrors and optical lenses, to produce high thermal energy density and temperature. Unlike non-concentrating systems, the diffused part of solar irradiation cannot be used in CSP system. CSP systems can be classified into two main categories based on the optical configurations: Line Collectors and Point Collectors.

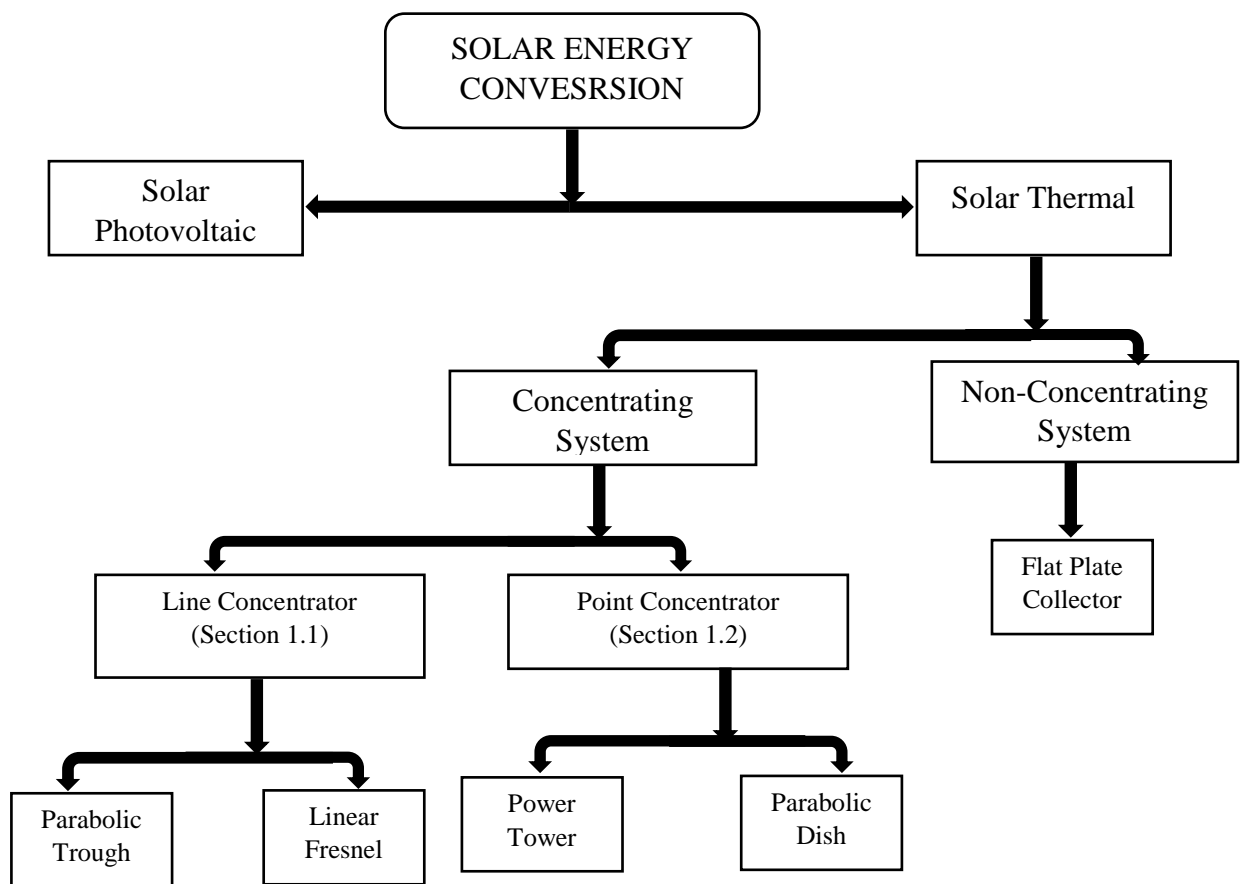


Figure 1: Solar energy conversion techniques

1.1 Line concentrating systems

Line concentrating systems focus the incoming radiation to a length of absorbing receiver placed at the focal axis by using reflecting mirrors. These types of systems meet the tracking requirement by rotating the optics about a single axis. The line concentrating systems can be classified into two important techniques:

- Parabolic Trough Collectors (PTC)
- Linear Fresnel Collectors (LFC)

Parabolic trough collectors are considered to be the most mature solar conversion system as they have the biggest share of CSP market due to low financial and technological risks. Figure 2 illustrates a typical schematic parabolic trough power plant layout. Parabolic trough collectors, consisting of an array of single axis tracking troughs, concentrate the solar beam radiation onto a receiver tube running at the focal length of collector. The solar radiation is absorbed by the fluid in the tubes which flows from the receiver to the conventional power plant.

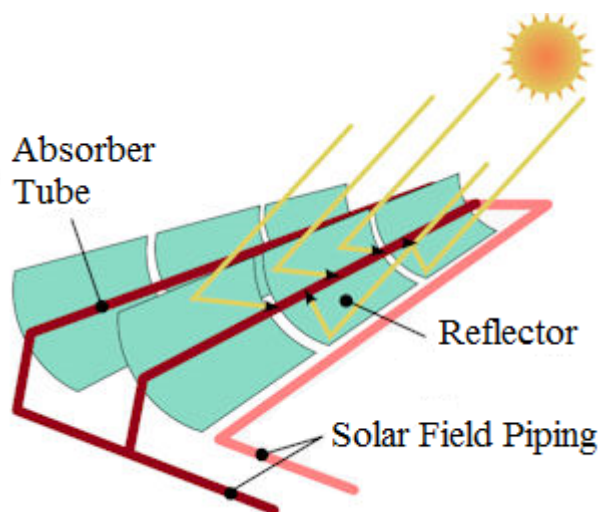


Figure 2: Schematic of parabolic trough system

(<http://www.energy-fundamentals.eu/17.htm>)

Linear Fresnel Collectors are a variation on the parabolic trough comprised of a series of one-axis parallel mirror facets, instead of parabolic bent mirrors, to concentrate the solar radiation onto a suspended linear cavity receiver well above the primary mirror field. The working fluid running through the selective coated receiver is utilized to absorb heat from incident concentrated solar radiation and transfer it to power plants. A typical Linear Fresnel Collector power plant is shown in Figure 3.

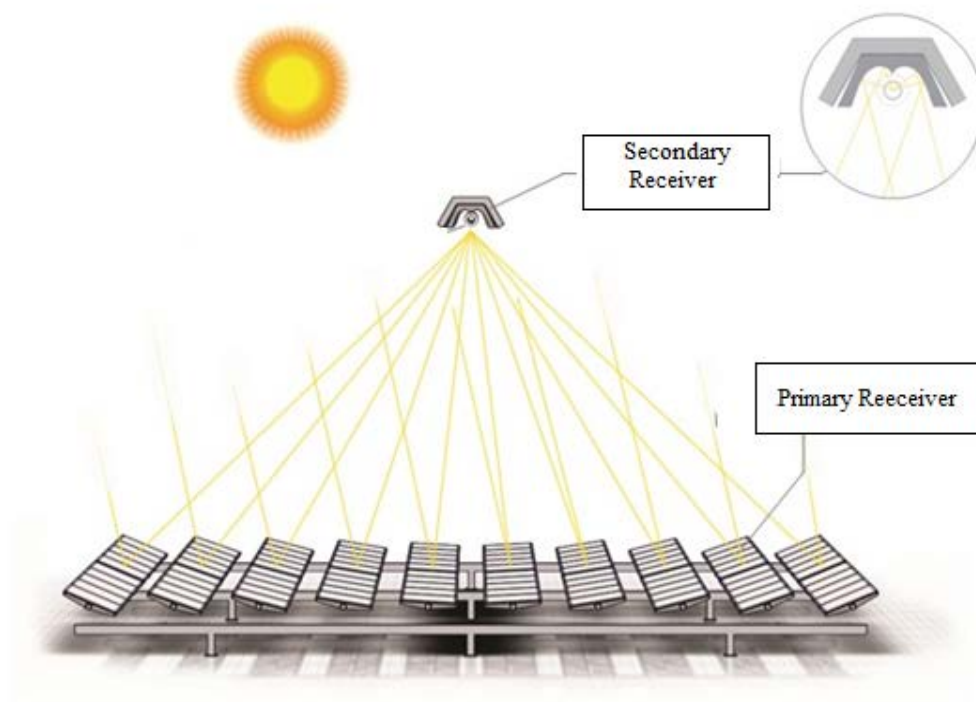


Figure 3: Schematic of linear Fresnel collector

(<http://www.millenniumenergies.com/nuestra-tecnologia/fresnel/>)

Depending on the design of parabolic trough and Linear Fresnel collectors, the thermal fluid is able to be heated to 400°C which constitutes a concentrated solar radiation flux of between 30 to 80 times (Hachicha et al., 2013a).

1.2 Point concentrating systems

Point concentrating systems focus the incoming solar radiations onto a point or a receiver as opposed to line concentration. As a result, they require two-axis tracking systems to achieve their high concentration ratios. . The dish collectors focus large amount of solar radiation, incident on their aperture, on a small receiver (or enclosure). Ideally, the parabolic dish systems can achieve the concentration ratio up to 10,000 Suns (1 sun=1000 W/m²) compared with 1000 Suns and 100 Suns achieved by the solar towers and the parabolic troughs, respectively. Research has been performed to estimate the convection and radiation from the different cavities used in point concentrating systems (Jilte et al., 2013). In these systems, cavity receivers are used in preference to volumetric receivers due to their lower radiative losses (Reddy et al., 2016). The solar radiation is focused to enter the cavity receiver through the opening, known as the aperture, and then absorbed by the enclosing walls. The most common techniques using point concentrating systems are:

- Solar Power/Central Tower (SPT)
- Parabolic Dish Collectors (PDC)

Solar power towers (or solar tower) are comprised of a large field of sun tracking reflecting, flat, moveable mirrors, known as heliostats, used to concentrate the solar radiation on a receiver on top of a centrally located tower (Figure 4). The ability to use a large number of heliostats results in these having a high concentration ratio. The working fluid, after absorbing heat from incident solar radiations, is pumped down to conventional thermal power generation systems to produce electricity. Absorbed heat is often stored in a tank, containing molten salt, for off-peak energy supply.

Despite achieving a very high operating temperature, a large amount of thermal loss is unavoidable due to the open area of the receiver and the high temperature. This causes a

reduction of the overall conversion efficiency of the system. Although solar power collectors are more complex than parabolic trough collectors, they are commonly used today to generate electricity due to lower cost and greater performance (Behar et al., 2013).

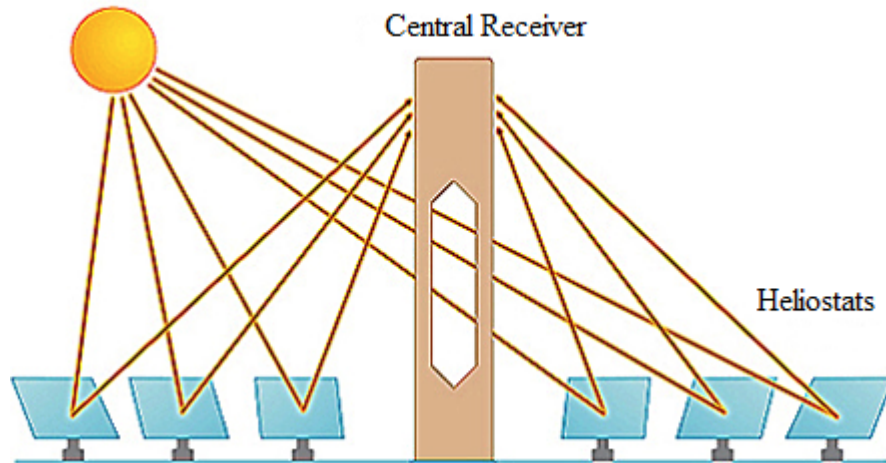


Figure 4: Schematic of solar power tower

(http://solarcellcentral.com/csp_page.html)

Parabolic dish technology is considered to be the oldest solar technology. The Greek mathematician Diocles described the geometrical properties, concentrating and collimating properties, of paraboloid mirrors around 200 BC (Gunther and Shahbazfar, 2012). In the 19th century Stirling-based dish systems were developed, which lead to the modern Stirling-based dish system, first built in the late 1970's.

Parabolic dish collectors concentrate the direct solar radiation onto a cavity receiver mounted at the focal point by its reflecting concave surface (Figure 5). The highly polished surface of parabolic dish reflects most of the solar irradiation without any significant increase in the dish's temperature. The working fluid transfers the absorbed solar radiation from the cavity receiver to the power generation system. The cavity

receiver used in parabolic dish systems and solar power tower are typically similar in geometry but vary in size. The typical inner length of a cavity receiver used in PDCs is less than 1 m whereas for a solar power tower the length is larger than 1 m (Robert et al., 2015).

PDCs are either stand-alone units, like those of CSP systems using a Stirling engine/generator module, or they can be used with a similar mode of operation as other CSP systems using modular collectors and cavity receivers (Paitoonsurikarn, 2006). Typical system sizes are usually in the range of few kilowatts, but on the other hand, the largest demonstration plant has an output capacity of approximately 5MWe (Holl and de Meo, 1990). PDCs are also used in desalination plants utilising the reverse osmosis (RO) process to provide energy input to the pumping and heat recovery section of the system. PDCs are capable of producing a concentration ratio of more than 3000 with highest annual efficiencies (Stine and Diver, 1994).

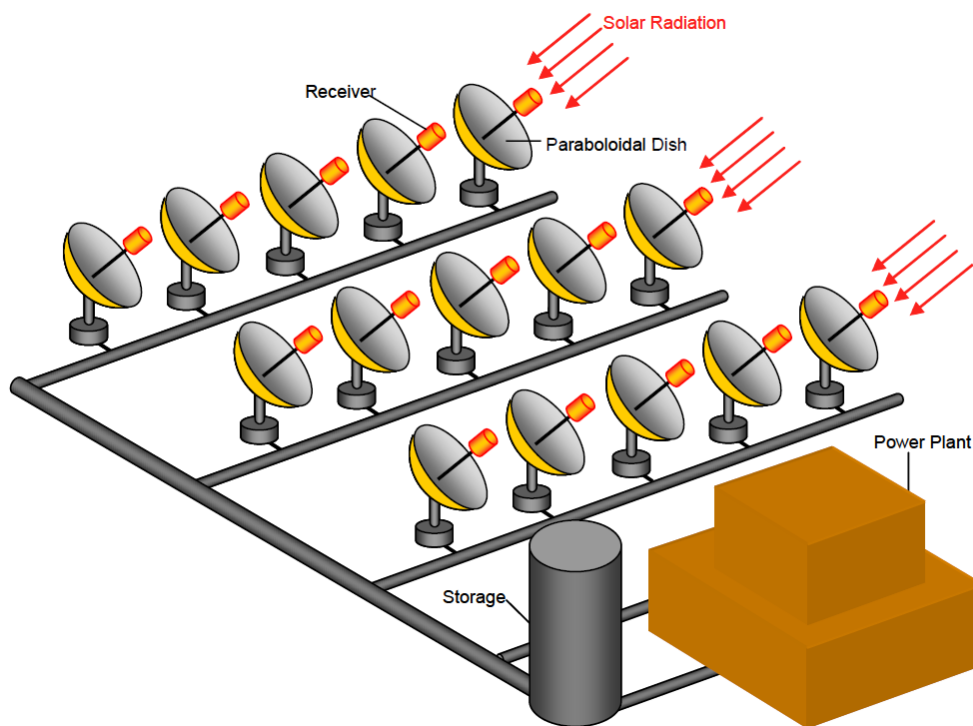


Figure 5: Schematic of parabolic dish system

(Paitoonsurikarn, 2006)

1.3 Heat loss from parabolic dish concentrators

The performance of CSPs is strongly influenced by the heat losses to the environment from the thermal receiver, particularly at high operating temperature. As such these heat loss from the receiver has been shown to have a decisive influence on the overall efficiency of the solar power plant (Price et al., 2002). In general CSPs are located in open terrain where the heat loss is sensitive to wind (Lupfert et al., 2001). Due to high temperature in the cavity and open atmosphere installation of the system, the thermal losses from solar receivers occur by convection, conduction and radiation losses. A precise assessment of thermal losses from the cavity plays an imperative role to improve the efficiency of parabolic dish system. There are many analytical techniques available (Holman, 1997) to determine the radiation and conduction heat losses from the receiver. The conduction losses are generally less compared with other modes of the heat losses. Also, the radiation losses are relatively constant for all the previous convection models due to radiosity method used does not changed and neither the characteristics of the insulation layer are (Samanes et al., 2015). However, determination of convection heat loss from the receiver is much more complicated due to the complexity of the temperature and velocity field in and around the cavity and usually relies on semi-empirical models (Wu et al., 2010). In this research, the main focus is about the convective heat losses and for a complete heat loss model, the radiation and conduction heat losses should also be considered with convective heat loss model.

For parabolic dish systems, the absorbing surface is typically placed inside a cavity. This protects it from wind and naturally driven air currents. The cavity position, internal temperatures and the wind conditions, including both the speed and the direction, were investigated and found to be significantly affecting the rate of heat losses from the cavity receiver (Paitoonsurikarn and Lovegrove., 2003). As expected, the findings showed that the heat loss from the thermal receiver drastically reduces the efficiency and hence

increases the operating cost value of system. Due to the importance of thermal losses from the receiver, both experimental and numerical studies on convective heat transfer (natural and forced convection) from the receiver have been the main area of the subject for researchers from late 1970's, and numerous models have been proposed.

Many researchers have investigated the natural and forced convection heat losses from different cavity receivers with various geometries and orientations. Thermally driven natural convection was investigated numerically and experimentally and a correlation was proposed showing the dependency of heat loss on the cavity inclination angle (Le Quere et al., 1981a; 1981b).

In three of the most frequently cited works, Clausing (1981, 1983) and Clausing et al. (1987) investigated the natural convection heat losses from large cavities based on the hypothesis that the convective heat loss from the cavity was dependent on (i) the ability to transfer mass and energy across the aperture and (ii) the ability to heat air inside the cavity. Based on the investigation, an analytical solution was developed. In their implicit solution, the cavity receiver was divided into two major zones, a convective zone and a stagnant zone. It was observed that the convective heat loss from the cavity receiver was highly affected by the ability to heat air inside the cavity. Similarly, Le Quere et al. (1981a, 1981b) performed a numerical and experimental study in order to develop a relationship between the Nusselt number and tilt angle. They examined the thermally driven laminar natural convection in an open cubical cavity and found the dependency of convective heat loss on the inclination of the cavity. In this vein, numerous further studies (Koenig and Marvin, 1981; Siebers and Kraabel, 1984; Stine and McDonald, 1989; Leibfried and Ortjohann, 1995) have attempted to quantify and deliver a relationship between the natural convection heat transfer from parabolic dish receivers and their orientation (tilt angle), aperture size and cavity geometry. Leibfried and Ortjohann,

(1995) found the modified Stine and McDonald's explicit model better than the Clausing's implicit model after comparing them with the measured data obtained.

In reality parabolic dish receivers are likely to be exposed to some degree of forced convection, however investigations of forced convection heat loss from these receivers are relatively scarce compared to those focussing on natural convection. In his study Ma (1993) examined a parabolic dish receiver without the presence of the dish and came to the conclusion that convection losses due to wind varied strongly with the receiver's tilt angle.

More recently, to predict the convective heat loss from the receiver, Taumoefolau and Lovegrove (2002), Lovegrove et al. (2003), Paitoonsurikarn and Lovegrove (2002, 2003), Taumoefolau et al. (2004) and Paitoonsurikarn et al. (2004) performed experimental and analytical studies on a model cavity receiver over a range of temperatures. This work did not include the presence of the dish. The proposed correlations predicted the natural convection heat losses at all tilt angles with high accuracy when compared with the previous available correlations. They identified the effect of receiver tilt angle on the combined convection heat loss for the side-on wind case.

Prakash et al. (2009) investigated the effects of external wind at two different velocities in two directions (head on and side on) without considering the effect of the reflecting dish on the air motion around the receiver. The head-on wind as well the higher wind speed, caused higher convection heat loss as than the side-on wind, which conflicted with the finding reported by Ma (1993) and Paitoonsurikarn and Lovegrove (2006b).

Many other studies (Tan et al., 2009; Kim et al., 2010; Fang et al., 2011; Xiao et al., 2012; Wu et al., 2013, 2014, 2015; Liovic et al., 2014; Flesch et al., 2014, 2015; Cui et al., 2014; Vikram and Reddy 2014, 2015; Reddy et al., 2015, 2016) have dealt numerically and experimentally with the convective heat losses from different types of cavity receiver

without considering the presence of the dish. In all of the studies, heat loss from the receiver was found to be dependent on the orientation of the receiver. It should be emphasised that in all the studies, the presence of the dish was not considered.

In almost all studies, researchers have treated the cavity receiver as an isolated entity, without considering the presence and influence of the dish/reflector structure. Wu et al. (2010) highlighted this issue in their review of the field, noting that there is a dearth of information relating to wind effects on heat loss and the interaction between the wind and dish, and by extension the influence on the heat loss.

1.4 Research objective

From examining the previous work on heat loss from parabolic dish concentrator receivers there is a significant lack of work on the impact of parabolic dishes on wind flow and heat loss at the receiver. Numerous studies have examined the heat loss from various receiver geometries under natural and forced convection conditions; however there is a marked absence of studies that take into account the effect that the dish may have on the heat loss, particularly for forced convection conditions. Given that forced convection could increase the heat loss from such systems, there is a need for an understanding of the effect of the wind velocity and flow structure around parabolic dish solar concentrators. In addressing this, the central question for this work is:

“What is the impact of the parabolic dish on the wind flow and hence the heat loss from the receiver of such a solar concentrator system?”

Chapter 2: Flow behaviour around a coupled dish-receiver system

From the literature review, it was shown that the performance of CSP systems utilizing parabolic dishes were sensitive to heat losses from the cavity receiver, particularly at high temperatures. In particular, the heat loss from the receiver is affected by the surrounding air movement, and consequently exposure to this results in increased heat loss, and decreased thermal performance (Lupfert et al., 2001). Also shown in the review (section 1.3), there is a marked absence of research on the effect of the dish structure on the flow near the receiver and its effect on the performance of parabolic dish solar power systems.

To begin to address the research question posed in the previous chapter, an understanding of the flow behaviour around the parabolic dish is required.

There are few numerical studies of wind flow around parabolic concentrators. In one study, Paitoonsurikarn and Lovegrove (2006a) numerically examined the local wind velocities near the cavity receiver in the presence of a dish structure. They found that the local wind speed at the aperture of the receiver was largest when the free stream wind was parallel to the aperture plane. Their simulation results indicated the significant effect of the dish structure on the local wind flow around the cavity receiver, but they did not investigate its effect on the convective heat loss. Christo (2012) numerically investigated the transient flow behaviour around the dish with regard to dust deposition on a dish surface and validated the simulation with wind tunnel testing by Hosoya et al. (2008). Neither did this study explore the effect on heat loss.

Naeeni and Yaghoubi (2007a, 2007b) numerically investigated the recirculation regions around a parabolic trough solar collector from the Shiraz solar power plant with different configurations, and Hachicha et al.(2013a, 2013b) proposed a Large Eddy Simulation

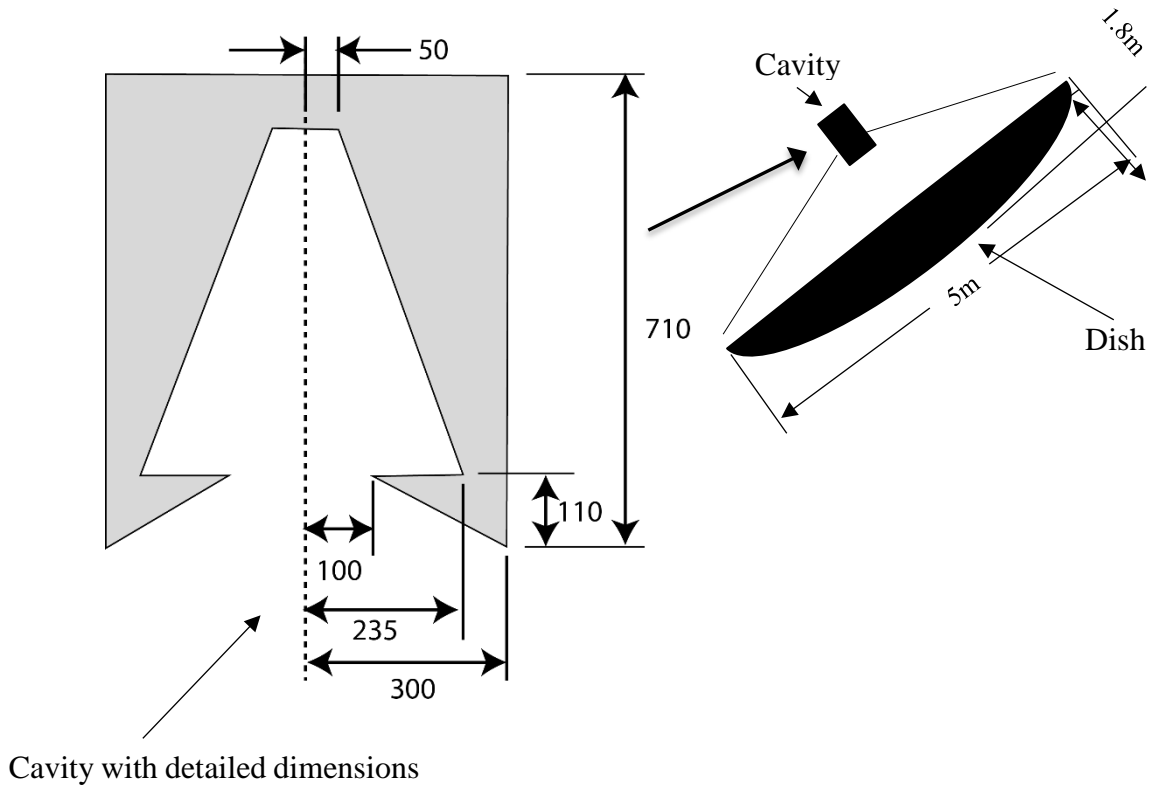
model to compute the fluid flow and heat transfer around a parabolic trough solar collector with different orientations using real working conditions.

None of these works included the effect of the dish structure on the wind flow around the receiver and subsequently the heat loss and efficiency of the system. Hence, there is clearly a gap in knowledge and a need to understand this in order to develop a model of the CSP systems able to deal with the effects of the wind and dish orientation on heat losses.

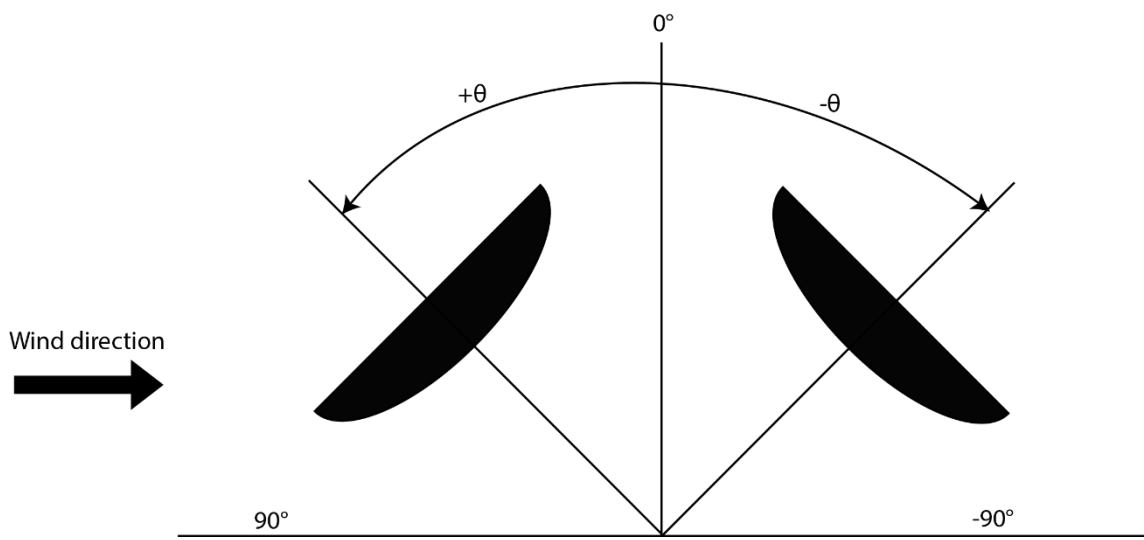
2.1 Numerical setup

In order to examine the effect of wind flow on the heat loss from the parabolic dish receiver it was decided to undertake a computational fluid dynamics (CFD) analysis of the flow around the Australian National University's 20 m² dish and frustum shaped receiver used in their solar thermochemical demonstration plant. This system was chosen as the basis for this study as previous numerical and experimental studies had been performed to assess the thermal characteristics of the receiver of this specific dish. However only a few numerical studies of the flow fields have been published (Paitoonsurikarn and Lovegrove., 2003).

This parabolic dish has an aperture diameter of 5 m and a nominal aperture area of 20 m², a focal length of 1.84 m and a rim angle of approximately 70°. The dimensions of the frustum shaped cavity receiver are shown in Figure 6 as well as the definition of angle of tilt (θ).



(a)



(b)

Figure 6: (a) Schematic of parabolic dish system (b) Orientation of dish with respect to different tilt angles

In previous studies of wind flow over solar concentrators, a time-averaged steady state simulation approach has been shown to be sufficient to examine the flow field and aerodynamic forces (Paetzold et al., 2014, 2015). Therefore, for this study, a steady state numerical simulation of the wind flow over the parabolic dish system was performed using the commercial CFD solver ANSYS CFX 15.0.7. Initial steady state simulations were performed by changing the tilt angle from 90° to -90° , under a free stream wind velocity of 5 m/s at 20°C ambient temperature.

As the flow around the dish was expected to be primarily turbulent, the Shear Stress Transport (SST) $k-\omega$ two-equation eddy-viscosity turbulence model was used to resolve the flow. The SST $k-\omega$ model can be used as a low-Reynolds turbulence model without any extra damping function and the model adjusts itself to a $k-\varepsilon$ behaviour in the free stream to avoid any sensitive effect of inlet-free turbulence properties (Menter, 1993; 1994). Further, it has been shown to be appropriate for both near-wall and far-field zones due to the absence of any non-linearity in the damping function in the model, meaning simulation results are more precise and robust (Christo, 2012; Fluent, 2005). Finally, the model has also been shown to be one of the most accurate two-equation models for separation prediction and has been successfully used for studies of wind flow over parabolic troughs to capture the effect of natural and forced convection (Paetzold et al., 2014, 2015).

To capture the flow field a domain was developed that extended 75m upstream (15 dish diameters – 15D) to allow the inlet velocity profile to fully develop, 105m (21D) downstream to capture all the affected parameters, and 30m (6D) in the lateral direction to avoid any shear effects of the walls on the flow field near dish (Figure 7). After defining the boundary conditions a mesh sensitivity analysis was performed to investigate the effect of grid sizes on the numerical results. A high-quality mesh was chosen with grid size of approximately 4.7 million elements, being used to perform simulations of the flow

around the dish. Regions further from the dish were meshed with larger grid sizes to improve computational speed. A detailed mesh sensitivity analysis and domain selection investigation is presented in Appendix A.

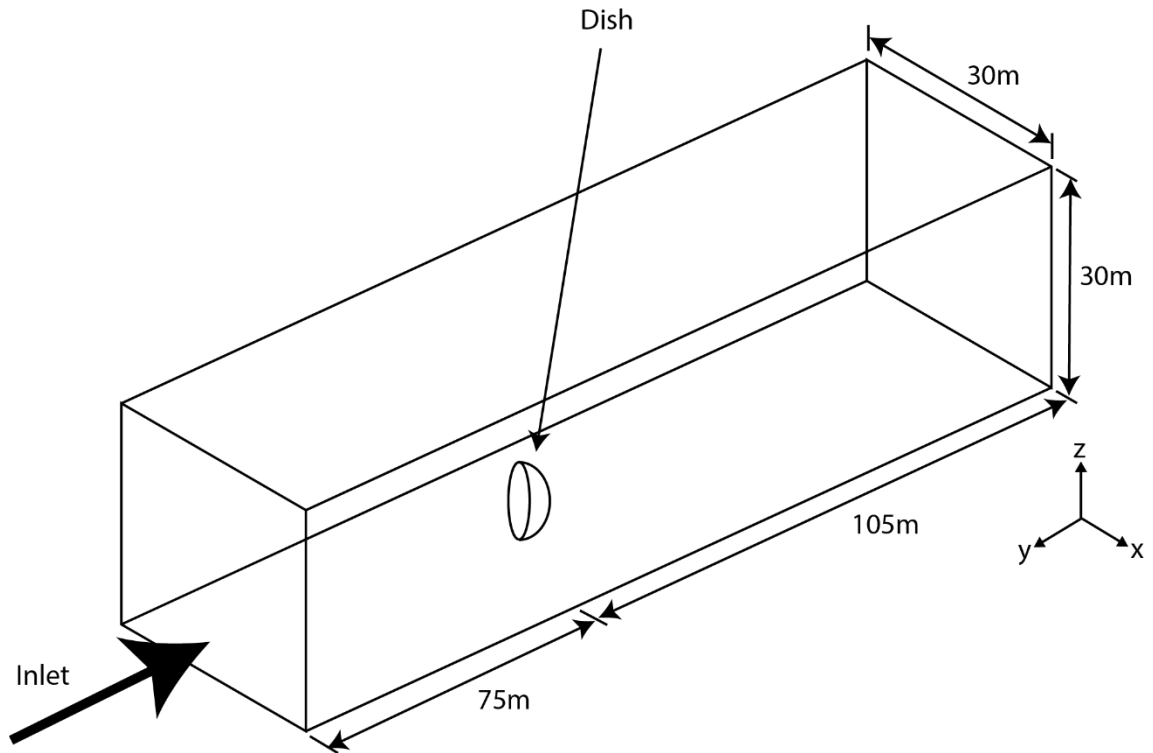


Figure 7: Simulation domain around dish cavity system

2.2 Experimental setup

In order to validate the numerical scheme, wind tunnel experiments were performed using a scale model of the dish. In doing this a model of the dish with a diameter of 150 mm (1:33 scale model of the original dish) was used to analyse the flow behaviour around the dish. Due to the very small size of the scale model of cavity receiver, it was very difficult to visualize the flow around the receiver. So, only the flow around the dish was analysed. A schematic representation of the experimental setup is shown in Figure 8. The base of the model was specifically designed in order to allow the adjustment of the dish tilt angle (θ) and orientation of the model in the wind tunnel.

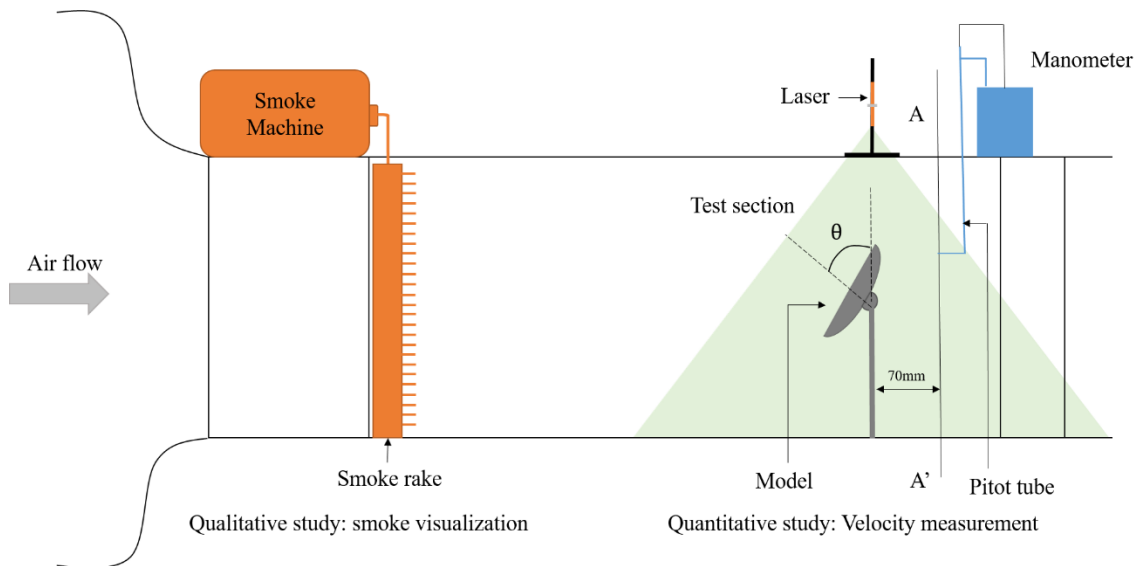


Figure 8: Schematic representation of the wind tunnel experiment

The scale model of the dish was manufactured using a three dimensional printing system. A honeycomb structure was mounted at the inlet of wind tunnel to provide a uniform flow velocity. The test section around the dish was 500mm x 500mm in cross section, and extended 500mm upstream and 1000mm downstream of the model. After testing of the wind tunnel to ensure homogenous flow (Appendix B), experiments were performed to qualitatively and quantitatively examine the flow patterns around the dish using smoke visualization.

In doing this a free stream velocity of 3.2 m/s was selected at a temperature of 20°C, leading to a free stream Reynolds number of 3.2×10^4 , taking the diameter of the parabolic dish to be the characteristic length. In order to diffuse the smoke in parallel lines inside the wind tunnel, a smoke rake was fabricated using the basic concept of Trinder and Jabbal (2013). The images of the smoke flow were captured in the presence of a green laser light sheet by a digital SLR camera.

In order to quantitatively examine the flow field, a Pitot-static probe, differential manometer was traversed across the tunnel to determine velocity profile at a plane 70mm

behind the rotation centre of dish. The Pitot-static sampling positions included 35 grid points shown in Figure 9.

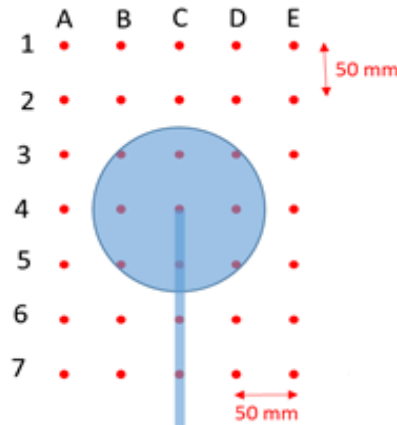


Figure 9: Cross section view at section AA'

2.3 Comparison between wind tunnel tests and numerical model

In order to validate the flow behaviour around the parabolic dish system, CFD simulations were performed for the dish at different tilt angles while visualization of the flow around a parabolic dish structure was performed using smoke. This allowed the simulation results to be verified qualitatively. For different tilt angles of the dish, velocity streamlines along the center plane of the CFD simulation domain (with flow moving from left to right) were compared with the smoke streak lines as shown in Figures 10-18. These results were similar to published streamlines of Paitoonsurikarn (2006) and Christo (2012).

The flow around the dish shows markedly different flow structures with different tilt angles. Starting from the case when flow is perpendicular to the aperture plane of the dish, i.e. 90° tilt angle; an accumulation of smoke in front of the plane of the dish can be seen (Figure 10) due to the dish structure blocking the horizontal movement of air. Under these conditions, the local velocity becomes normal to the original flow near the dish's edge. In turn the velocity in the front of the dish structure moves towards a stagnation condition

and at the edges of the dish structure the velocity values increase to maintain continuity. As a result, the velocity behind the dish is reduced and two strong recirculating vortices are generated in the dish's wake. Figure 10 shows similar results for the stream lines from the CFD and smoke visualization from the wind tunnel test.

By changing the tilt angle to 60° flow separation occurs at the upper and lower edge of dish, resulting in two large vortices behind the dish. From the streamlines shown in Figure 11, it can be seen that as the velocity increases at the upper and lower edge this leads towards a flow separation. This phenomenon is also observed while investigating the smoke pattern around the dish in the wind tunnel test (Figure 11). Similarly, Figure 12 shows flow separation occurring from the upper edges, creating a vortex behind the dish, at a pitch angle of 45° .

However as the angle is reduced further, to a tilt angle of 30° (Figure 13), the flow becomes more uniform and there is no major flow separation except a smaller recirculation region near the lower portion of dish. As a result, the flow orientation is mainly upward due to the low pressure generated by the acceleration of the flow over the dish. This uniform flow is clearly demonstrated in numerical results as well as in smoke visualization.

The recirculation regions have effectively vanished as the dish reaches a 0° tilt angle (Figure 14), and it suggests that the dish does not affect the air flow on the top side of dish for this orientation. Under these conditions, the receiver location would be in such a position that the shape of the dish would not influence the flow near it.



Figure 10: CFD streamlines and flow visualization for 90° tilt angle

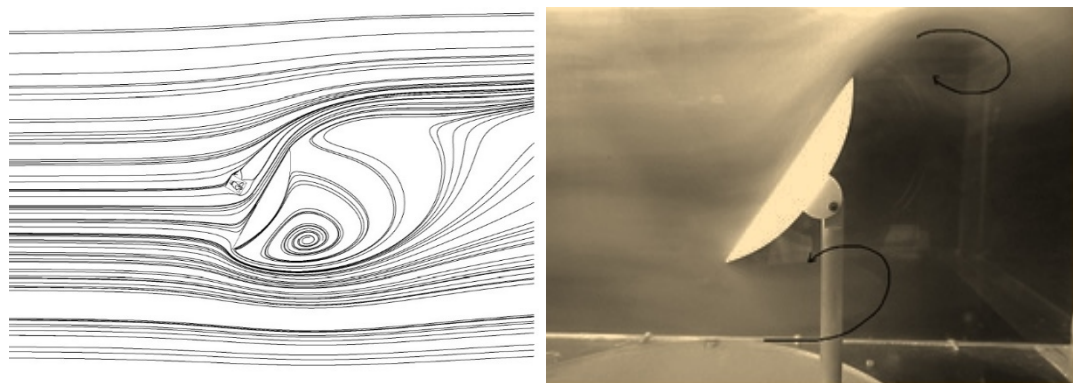


Figure 11: CFD streamlines and flow visualization for 60° tilt angle

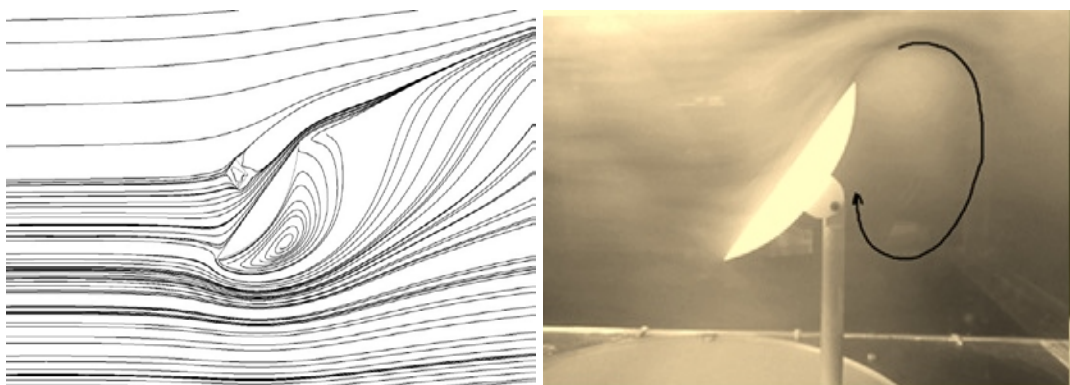


Figure 12: CFD streamlines and flow visualization for 45° tilt angle

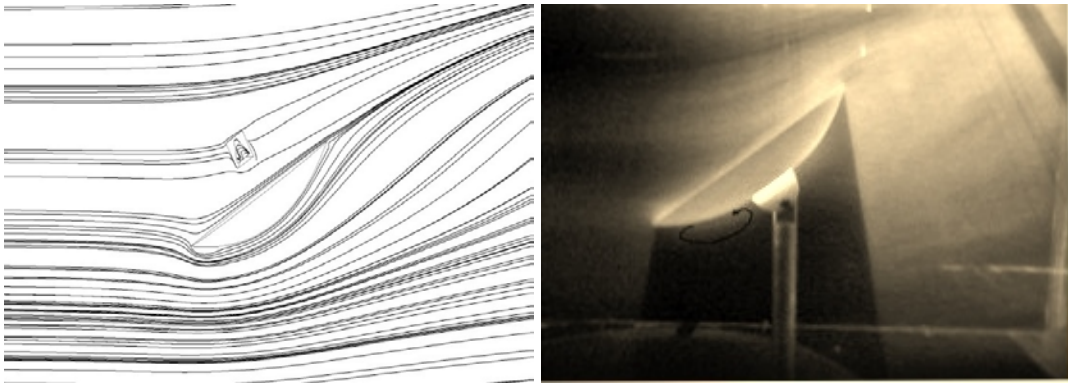


Figure 13: CFD streamlines and flow visualization for 30° tilt angle

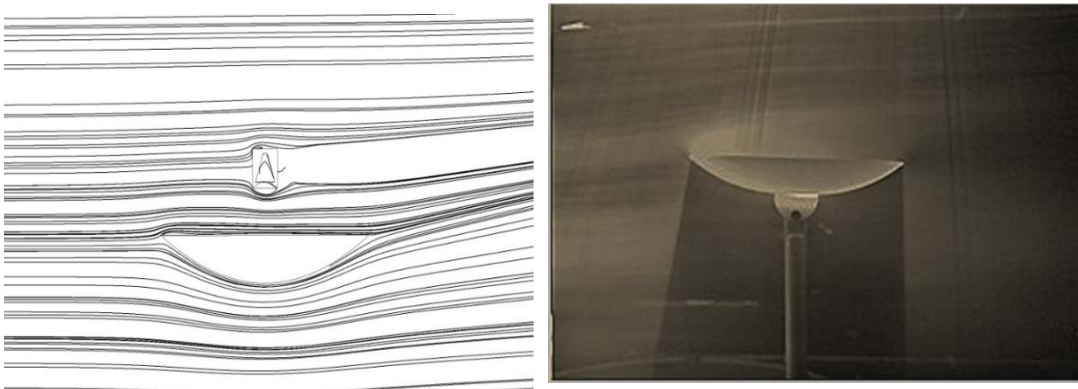


Figure 14: CFD streamlines and flow visualization for 0° tilt angle

By changing the tilt angle to -30° , such that the flow is from the backside of the dish structure, the dish creates a vortex in its wake. As is visible in Figure 15, smoke is trapped behind the dish and rotates locally. This smoke cloud is especially visible when the smoke generation is stopped, and takes a significant amount of time for the cloud to disperse. This is important to note, as this is where the cavity receiver would be and implies low transfer rates in this region. This would suggest that for this orientation natural convection would be significant whereas for other orientations the forced component might be dominant.

By increasing the tilt angle to -45° , again a large recirculation can be viewed in the wake region of dish creating a disorderly airflow in this area, while a small recirculation can be

viewed near the lower edge (Figure 16). Similar to -30° tilt angle, the local flow velocity behind the dish structure reduces sharply. In this respect, it is apparent that the flow near the aperture is dominated by the tangential components for tilt angles in the range 45° to -45° . Figure 17 shows the flow pattern for a tilt angle of -60° , showing the high velocities at the edges of dish structure producing the negative pressure in the vicinity of the wake region. The low pressure generates strong vortices behind the dish and like a 90° tilt angle, the circulation region increases sharply at a tilt angle of -90° generating two large vortices behind the dish structure (Figure 18). The overall effect is that as the dish moves to the vertical, the region near the receiver aperture is better shielded by the dish, the height of the wake increases and the local velocities reduce.

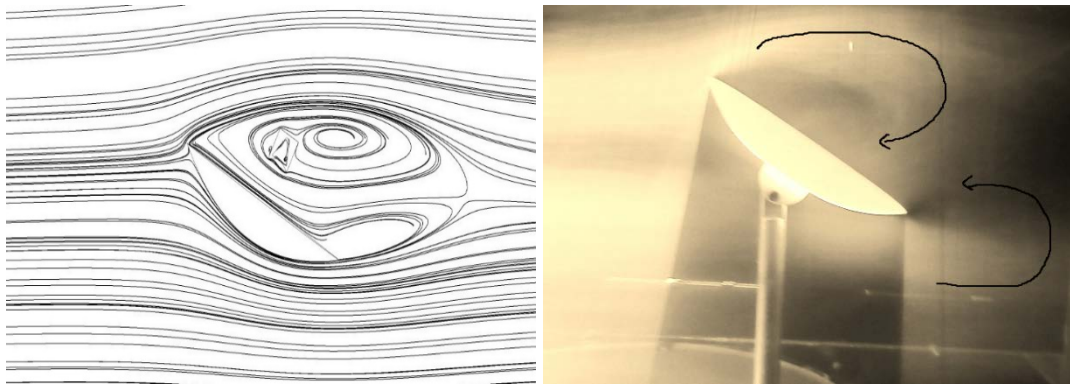


Figure 15: CFD streamlines and flow visualization for -30° tilt angle

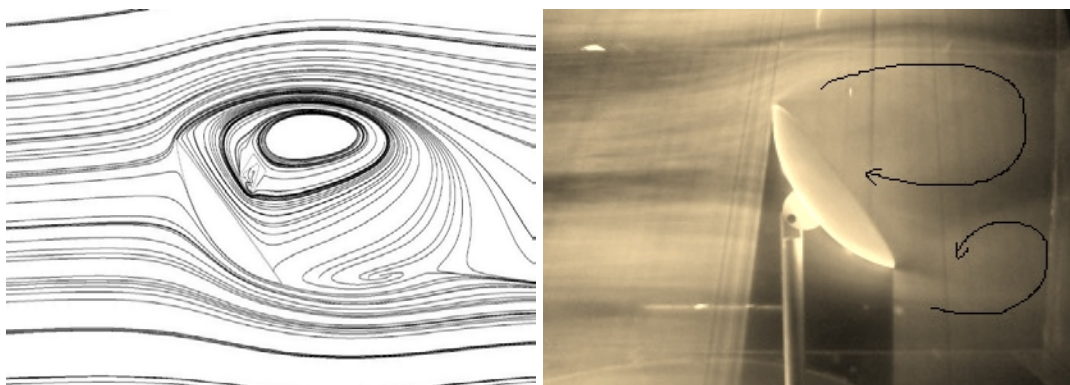


Figure 16: CFD streamlines and flow visualization for -45° tilt angle

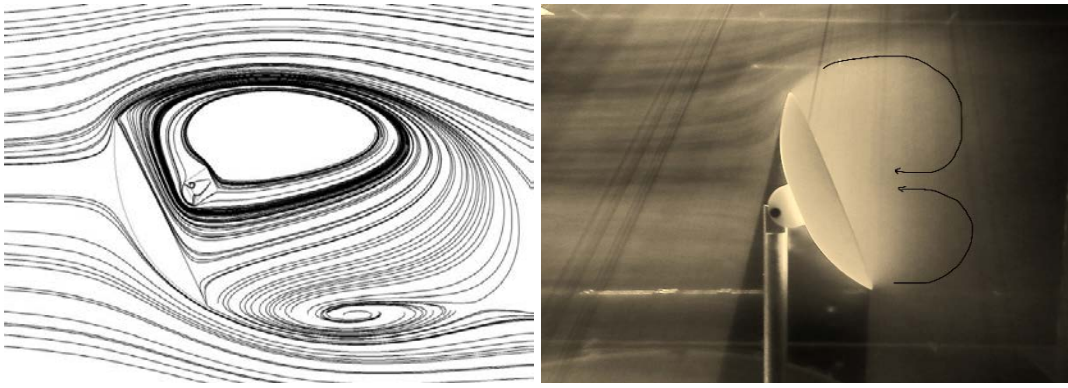


Figure 17: CFD streamlines and flow visualization for -60° tilt angle

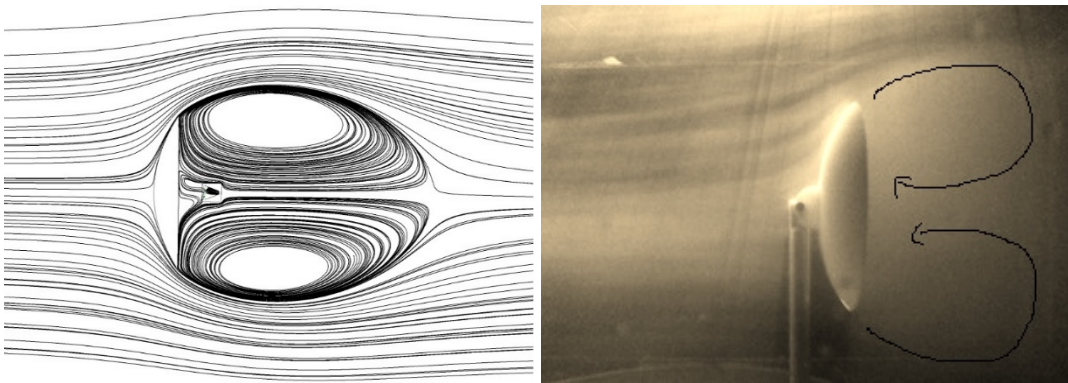


Figure 18: CFD streamlines and flow visualization for -90° tilt angle

In examining these images the streaks of the flow stream illustrate a shear layer that can also be observed from the simulation results. It can be clearly seen that the shear layer's trajectory is dependent on the tilt angle of dish structure. In turn, the shear layer disturbance at the edge of dish structure defines the drag force acting on the dish. It is observed that the maximum disturbance in the shear layer is in the case of 90° tilt angle, when the flow is approaching perpendicular to the aperture plane of dish from front side, implying the drag forces are maximum. The disturbance of the shear layer reduces with a decreasing tilt angle and it can be observed that the minimum shear layer disruption is the case of 0° tilt angle, when the aperture plane of the dish is facing vertically upward. The increase in the shear layer by increasing tilt angle can also be visualized with air flow from back side of dish.

Based on these observations, it can be concluded that the numerical model has generated similar flow patterns as seen in wind tunnel tests. The similarities between experimental and simulation results provide validation for the accuracy of the numerical model. Therefore, the results from the CFD solver can be used with confidence to predict the flow behavior around the dish structure.

It can also be seen that the orientation of a parabolic dish has a significant effect on the local air motion near the dish and consequently the air velocities near their receivers. These velocity disturbances and recirculation areas near where the receiver would be located would affect the heat losses and subsequently the overall performance of the parabolic dish concentrator.

2.4 Validation with available data of drag and lift coefficients

Having validated the numerical simulation qualitatively, it was decided to validate the numerical simulation quantitatively as well. To do this the drag coefficient (C_D) and lift coefficient (C_L) of the dish was determined from the steady state simulations and compared with data published by Wagner (1996) and Christo (2012) as shown in Figures 19 and 20. The aerodynamic coefficients, drag coefficient and lift coefficient are defined as:

$$C_D = \frac{F_D}{\rho V^2 A / 2} \quad (1)$$

and

$$C_L = \frac{F_L}{\rho V^2 A / 2} \quad (2)$$

Where, F_D and F_L are the drag and lift forces experienced by the dish, ρ is the density of air, V is the speed of the wind and A is the projected area of the dish.

For this study, the coefficients are seen to correspond well with the drag and lift coefficients of these previous two studies. This implies that, in addition to qualitatively predicting the flow shown previously, the CFD can quantitatively match the flow effects of the parabolic dish. This is significant as it supports the use of such a technique in exploring the heat transfer from such systems.

It can be observed by overlapping curves that the wind velocities had no significant impact on the drag and lift coefficients at any particular angle. They show that the parabolic dish receives the maximum drag force when air flow approaches perpendicular to the aperture plane of dish from front side i.e. 90° tilt angle. The wind produces the high pressure on the inside of the concave surface of dish resulting high drag coefficient. By changing the tilt angle, the drag coefficient decreases due to decrease in the projected area and the minimum drag force can be observed for a case when dish aperture is facing vertically upward (0° tilt angle). The drag force again increases by changing the tilt angle from 0° to -90° but the value of drag force remain lower than 90° tilt angle as the convex surface generally generates lower drag coefficient compared to concave surface (Figure 19).

Opposed to drag forces, Figure 20 shows that the dish experiences approximately zero lift force at 90° and -90° tilt angles due to minimum lift area (maximum drag area) and the positive and negative lift forces are experienced by varying the tilt angles from 90° and -90° . In the case of zero degree tilt angle, due to the low pressure and high velocities below the structure, dish experiences a slightly negative lift force. The negative lift coefficient indicates that the downward directed lift force due to the curved structure of dish. By changing the tilt angle, the maximum negative lift force can be observed at 30° due to high pressure on the front side of dish and after that the lift forces approaches almost linearly towards an approximate value of zero at 90° tilt angle. In case of negative tilt angles, the lift force first increases to a maximum value at -60° tilt angle and then due

to upward stronger forces from back side, the lift force again decreases to a zero value. Although all the data set are matching each other except there is a great deviation in case of lift coefficient at 30° tilt angle. This might be due to experimental error by Wagner (1996).

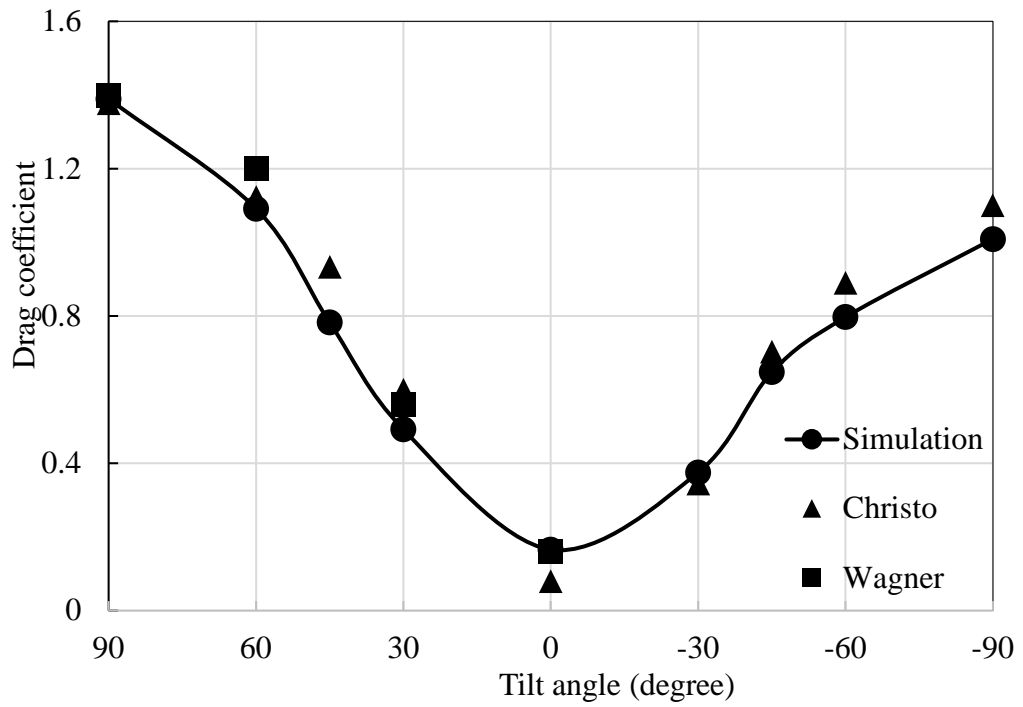


Figure 19: Comparison of drag coefficient at different tilt angles

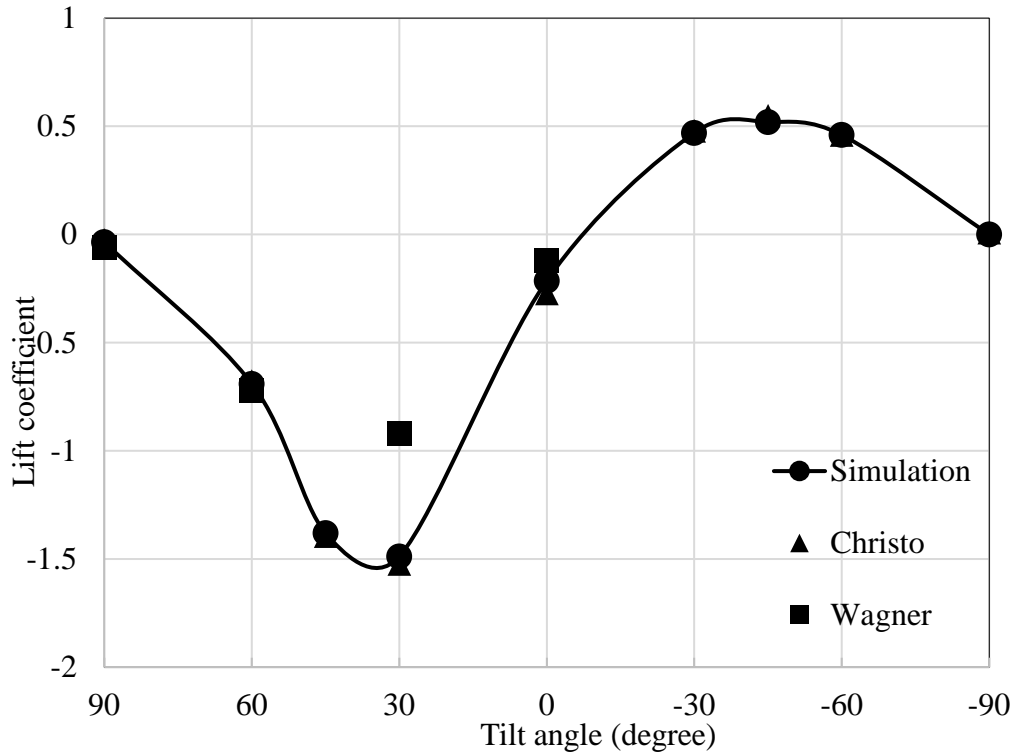


Figure 20: Comparison of lift coefficient at different tilt angles

2.5 Velocity profile in wake region of the dish

As further validation of the computational approach, a pitot-static probe was used to measure the velocity, in the flow direction, for a plane in the wake of the dish 70mm behind of dish. On the selected plane, 35 uniformly distributed points were selected to compare the velocities obtained numerically and experimentally (Figure 9). The experimental and simulated values of velocity in the direction of flow at the selected plane with a tilt angle of 90° are shown in Table 1. The deviation of experimental and simulations results was recorded and found to be not more than 20% for other tilt angles, which is an accepted experimental error range.

Experimental Simulation	Location				
	A	B	C	D	E
1	4.1 3.74	4.3 3.92	4.3 3.95	4.2 3.92	4.2 3.72
2	4.3 3.95	1.5 1.78	0.6 0.736	2 1.81	4.2 3.96
3	3.6 3.94	0 -0.792	0 -1.44	0 -0.72	3.4 3.9
4	0.6 0.738	0 -1.368	0 -1.934	0 -1.37	0.6 0.74
5	2 1.812	0 -0.708	0 -1.33	0 -0.75	2.1 1.95
6	4.2 3.92	1.6 1.85	0 0.7917	2.1 1.95	4.2 3.99
7	4 3.74	4.2 3.96	3 3.96	4.1 3.94	4 3.94

Table 1: Experimental and simulation velocities values at selected plane with 90° tilt angle

As the pitot-static probe measures the velocity in the direction of the original air flow, normal to the wind tunnel section, a velocity of 0 m/s in these results indicates a zero velocity vector in the direction of flow at the measurement point. However it can have a value in opposite direction if there is a recirculation zone as is observed by the negative values in the simulation data. It is evident from data that the velocities of free stream air flow accelerate when passing through the edges of the dish structure, while there is

negative velocity behind the dish. The obtained experimental velocities values were in a good agreement with the simulation values.

2.6 Effect of dish shape and focal length on flow field

In the previous sections, the impact of the dish structure on the flow field near the receiver was explored. However, one may argue that this result is not generalizable, and that changing the geometry of the dish the flow field may be significantly changed, and hence the transfer rates could be different. To address this possibility, a series of further simulations were undertaken, where the dish diameter was fixed but the rim angle and focal length were changed. Based on the variation of the shape, the dish structure can be defined as either being a shallow dish or deep dish, due to the relative position of the receiver at its focal length.

In order to investigate the effect of the cavity receiver's position, the flow behaviours were investigated around three different geometries with a constant dish diameter of 5m. The selected ANU dish having focal length of 1.84m was chosen as reference to define the other two dishes as a shallow and a deep dish respectively. Based on the focal lengths, the selected dishes were defined as (i) deep dish with focal length at 1.3m (ii) medium dish with focal length at 1.84m and (iii) shallow dish with focal length at 2.5m (Figure 21). These simulations were performed with a wind free stream velocity of 5 m/s with the other conditions fixed to be the same as discussed in Section 2.1. In the simulations, the incidence angle was fixed at 90° and the dish was rotated from -90° tilt angle to 90° tilt angle.

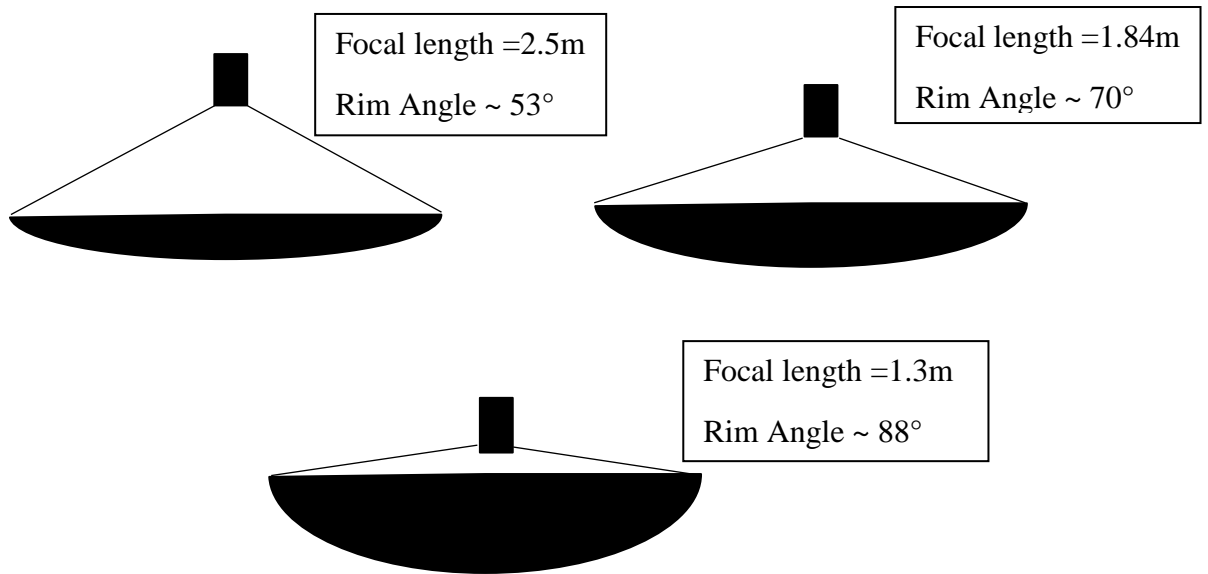


Figure 21: Sketched of dishes of different shape showing the focal length for same diameter

By comparing the drag coefficient of the three dishes, it was found that the maximum drag coefficient, as one may expect, was observed in deep dish structure (Figure 22). However it can be seen that there is a relatively small difference in the drag coefficients for the three dishes. This implies that the aerodynamic behaviour described previously applies to all these dishes, and in turn, that the transport behaviour of one dish would be representative of the others.

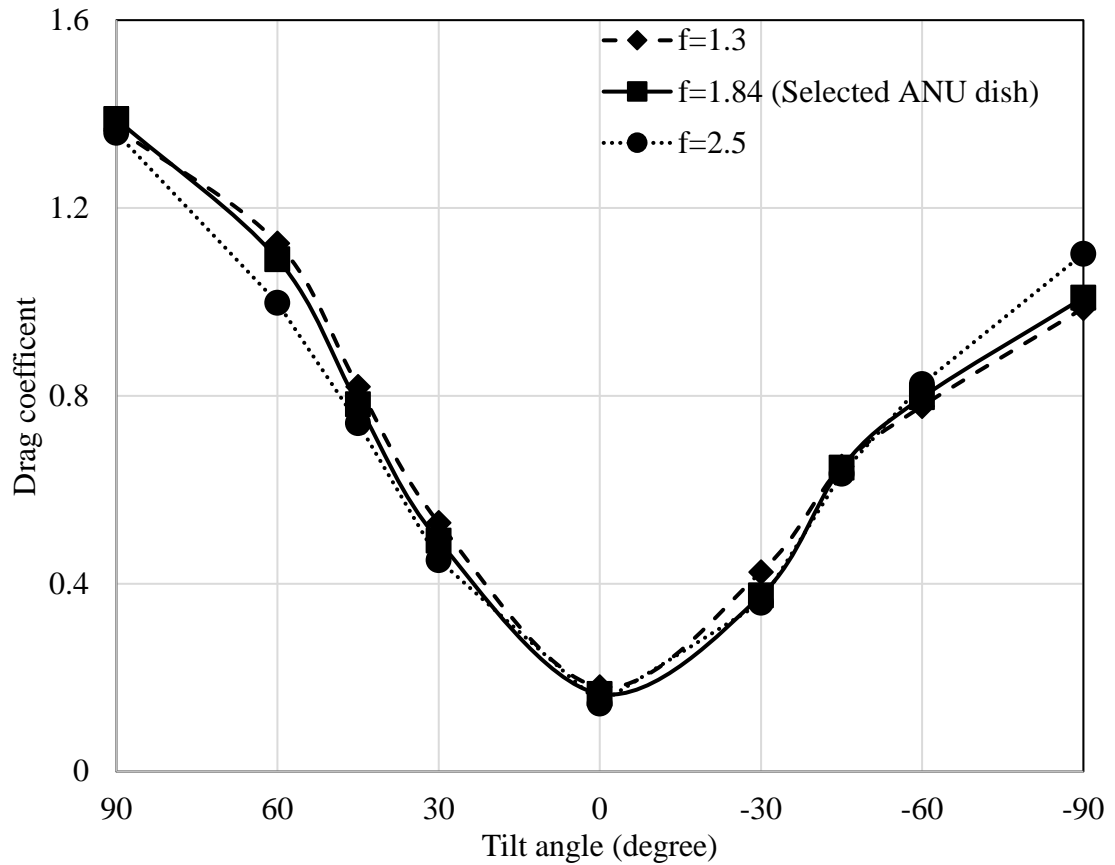


Figure 22: Drag coefficients at different tilt angles for the selected dish geometries

2.7 Significance of inclusion of the dish

As discussed in previous section, the interaction between the wind and the dish structure effect the local air motion at the cavity inlet. However, many of these studies (Harris and Lenz, 1984; Kaushika, 1993; Yasuaki et al., 1994; Kaushika and Reddy, 2000; Khubeiz et al., 2002; Yeh et al., 2005; Kumar and Reddy, 2007, 2008, Reddy and Kumar, 2008, 2009; Prakash et al., 2009) examine heat loss from the receiver in isolation. In all these works, the presence or the effect of the dish on the air motion around the receiver was not included. As a result, the range of applicability remains unclear due to the lack of dish in the analyses and therefore caution should be exercised when using them.

2.7.1 Flow behavior with and without the presence of the dish

In order to understand the effect of the dish, the CFD flow around the receiver was compared with and without the dish structure, using the conditions described in Chapter 2. To illustrate the significance of the dish, velocity contour plots along the longitudinal cross-section of the domain at different tilt angles are shown in Figure 23-Figure 31.

With the wind normal to the reflective surface of the dish (90°) (Figure 23a), it can be seen that there is a low-velocity stagnation zone around the receiver aperture in the presence of the dish structure. In contrast, without the dish, the velocity near the opening of the receiver is much higher (Figure 23b).

Similarly, at -90° (Figure 24a), there was a low velocity air flow toward the receiver aperture plane. In this situation the dish structure provided a barrier to the flow and a very low velocity can be observed around the receiver. In contrast, with no dish, the free stream wind directly enters the receiver, and the receiver is surrounded by high velocity air (Figure 24b). The air movement, with higher velocity, inside the cavity contrasts with almost stagnant air inside the cavity in the presence of the dish. In both cases (90° and -90°) the dish structure provided shelter from the flow and the receiver was surrounded by a low velocity zone.

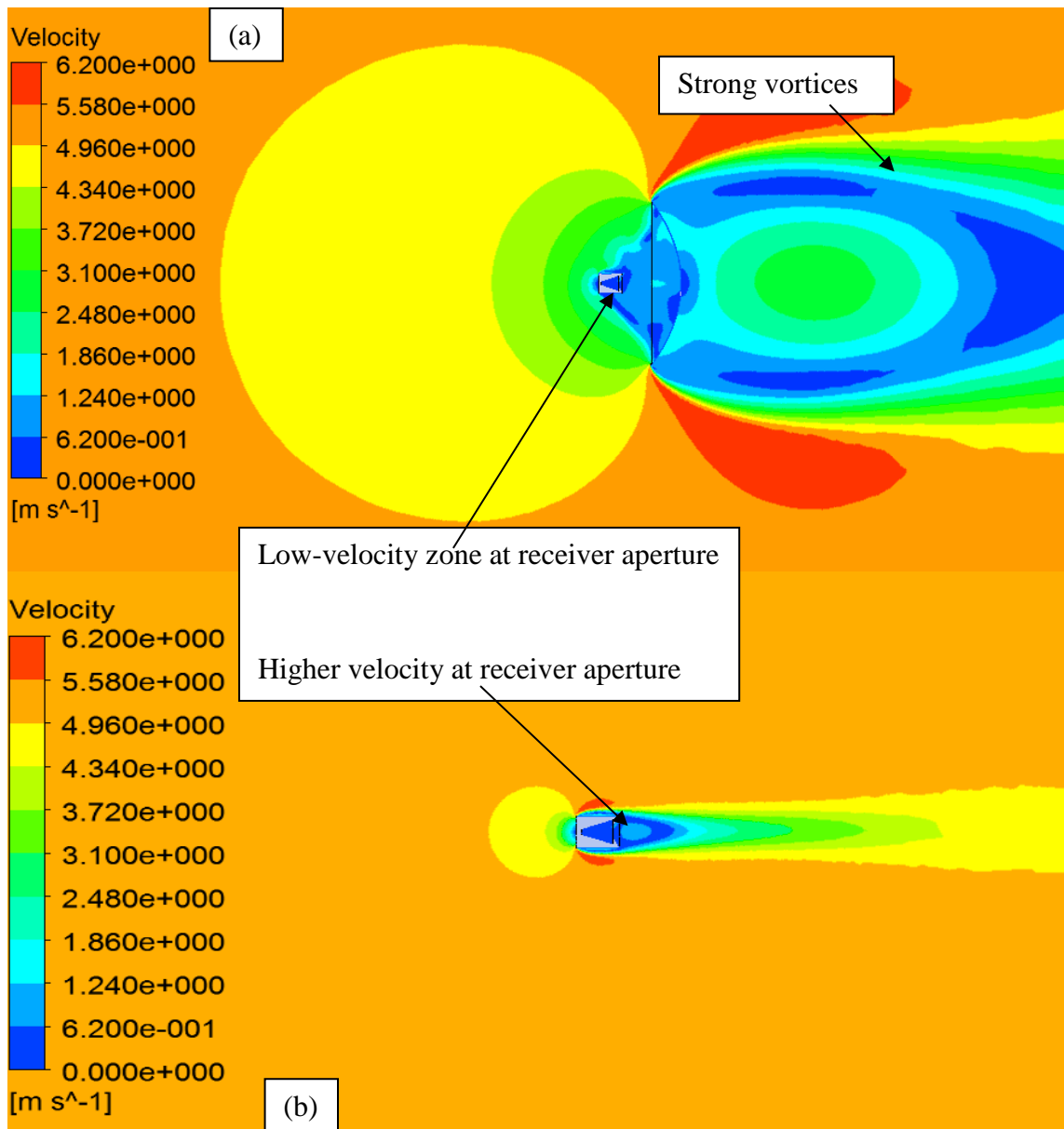


Figure 23: Flow at 90° (a) with dish (b) without dish structure

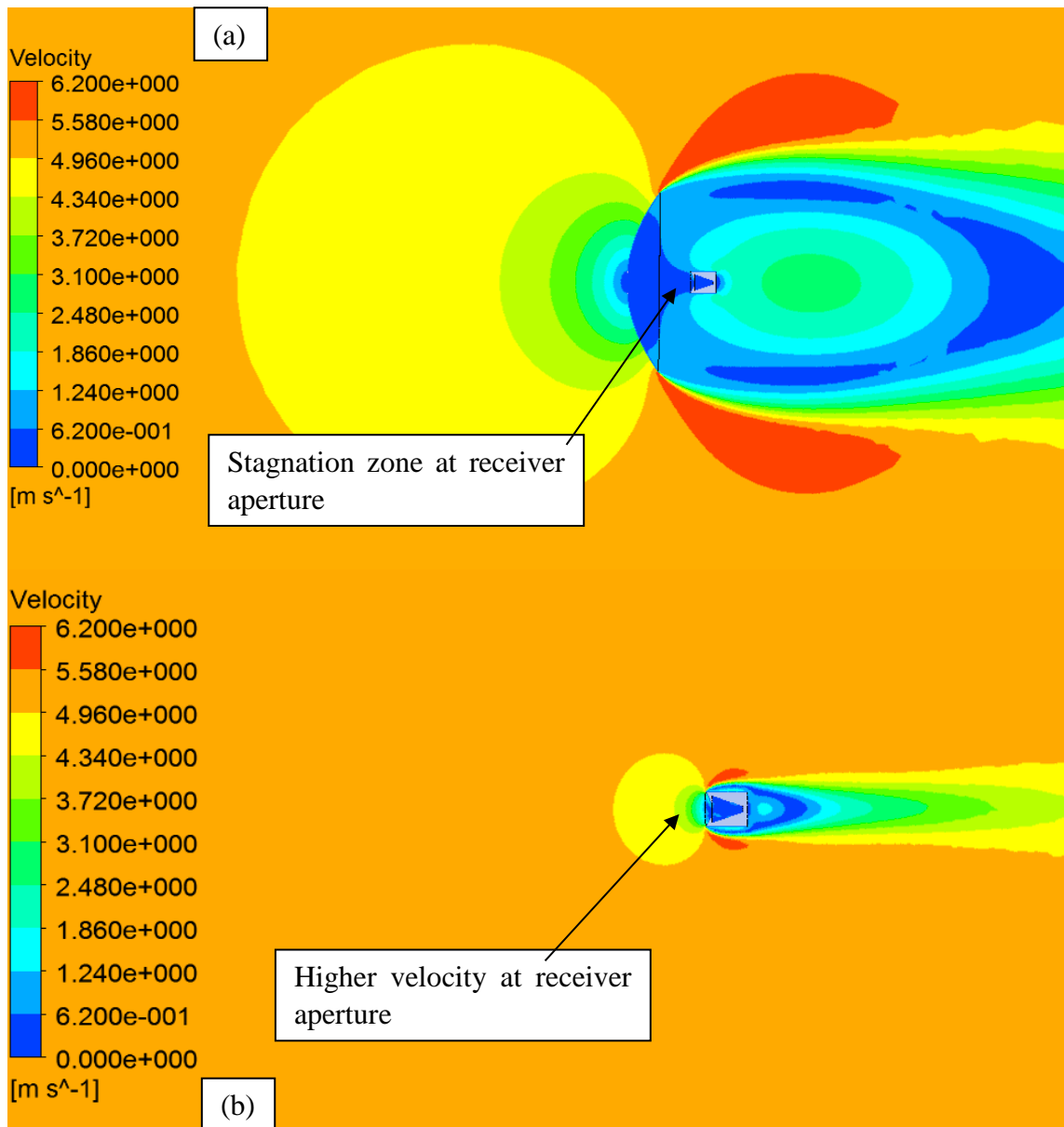


Figure 24: Flow at -90° (a) with dish (b) without dish structure

In the case of 60° flow with the dish present, the velocity contours (Figure 25a) show a low velocity near the cavity zone and flow separations from the upper and lower portion of the dish structure. This flow separation generates two large recirculation vortices behind the dish. Without the dish, it is clear that the local velocity is relatively high (Figure 25b) and the dish structure has a pronounced impact on the wind flow and the local velocity near the receiver.

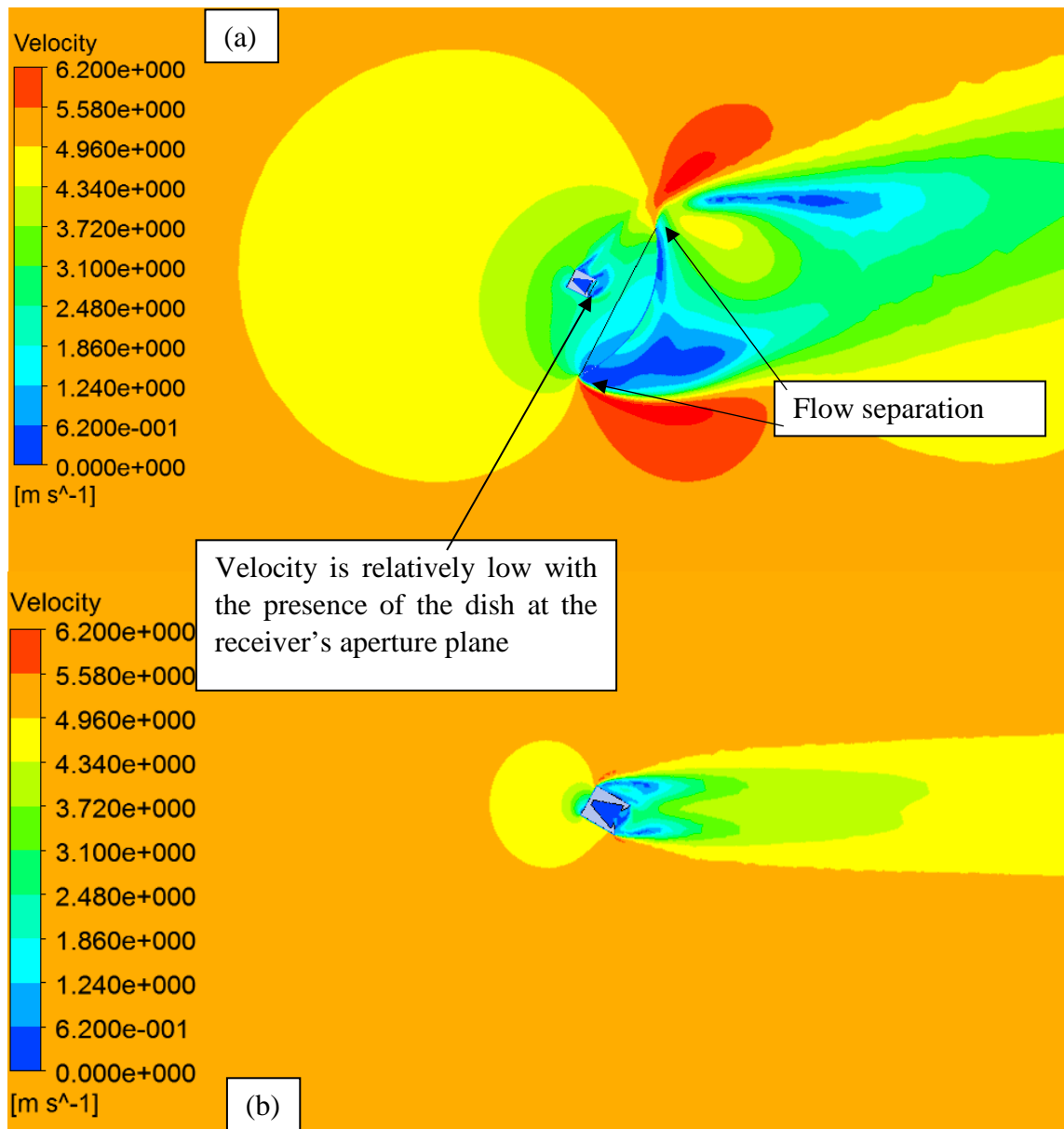


Figure 25: Flow at 60° (a) with dish (b) without dish structure

Similar to the 60° tilt angle, there was a very low wind velocity around the cavity receiver for -60° flow, where the velocity contours showed the formation of strong vortices around the cavity (Figure 26a). On the other hand, without the dish, Figure 26b shows higher velocities around the receiver without the dish. Like the -90° tilt angle case, the free stream air directly approaches the opening of the receiver and a significantly higher velocity is noticeable.

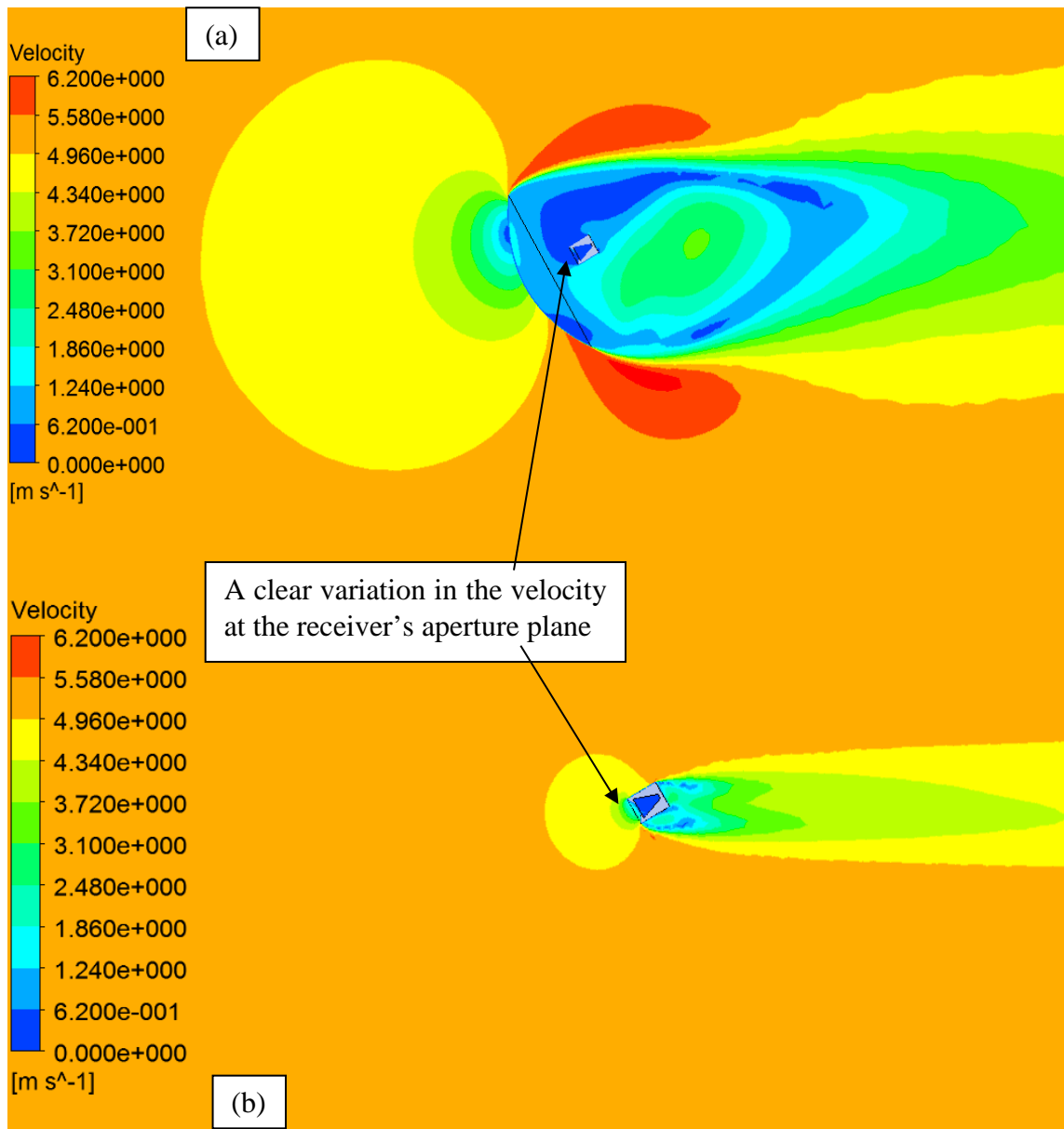


Figure 26: Flow at -60° (a) with dish (b) without dish structure

Figure 27 and Figure 28 show the velocity contours for 45° and -45° tilt angles. In both cases, with the dish present, a large circulation surrounding the receiver created the stronger tangential flow at the aperture plane. Meanwhile, in both cases, without the dish a markedly different flow behaviour and higher velocity can be seen.

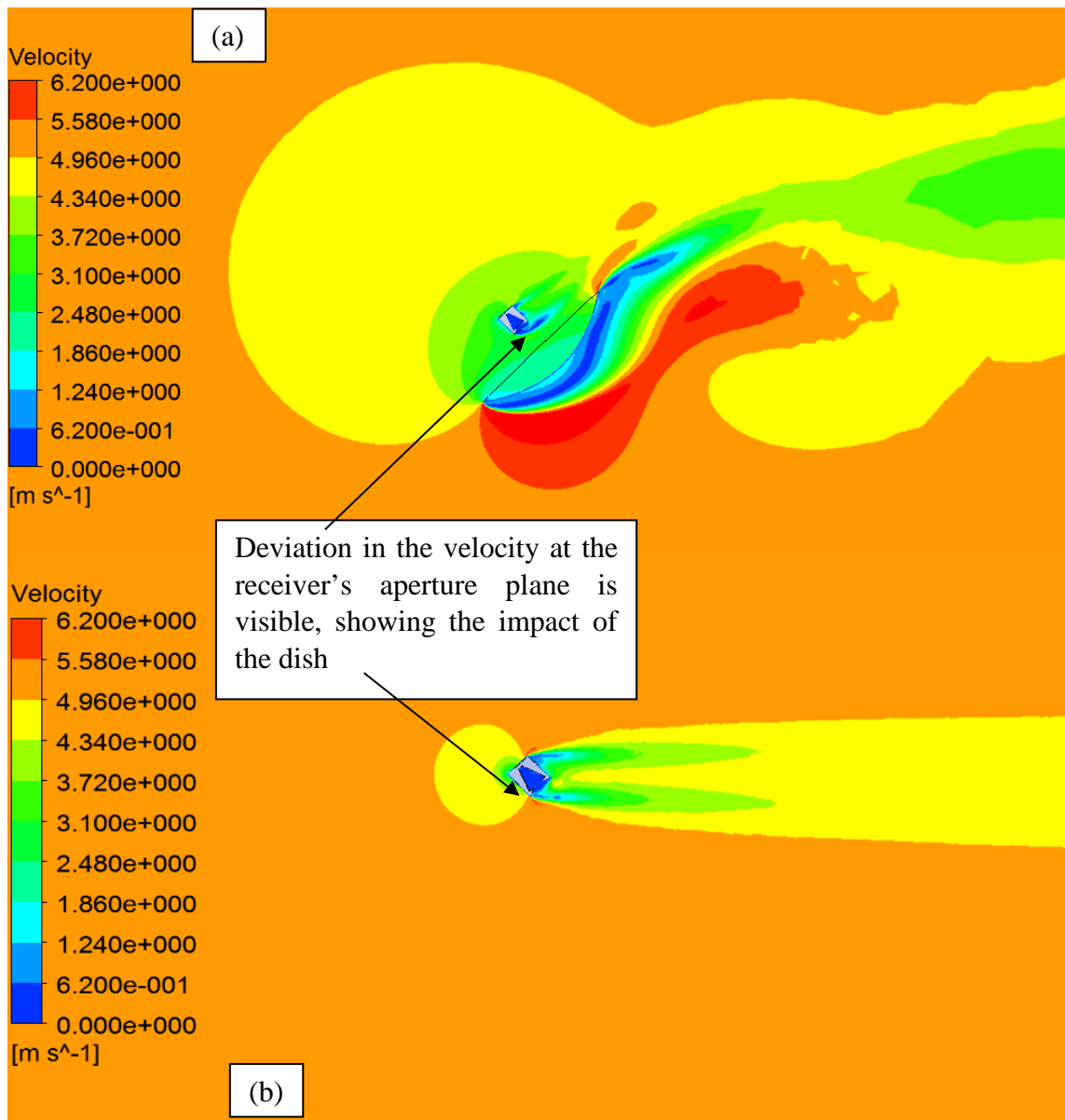


Figure 27: Flow at 45° (a) with dish (b) without dish structure

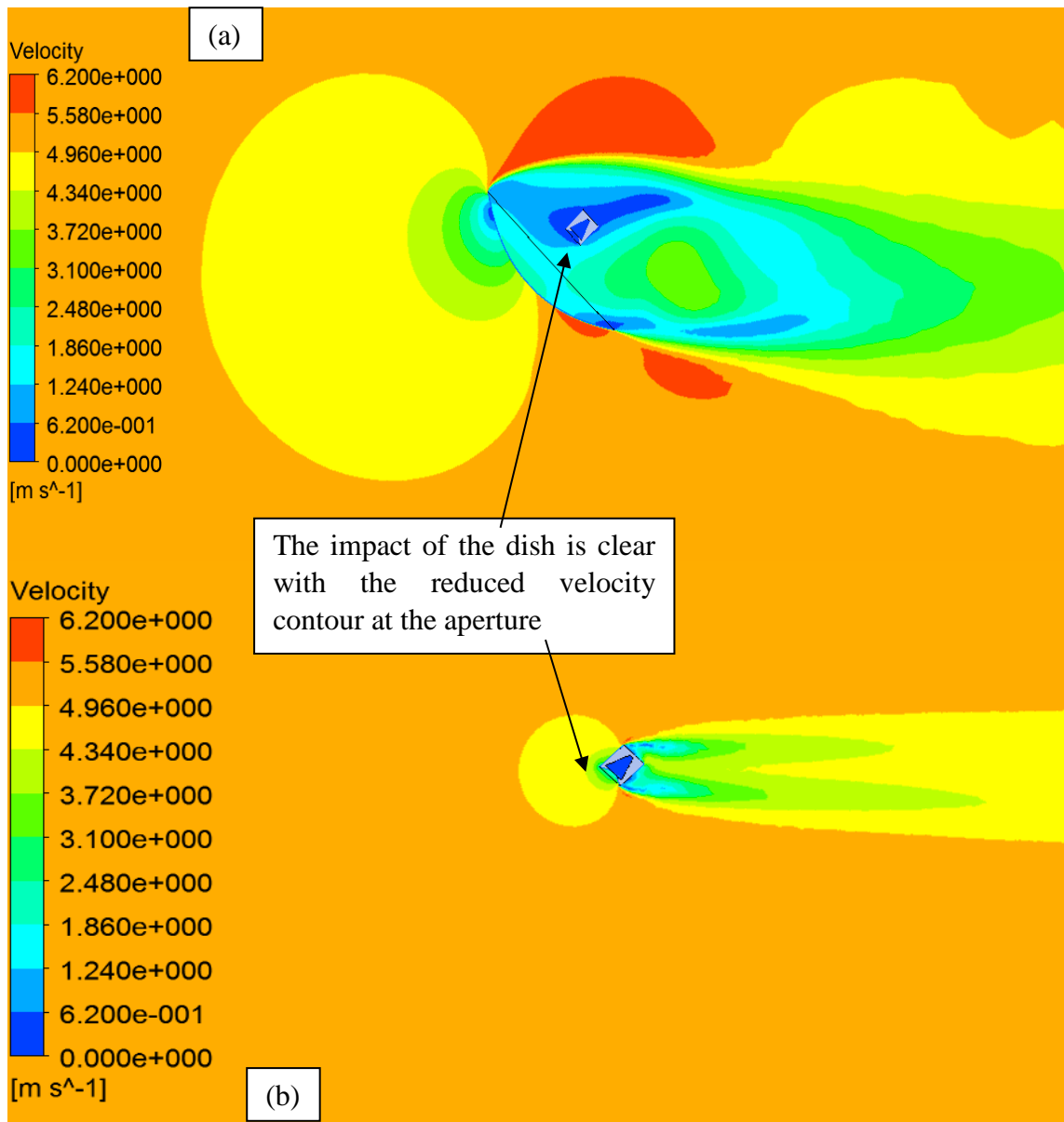


Figure 28: Flow at -45° (a) with dish (b) without dish structure

Figure 29 shows the results for 30° tilt angle. In both cases, with and without the dish, the simulation shows a streamlined wind flow with no larger flow separation near the receiver other than a flow recirculation region behind the lower portion of dish.

Figure 30a shows the velocity contours for -30° tilt angle, with the dish present. Without the dish, the higher velocity is clearly visible near the receiver aperture plane. It is evident

that the dish protected the receiver from free stream flow and this produced a comparatively low velocity zone near the receiver.

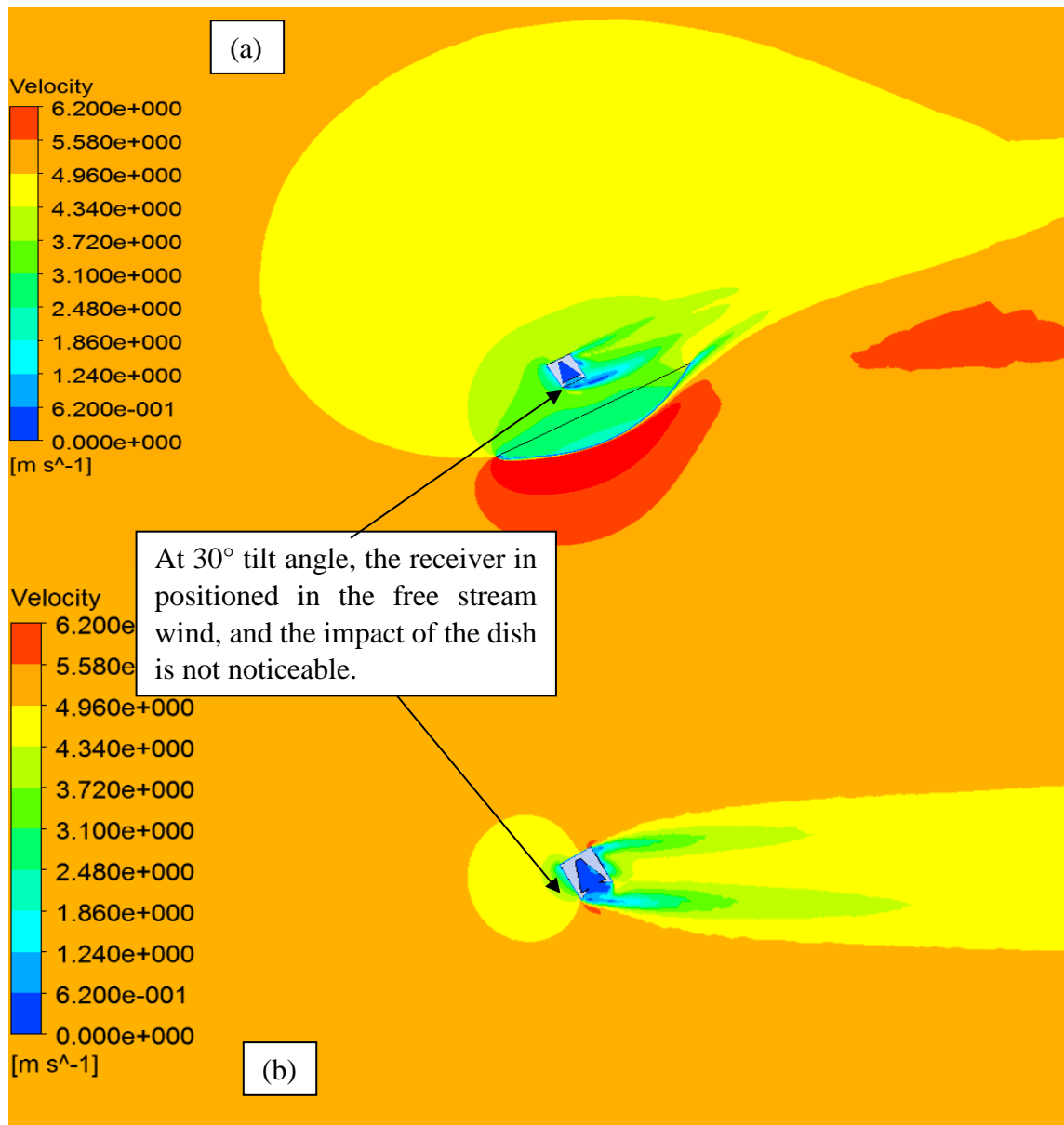


Figure 29: Flow at 30° (a) with dish (b) without dish structure

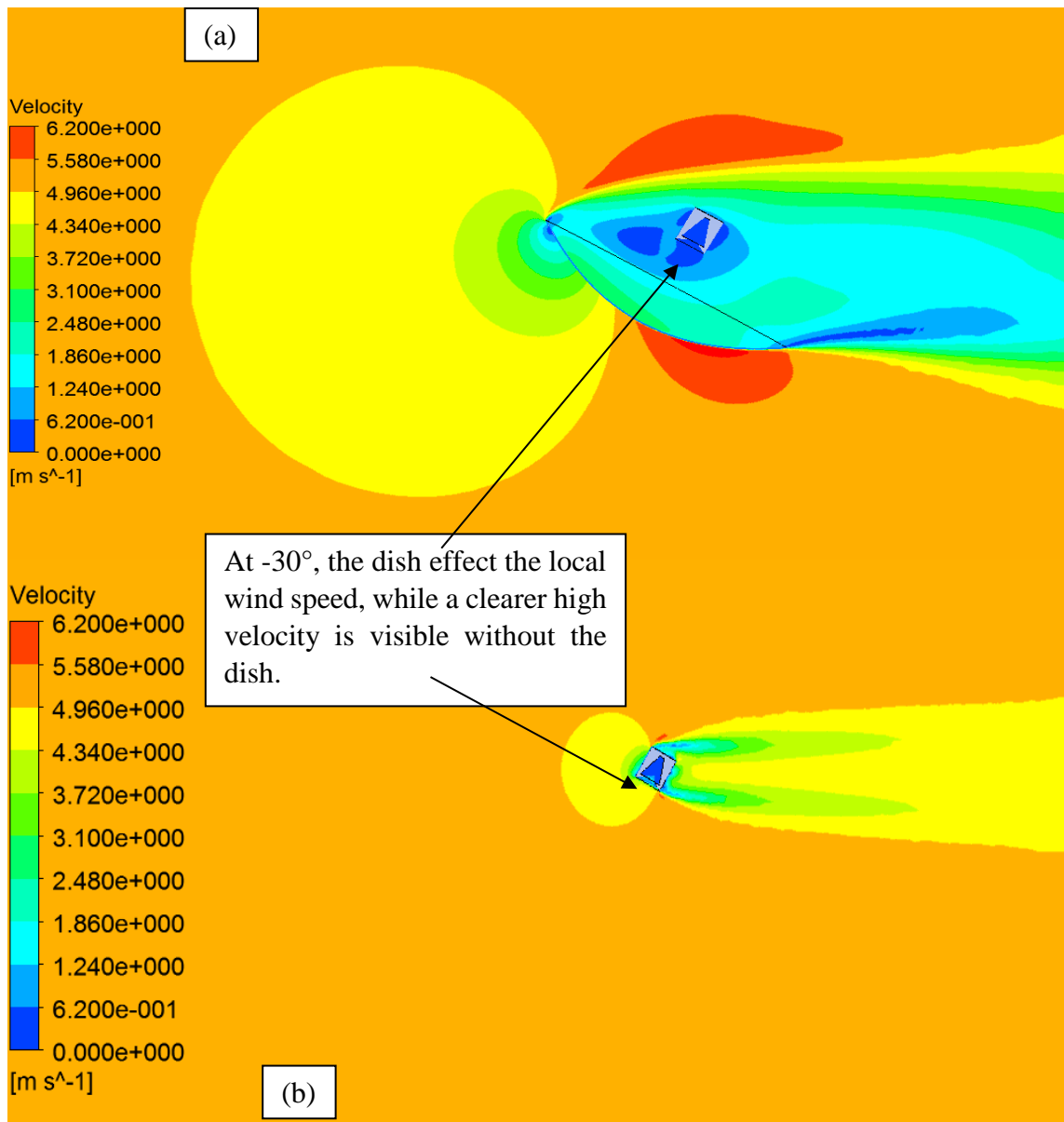


Figure 30: Flow at -30° (a) with dish (b) without dish structure

Figure 31 shows the case for 0° tilt. Both with and without the dish results are similar as the receiver is exposed to the free stream and the impact of the dish on the flow is not noticeable.

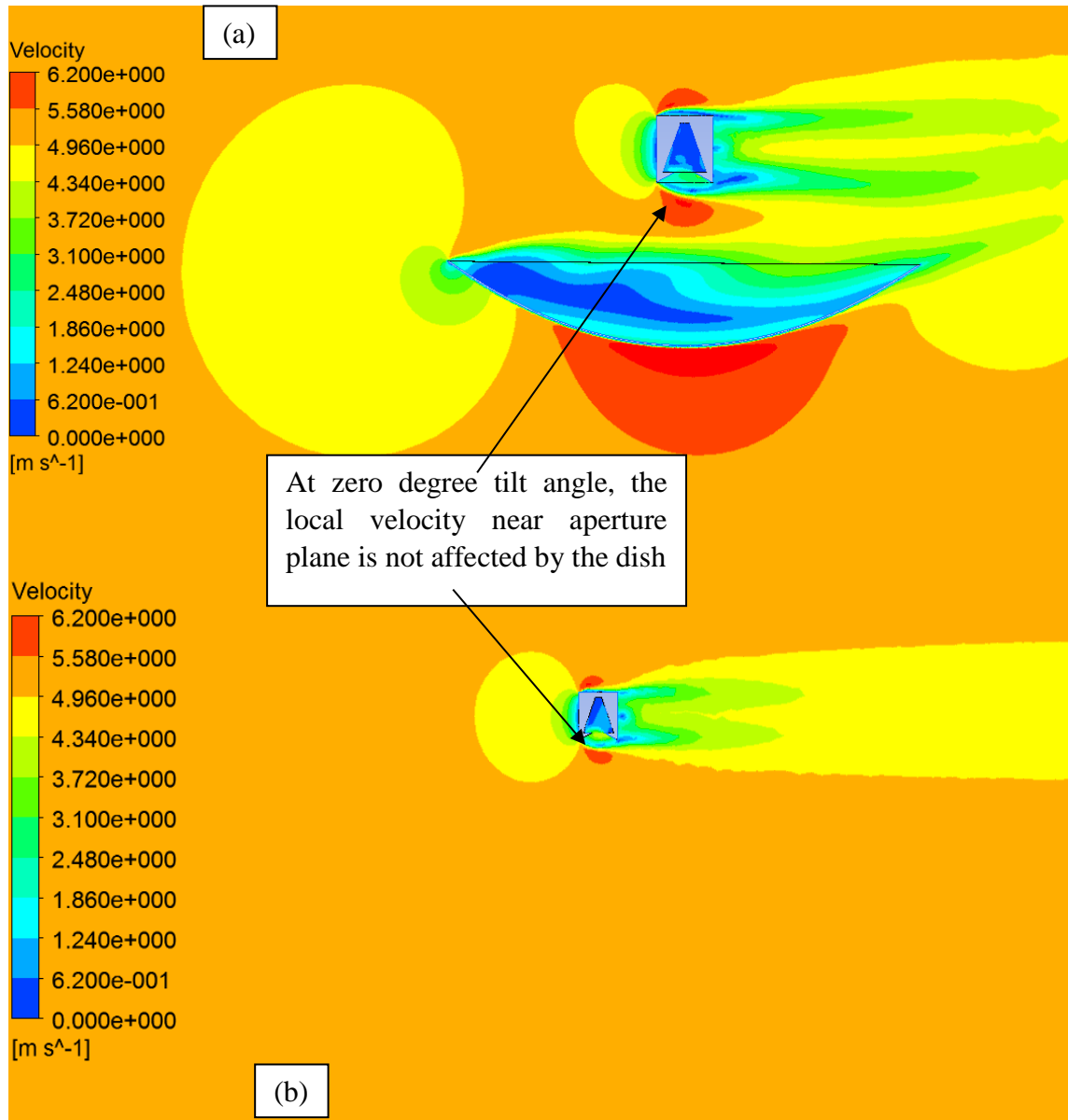


Figure 31: Flow at 0° (a) with dish (b) without dish structure

2.8 Chapter Summary

In this chapter, CFD modelling and experimental work of flow around a model of the dish are compared. The CFD has shown agreement between qualitative and quantitative experimental results. The wind tunnel test results provided a strong resemblance with the flow streamlines obtained from the numerical model used. Also, the numerically determined aerodynamic coefficients were in agreement with the previous studies. The numerical study has also shown minor impact of the focal length of the receiver on the drag coefficient, and so this work could be taken as a general outcome for a range of dish shapes.

This study provided a validation for the numerical model used with confidence. On this basis, it would appear that the use of the CFD model in the determination of heat losses from dish receivers holds significant promise.

It has also demonstrated that the dish structure significantly impacts the local velocity at the receiver. Based on the results, it can also be concluded that the orientation of a parabolic dish has a significant effect on the local air velocity near the dish and consequently the air velocities near their cavity receivers. These velocity disturbances and recirculation areas near where the receiver would be located, would affect the heat losses and subsequently the overall performance of the parabolic dish concentrator. The finding of this study also indicated a significant disturbance to the local air velocities at most tilt angles, except in the case of flow parallel to the aperture of the dish.

Chapter 3: Investigation into the presence of the dish on heat loss from the cavity receiver

Based on the validated simulation scheme, the interaction between the free stream air velocity and the dish structure was shown to significantly affect the local air velocity near the receiver. As such there is a need to examine the magnitude of the effect of the dish on the heat loss from the receiver in the CSP system. This chapter will therefore determine the heat loss due to these wind effects.

The heat loss from an open solar cavity receiver take places by conduction, convection and radiation. The conduction and radiation losses remain constant for any specific operating temperature, but the convection heat loss is greatly influenced by the tilt angle of receiver (Taumoefolau and Lovegrove, 2002). In general, the conduction and radiation heat losses can be determined by available analytical techniques with great accuracy just by knowing the accurate information of surface emissivity, conductivity and temperature values (Holman, 1997; Bergman et. al., 2011). However, determination of convection heat loss from the receiver is much more complicated due to the complexity of the temperature and velocity field in and around the cavity receiver, and usually relies on semi-empirical models (Wu et al., 2010).

A number of studies on convection heat loss from the cavity have been carried out and can be classified into natural and forced convection studies. It is obvious that without wind, there would be little impact of the dish on the convective heat loss. However, the interaction between the wind and the dish structure can affect the local air speed at the cavity inlet and thus the heat loss as well. From this one would also expect to see a transition from natural to forced convection as wind speeds increased. Both natural and forced convection would have to be combined to analyse the effect of a wide range of wind speeds on heat losses.

3.1 Natural convection from the receiver

3.1.1 Numerical setup

To establish a benchmark for comparison, it was decided to undertake a heat loss analysis for the no-wind condition, so that this work could bridge the complete range of wind conditions. In order to investigate the heat loss from the receiver, the validated numerical model discussed in Chapter 2 was used. Due to the large temperature difference between the cavity wall and the ambient air, the air cannot be treated as a constant density fluid. In these simulations, the internal cavity walls of the receiver were considered as isothermal at a temperature of 600°C and outer walls were assumed to be adiabatic. Figure 32 shows the boundary conditions used for heat transfer analysis. In order to accommodate the buoyancy induced flow, the fluid properties were allowed to vary across the domain as a function of temperature with the assumption that the pressure does not change significantly in the flow domain (Paitoonsurikarn, 2006).

Due to high temperature achieved in the cavity receiver, the walls radiates. As a result, the atmospheric air can be heated up and the convective heat loss will be different. However the effect of the radiative heat transfer is very negligible on the convective heat loss (Paitoonsurikarn, 2006). Therefore, no radiation model was used in addition to convective heat loss model in CFX.

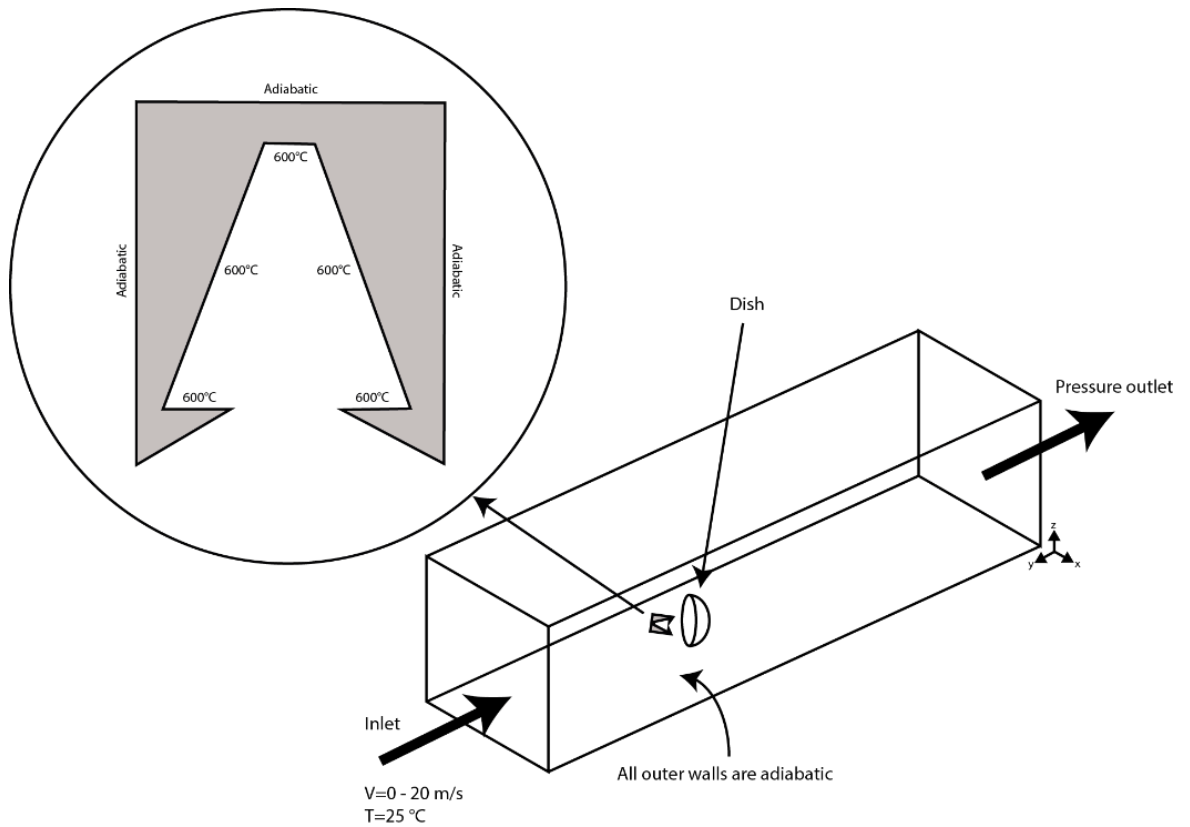


Figure 32: Boundary conditions

3.1.2 Validation

The simulation results of natural convective heat loss were compared with previous models of Stine and McDonald model (1994), Taumoefolau (2004), Paitoonsurikaran and Lovegrove (2006a), and Koenig and Marvin (1981), and a similar trend in the reduction of the convective heat loss pattern was observed in all cases. The same selected cavity was used to investigate the convective heat loss in all of these models. Figure 33 shows the comparison of heat losses between the simulation and the predicted values from these correlations.

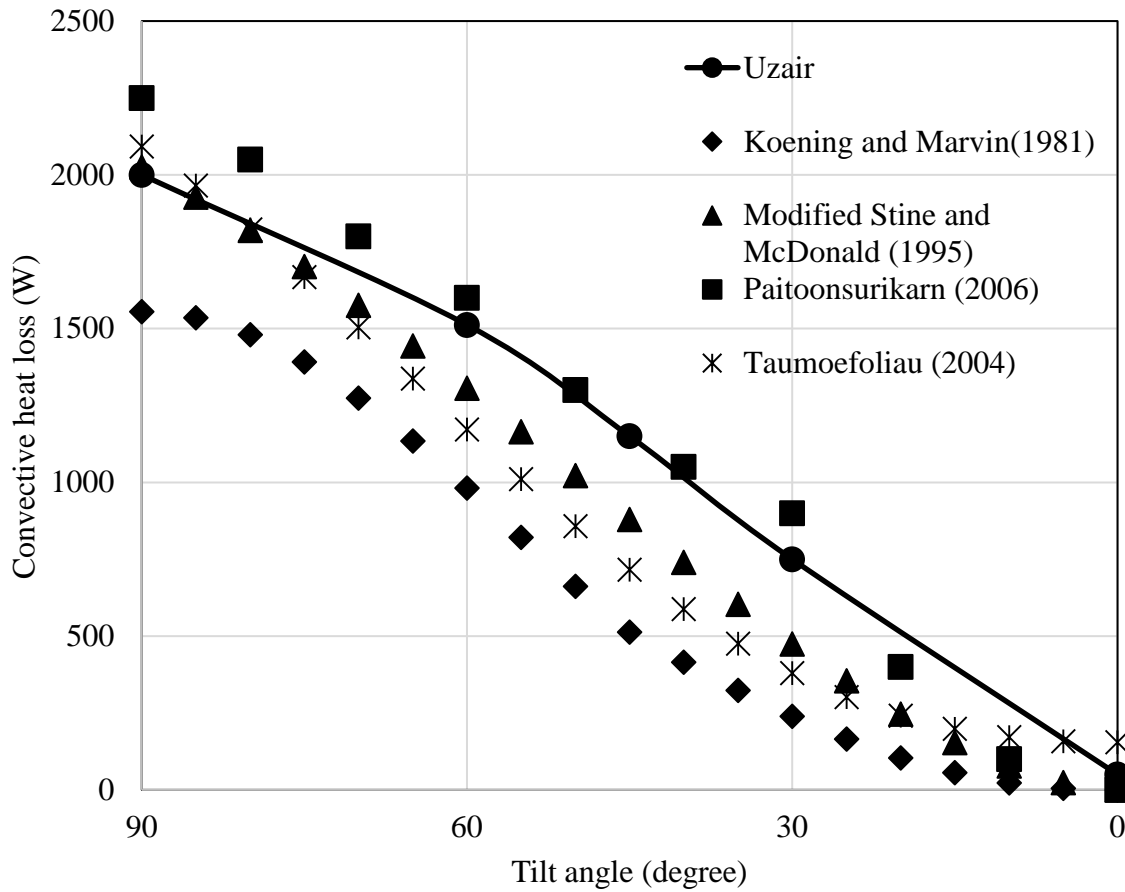


Figure 33: Validation of numerical simulation with other correlations

From the results, it is clear that the convective heat loss is strongly dependent on the tilt angle of the cavity receiver. Expanding on this, the temperature and velocity contours under natural convection conditions (i.e. the no wind condition) at different tilt angles are shown in Figures 34-38. By changing the tilt angle from 90° (facing horizontally sideway) to 0° (facing vertically downward), the convective heat loss from the receiver was gradually decreased. This phenomena is apparent as the plume velocity decreased over this range (Figures 34-38) and a dominant stagnation zone inside the receiver at 0° is also clearly visible. The stagnation zone is generated due to the trapped hot air inside the receiver resulting in the heat loss being at a minimum at the 0° tilt. This stagnation zone is markedly decreased for the case of 90° tilt angle. The reduction in the stagnation zone

indicates less hot air trapped inside the receiver, resulting in an increase of heat loss being evident at 90° tilt angle.

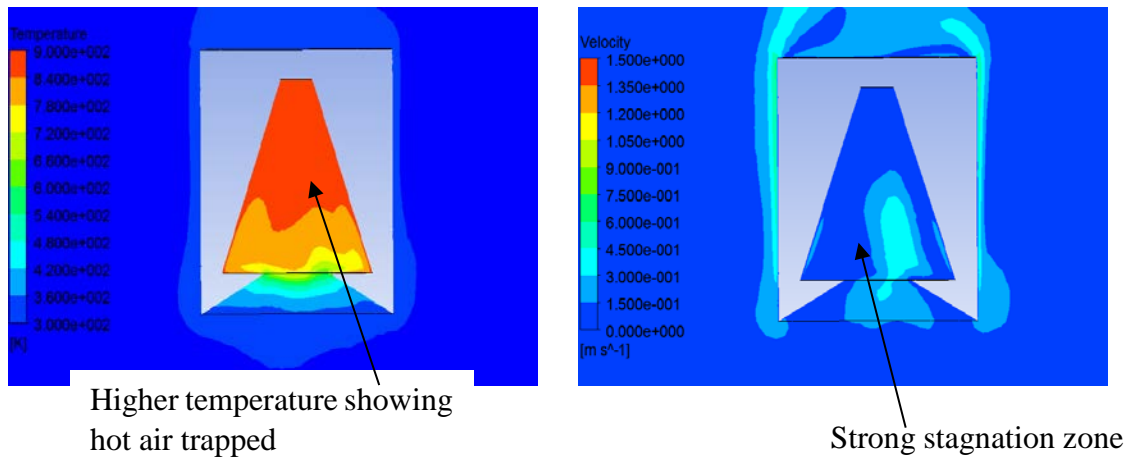


Figure 34: Temperature and velocity contours at 0°

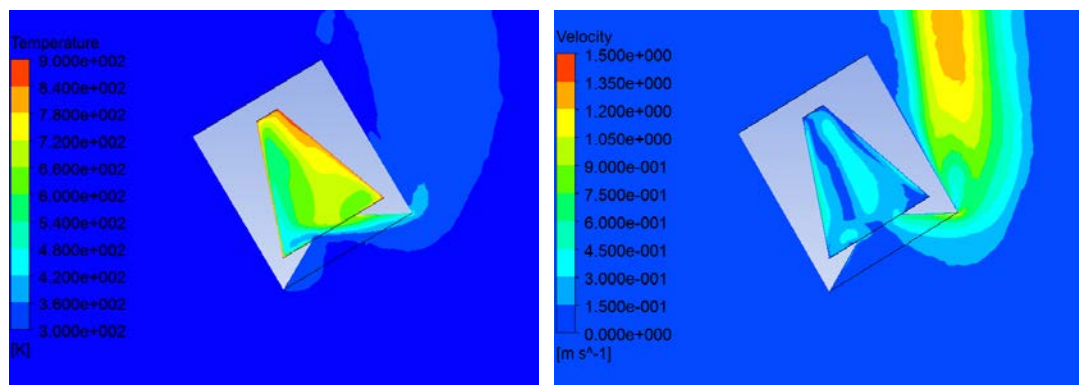


Figure 35: Temperature and velocity contours at 30°

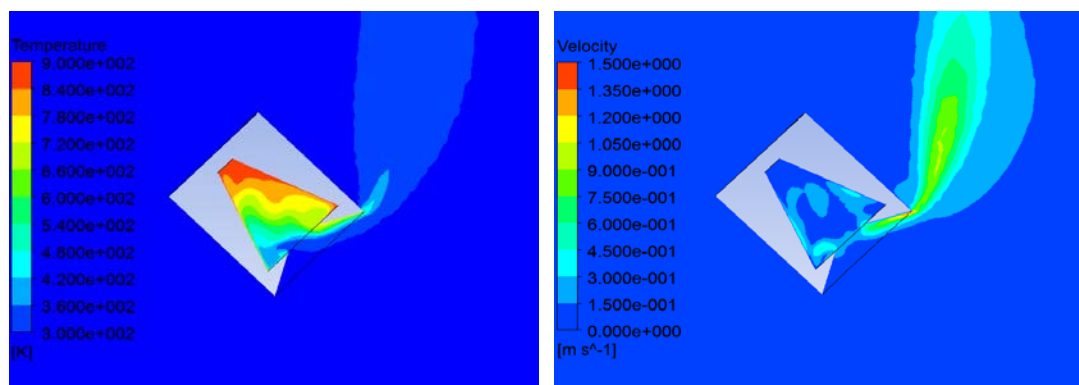


Figure 36: Temperature and velocity contours at 45°

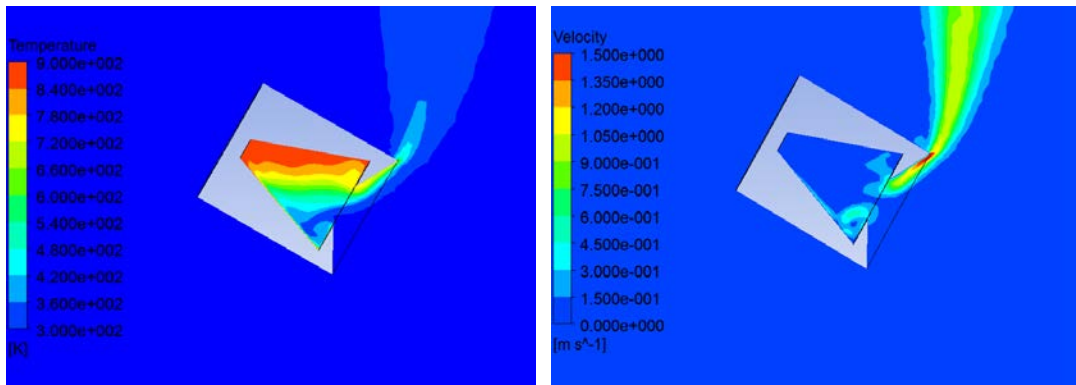


Figure 37: Temperature and velocity contours at 60°

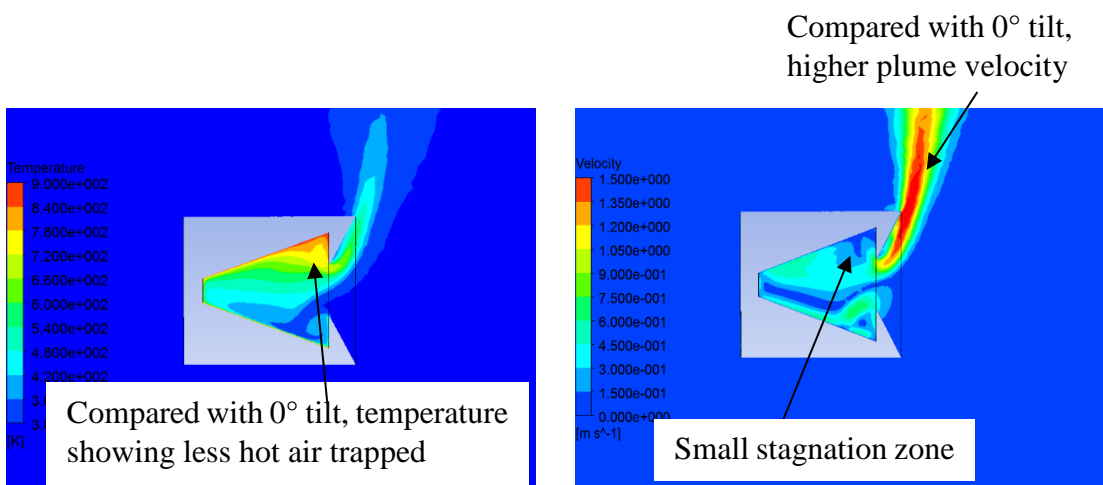


Figure 38: Temperature and velocity contours at 90°

In summary, at the position when the cavity receiver is facing vertically downward, the receiver is dominated by a large stagnation zone. The hot air rises up, resulting in a high temperature of the interior air close to the wall temperature. As a result the minimum heat transfer occurs when the cavity receiver is facing vertically downward. On the other hand, by tilting the receiver, the stagnation zone starts to decrease with the increase in the tilt angle resulting in some portion of hot air going out of the receiver and cold air flowing into it, producing a rising main air flow and heating up along the receiver's wall. The increasing heat loss with tilt angle results from the strengthening convection caused by the raised lip of the cavity releasing the heated air. Furthermore, this section has validated

the natural convection model and detailed the heat loss as a function of tilt angle for the no-wind condition.

3.2 Forced convection heat loss from receiver with and without the dish

Having shown that the model worked for natural convection conditions a detailed numerical comparison was performed to investigate the heat loss from the receiver with and without the dish present in the flow field. The simulations were carried out with a free stream velocity of 5 m/s and over a range of tilt angles with the cavity walls maintained at a temperature of 600°C.

Now, in the previous chapter, some of the airflow had very low velocities in the recirculation zone behind the dish compared to the free stream velocity. Hence, the convection heat losses from the cavity receiver might be forced or mixed convection subject to the tilt angle of the dish. Figure 39 shows the convective heat loss from the receiver without the presence of the dish and can be seen to agree with Paitoonsurikarn's model (2006) and therefore validate the method.

Extending on this, Figure 40 compares the convective heat loss from the cavity with the dish present and absent. It can be seen that, for the cases where the dish is neglected, the convective heat loss decreases as the tilt angle moves from $\pm 90^\circ$ (cavity axis aligned horizontally) to 0° (cavity facing downward). This is because at 0° the buoyancy forces move to their maximum and inhibit any flow from the aperture at the bottom of the receiver. However, what is most noticeable is that with the dish structure being present the convective heat loss is significantly lower than the cases where it is absent, except for the case of a zero degree tilt angle.

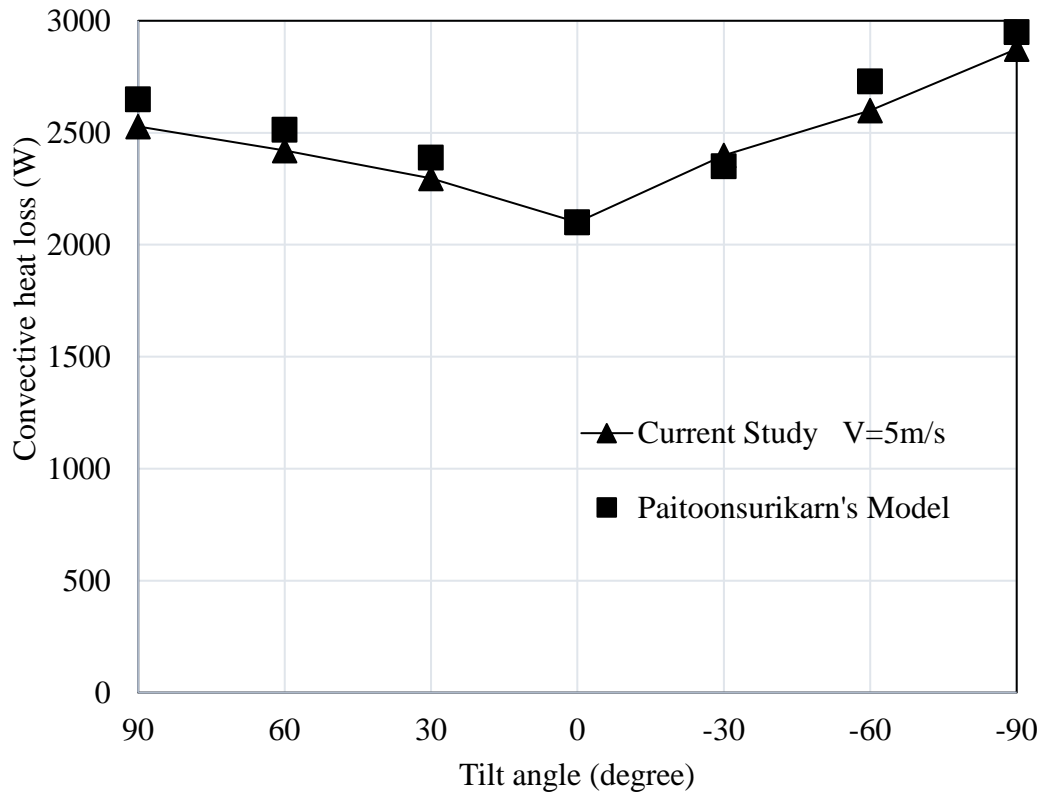


Figure 39: Validation of heat loss from the receiver without the dish structure

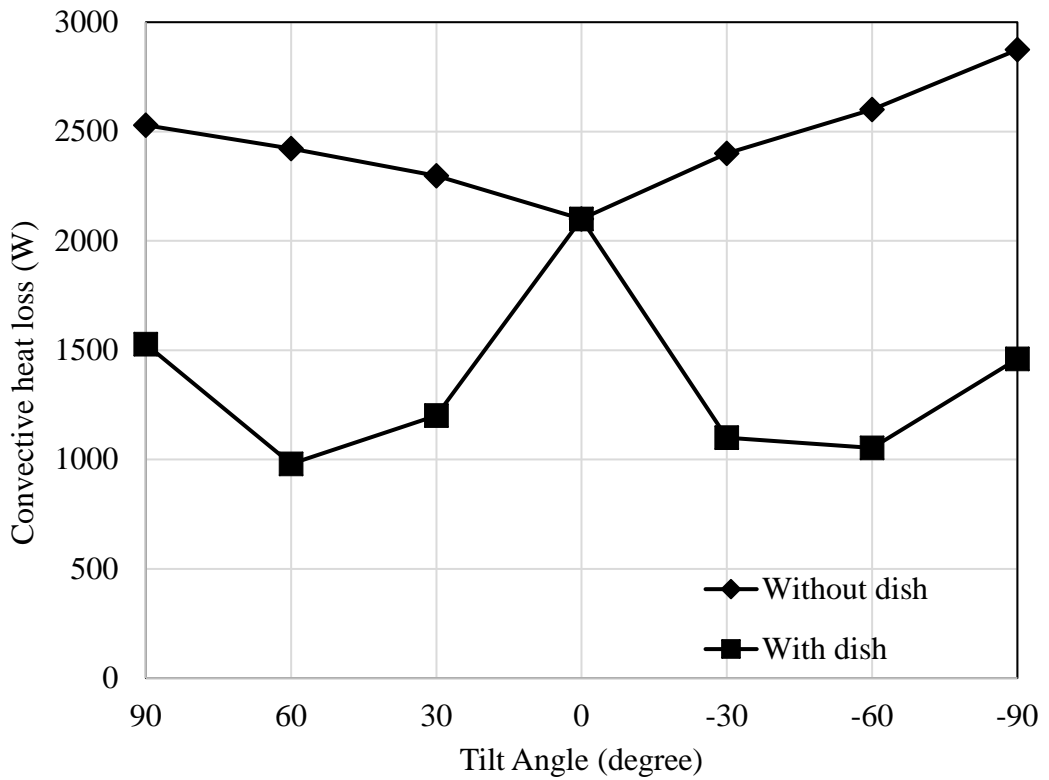


Figure 40: Convective heat loss at various tilt angles with a wind velocity of 5 m/s

It is clear from Figure 40 that the presence of the dish structure reduces the convective heat loss significantly (up to 40%). For most of the positive tilt angles (dish facing directly at the air flow), the heat loss is much lower than in the case when having no dish due to the lower velocities observed previously. For negative tilt angles, the cavity receiver is located in the wake region of the dish and is surrounded by the large vortices described earlier, and once again there is a marked change in the heat loss. This change in heat loss arises due to the fact that without the dish structure being present the cavity is exposed to strong forced convective flows, whereas in the presence of the dish the heat loss is driven by the weaker natural convection mechanism.

What is interesting to note is that for tilt angles between $\pm 30^\circ$ and 0° the heat loss increases. This can be attributed to the receiver moving into the free stream (by virtue of the dish's geometry) and being subject to stronger forced flow, rather than residing in the wake as illustrated by Figures 41-42.

For the case of zero degree tilt angle, the dish does not affect the convective heat loss from the receiver. This can be explained by the fact that at a zero degree tilt angle, the dish structure does not markedly affect the air flow on the top side of the dish (Figure 41). As a result there is no impact on the flow near the cavity receiver and hence the heat loss from the cavity. Within the range of 0° to $+30^\circ$ tilt angle, the receiver experiences free stream wind at the receiver aperture (Figure 42). However, at the -30° tilt angle, the receiver is located in the wake region of the dish and the recirculation can be observed easily (Figure 43).

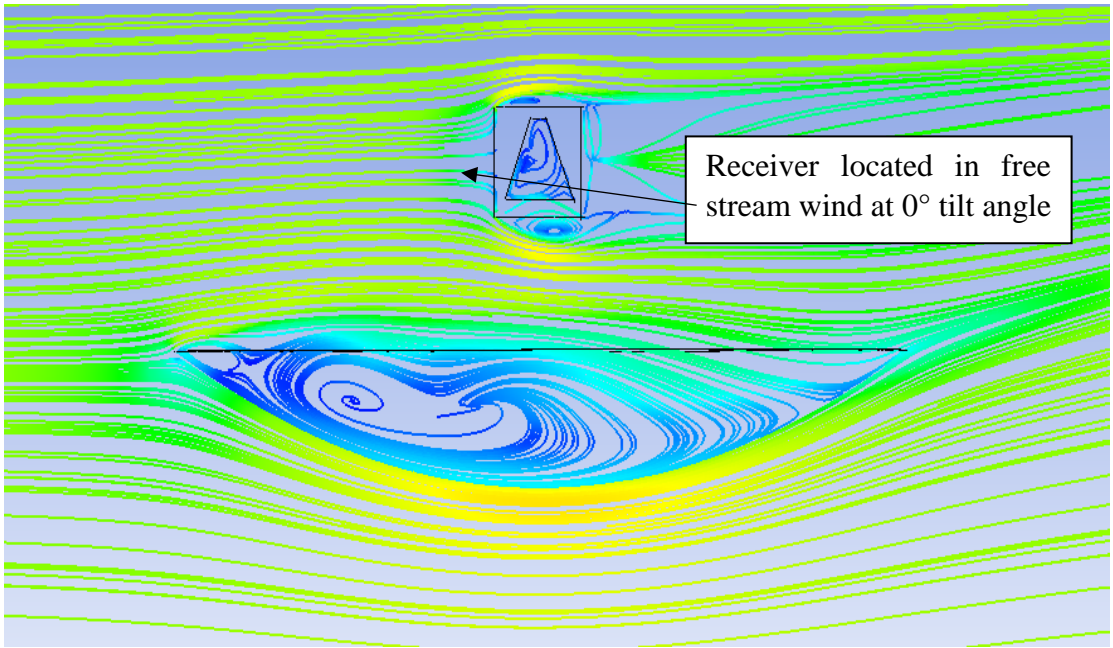


Figure 41: Location of the receiver at 0° tilt angle

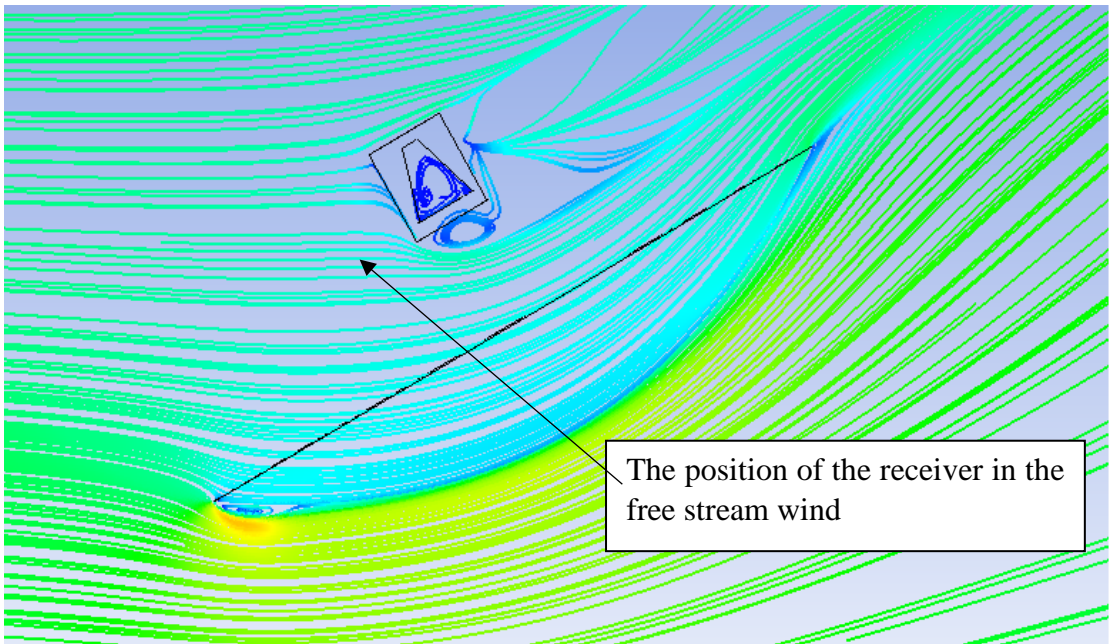


Figure 42: Location of the receiver at 30° tilt angle

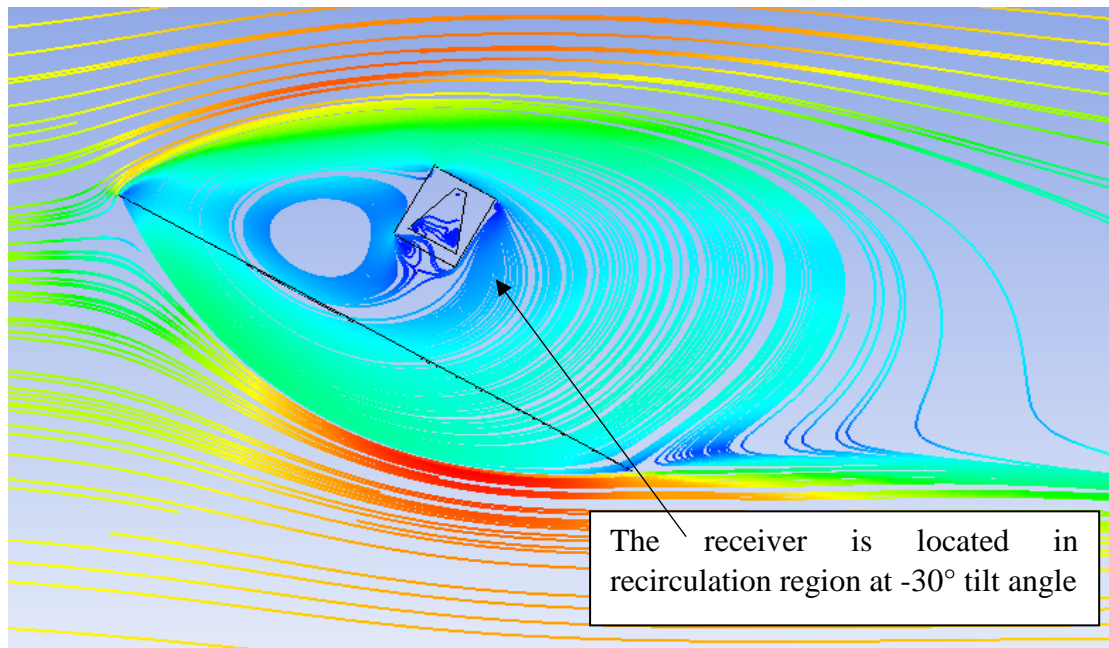


Figure 43: Location of the receiver at -30° tilt angle

The overarching conclusion is that parabolic dish CSP systems designed without consideration of the effect of the dish on heat loss will be significantly oversized and hence more expensive than they could be.

3.3 Effect of dish shape on convective heat loss from the receiver

Based on the observations discussed in Section 2.5, there is minimal difference in the drag coefficient when comparing dishes having different focal lengths. In turn this raised some interesting questions into how the heat loss from the receiver is influenced by this change. In considering how the positioning of the cavity receiver may impact on the heat loss, an investigation around three different geometries with a constant dish diameter of 5m was performed (Figure 44). Figure 45 shows the convective heat losses from the cavity receiver of these three cases.

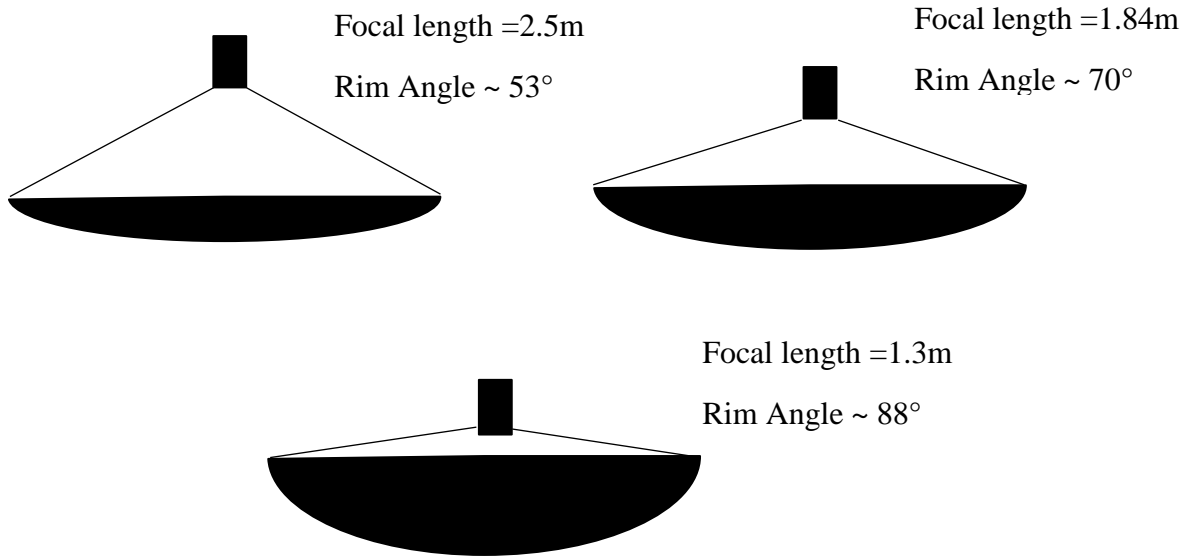


Figure 44: Sketched of dishes of different shape showing the focal length for same diameter

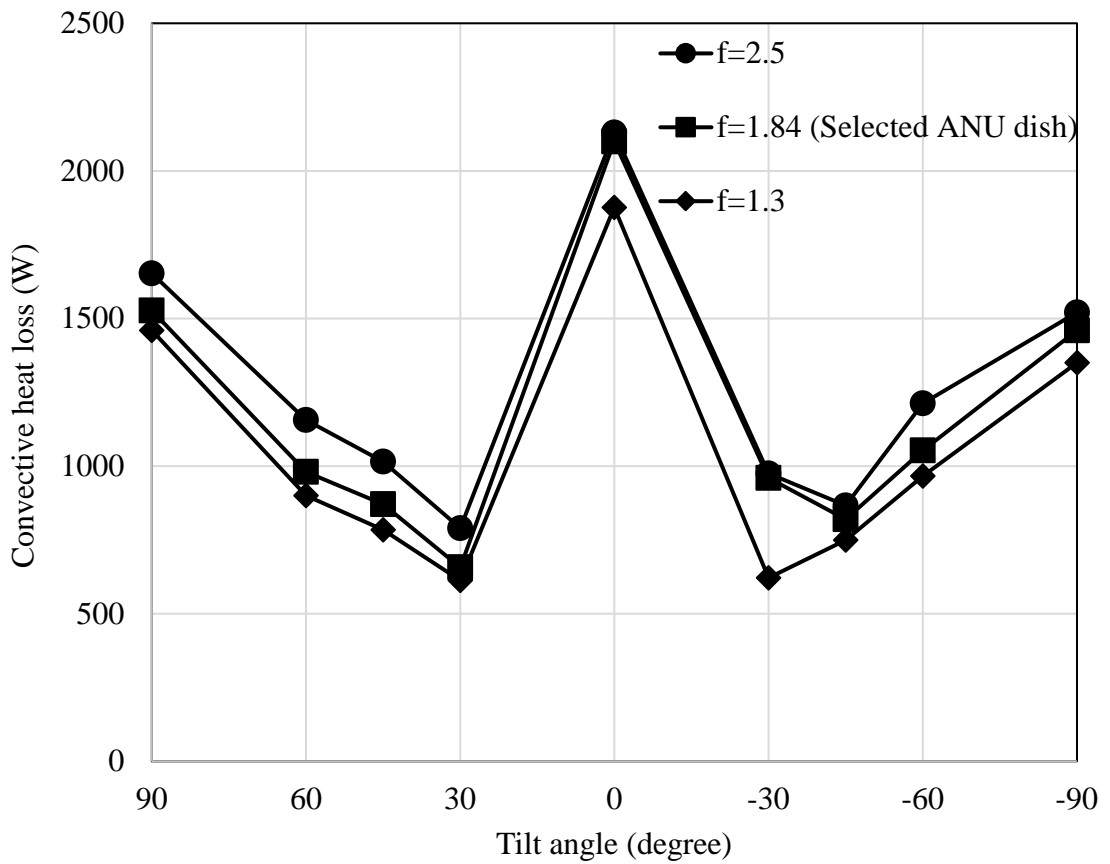


Figure 45: Convective heat loss from the cavity receiver with different focal lengths

The results show a slightly lower heat loss from the three dishes described in Chapter 2, over a range of tilt angles. It is clear from the Figure 46 that the deep dish provides a slightly greater sheltering effect on the receiver due to their shorter focal length.

Due to the sheltering effect of the deep dish on the receiver, the local air velocity near the cavity receiver was lower than the free stream air velocity. The reduction in the local air velocity prevented the heat loss from the receiver. Whereas, the heat loss from the shallow dish was observed to be maximum in all cases due to the location of the cavity receiver in the region of highest free air stream velocity.

Despite this observation, it is important to note that the heat loss from the receiver varies more with tilt angle than it does with focal length (or dish depth). So, it can be concluded that the heat loss is a stronger function of tilt angle rather than focal length, and in essence, the heat loss due to variation of this are negligible.

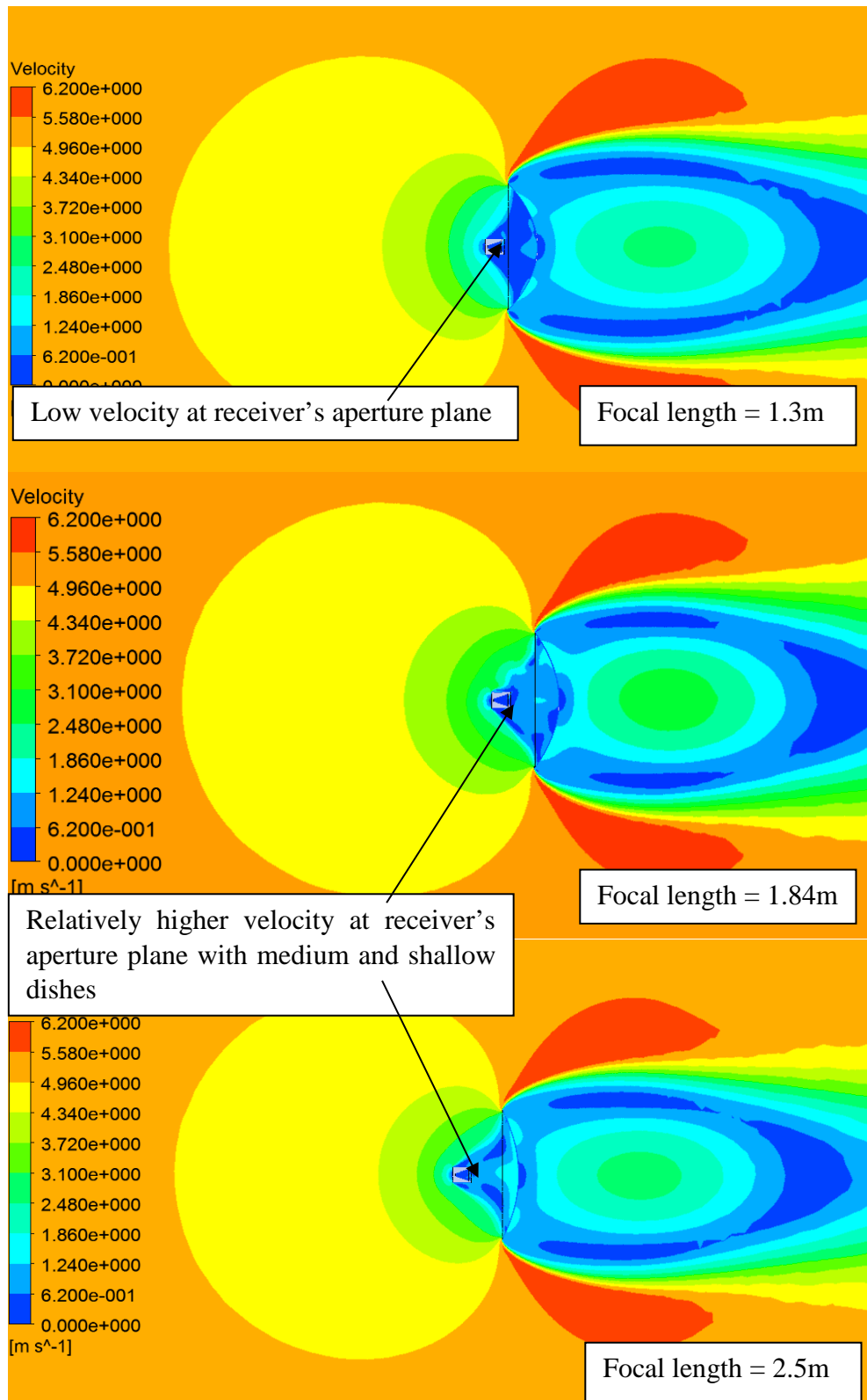


Figure 46: Velocity contour around different dishes at 90° tilt angle

3.4 Chapter Summary

In this chapter, convection heat losses from the receiver were numerically examined with no-wind condition and a 5 m/s wind condition. The numerical results were in agreement with previously published natural convection studies. From the results, it is clear that with a no-wind condition the natural convection heat loss is dependent on the tilt angle of the dish. Natural convection heat loss was reduced as the orientation of the cavity receiver was changed from 90° to 0° tilt angles. The minimum heat loss was observed with 0° tilt angle.

With a wind velocity of 5 m/s, the results revealed a significant reduction in the convective heat loss from a cavity receiver in the presence of the dish structure at various tilt conditions. Similar to the natural convection, the convective heat loss showed a dependence on the tilt angle. However, the maximum convective loss was observed when the cavity receiver was facing straight downward. Based on results, it was seen that the presence of a dish has a significant effect on the heat loss from receivers.

The numerical study has shown a minor impact of shape of the dish on the convective heat loss from the receiver. Different flow behaviours around the receiver were observed around different types of dishes. However, the convective heat loss was slightly different from the receiver using shallow dish, though this was not significant. In all cases, the heat loss from the receiver showed a great dependency on the tilt angle rather than the positioning of the receiver.

In the presence of the dish, for tilt angles between +/-30° and 0°, the receiver was mostly located in the free stream wind and the results demonstrated a significant reduction in convective heat loss from most of the tilt angle. The reduction in the heat loss emphasises the need to consider the dish structure in the flow field to determine the convective heat loss from the receiver.

Chapter 4: Effect of wind and dish orientation on convective heat loss

The results in previous chapters have indicated that the dish structure significantly affects the local air speed near the receiver, and hence the heat loss. This is because the convective heat loss from the cavity receiver is influenced by the local air velocity around the cavity receiver and the amount of air entering and leaving the cavity. The local velocity patterns generate recirculation and stagnation zones near and inside the cavity, which ultimately impact the heat loss in the presence of the dish. That said, the previous chapters have only dealt with the variation in heat loss with tilt angle for a single wind speed and direction. However, there is also a need to investigate the effect of the wind speed and angle of attack under these conditions to develop a fuller understanding of their effect on the heat losses from the dish-receiver system.

4.1 Convective heat loss from cavity receiver

As the dish system operates on a 2-axis tracking system the wind can approach the dish/receiver from any direction. Therefore, to model the wind from all directions (0° to 360°), steady state simulations were performed while varying: (i) tilt angle (θ) and (ii) wind incidence angle (φ), as shown in Figure 47 and Figure 48 respectively.

For this study, the tilt angle was varied from -90° to 90° , where 0° represents the dish facing vertically upwards, and $\pm 90^\circ$ represent the dish system facing in a horizontal attitude. Hence, when the wind movement is parallel to the aperture plane of the dish/receiver, the wind incidence angle is 0° .

The range of wind incidence angles (φ) was from -90° (the wind impinging directly on the back side of dish) to 90° (the wind directly striking the reflective surface of the dish structure).

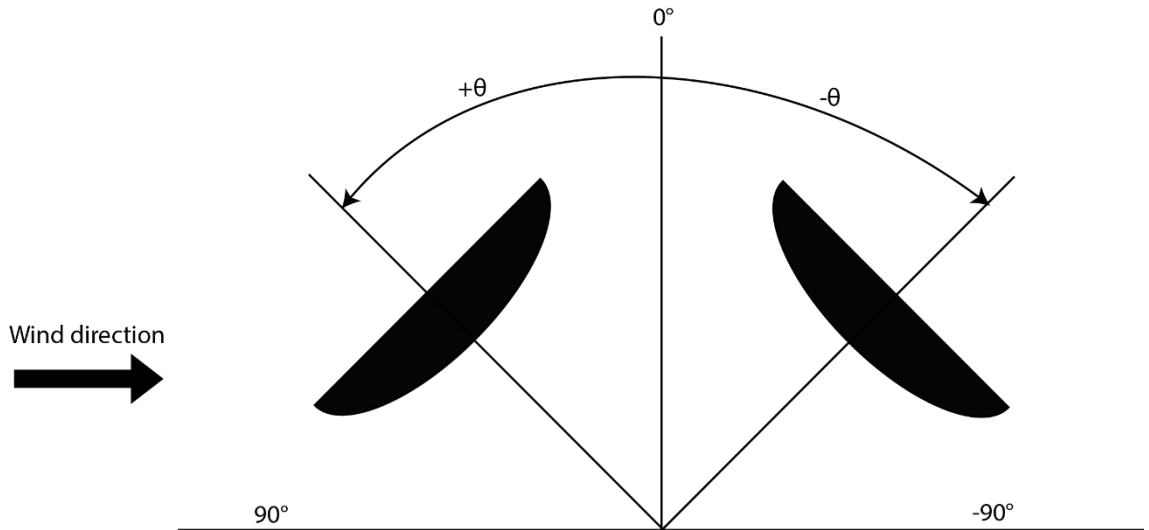


Figure 47: Definition of tilt angle (θ)

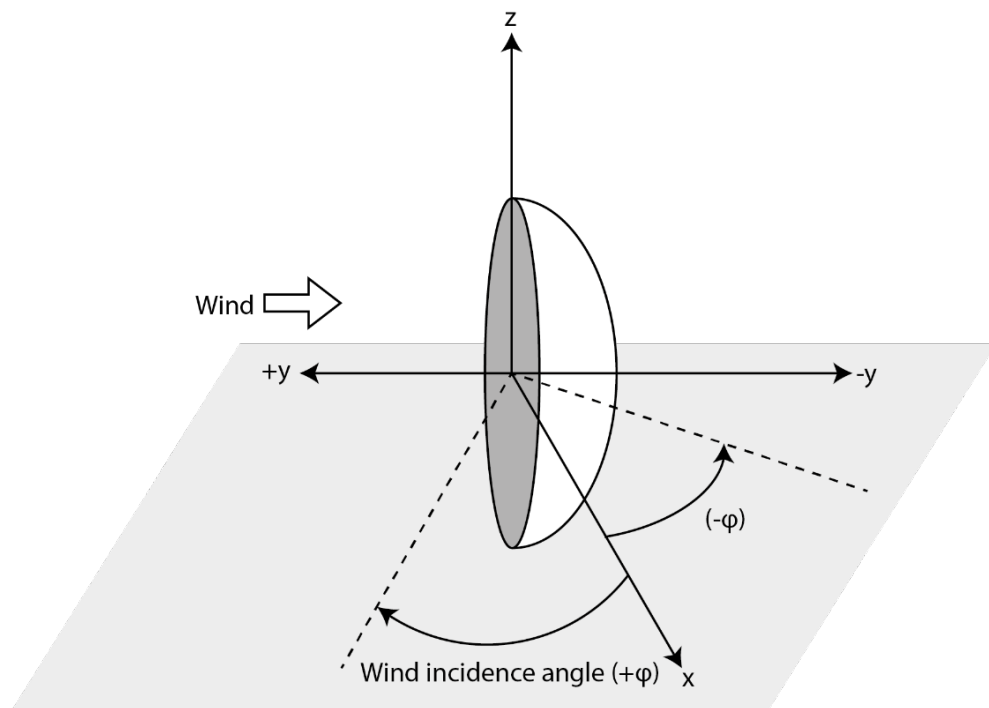


Figure 48: Orientation of dish-receiver system

As discussed, the angle of attack of wind can vary from 0° to 360° , but due to the symmetrical structure of the dish and cavity about a vertical axis, the range of wind incidence angles (φ) only needs to be varied from -90° to 90° . Similarly, due to flow

parallel to the aperture plane of dish, the flow showed symmetrical behaviour for positive and negative tilt angles, so only the positive tilt angles were considered. In this sense, a full range of incidence angles (positive and negative), with a wind velocity range of 0-20 m/s and tilt angles ranging from 0° to 90° were evaluated.

4.2 Effect of wind incidence on heat loss:

4.2.1 Wind flow parallel to the aperture plane (zero incidence angle)

In the case of parallel or side-on wind flow conditions, the bulk flow is parallel to the receiver opening, meaning the dish structure does not affect the local air flow around the receiver for higher wind speeds nor the heat transfer as shown in Figure 49. At speeds greater than 3 m/s, the convective heat loss values converge, implying a transition from forced convection to natural convection. For tilt angles between 90° and 45° at lower speeds, a reduction in heat loss was observed due to fact that there was insufficient air movement to carry away the heat from the inside of the cavity receiver

For higher wind velocities, greater than 3 m/s, the difference in the heat loss from the receiver at different tilt angles was negligible due to the dominance of forced convection. From this, it can be concluded that the receiver tilt angle has an almost negligible effect on convective heat loss for wind flow parallel to the aperture plane.

However, what is interesting to note was the initial decrease in heat loss that occurred at very low wind speeds. This suggests that at low wind speeds the wind acted as an air curtain that suppressed convective losses from the receiver.

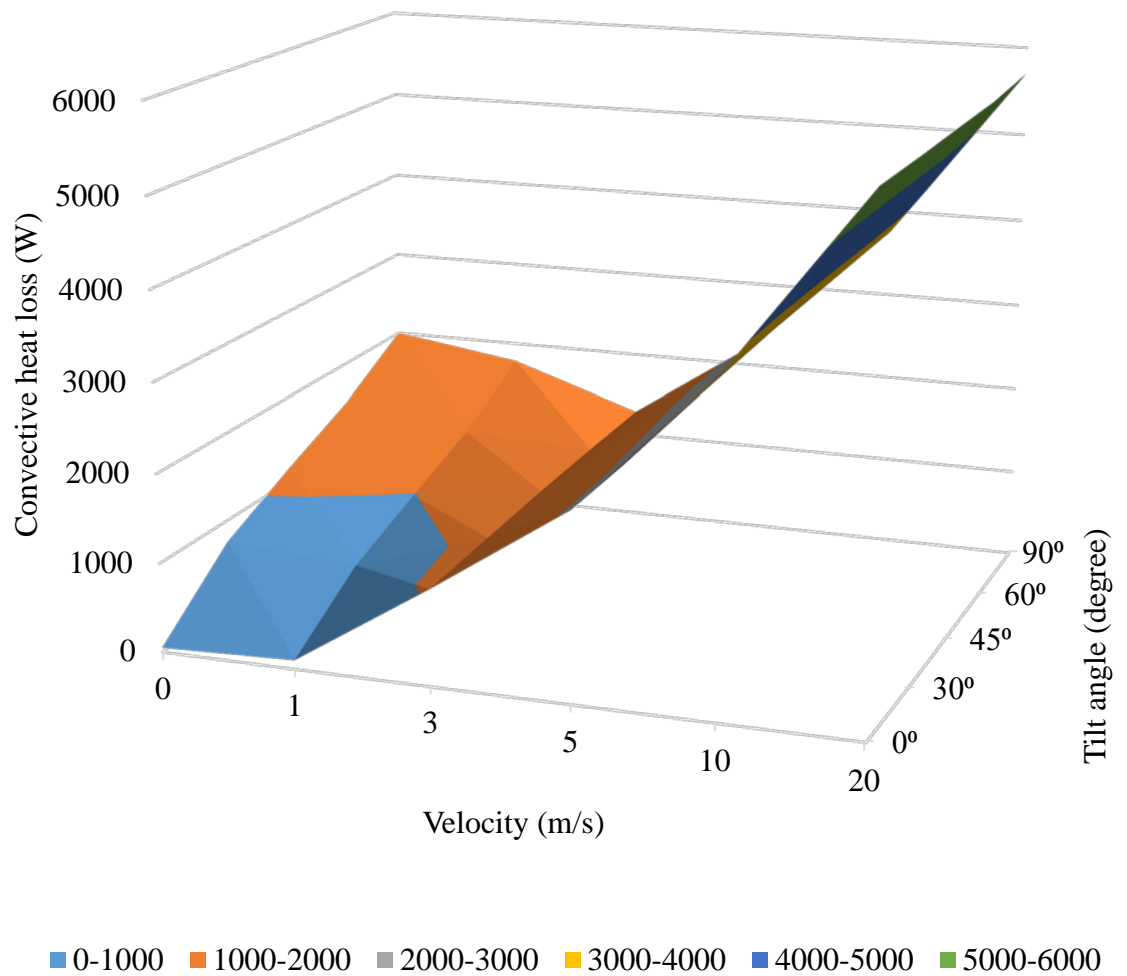


Figure 49: Parallel flow to the cavity aperture plane ($\varphi = 0^\circ$)

4.2.2 Wind flow from the front of the dish (positive incidence angles)

In the previous chapters, for the case where the wind approaches the reflective (front) surface of the dish ($\varphi = 90^\circ$), the flow patterns around the receiver were shown to be greatly affected by changing the dish's tilt.

Exploring this, Figure 50 shows the heat loss for the condition of wind impinging on the front surface of the dish ($\varphi = 90^\circ$). Similar to Figure 49, the impact of the dish on heat loss was negligible at low velocities (Figure 50) though it can be seen that, as the wind speed increases above 3 m/s, the magnitude of the heat loss is significantly lower than those

observed in Figure 49. This was due to the dish structure providing an impediment to the flow, thus creating a region of stagnant, low-velocity air near the cavity receiver (as shown in Figure 51). The stagnation region generated by the dish reduced the convective heat losses relative to those where the receiver was exposed to free stream wind alone, as is the case for a tilt angle of zero degree.

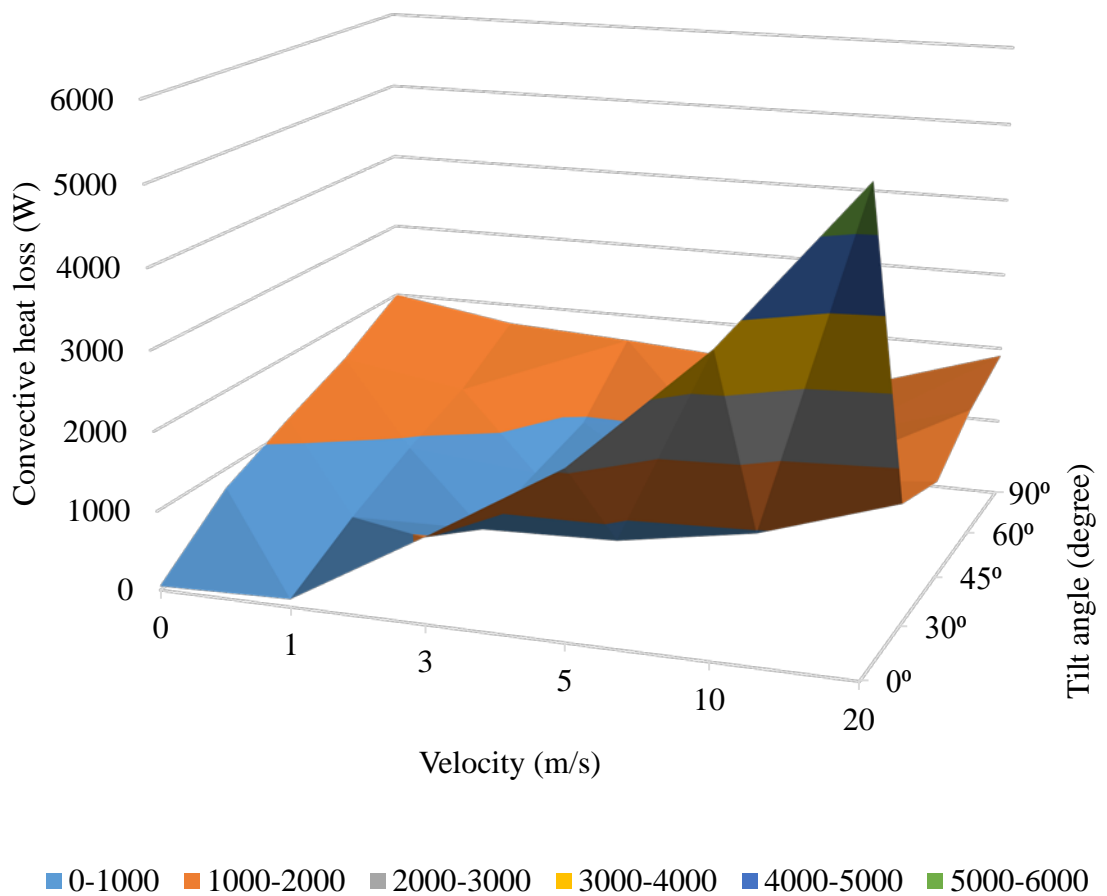


Figure 50: Flow impinging directly on the reflective (front) surface of the dish ($\varphi = 90^\circ$)

At higher velocities, the dish causes a very low velocity zone near the receiver, relative to the free stream wind velocity. As such, for positive dish tilt angles from 90° to 30° , the

local velocity was observed to be predominately parallel to the receiver aperture plane (Figure 51), therefore yielding greater convective heat transfer.

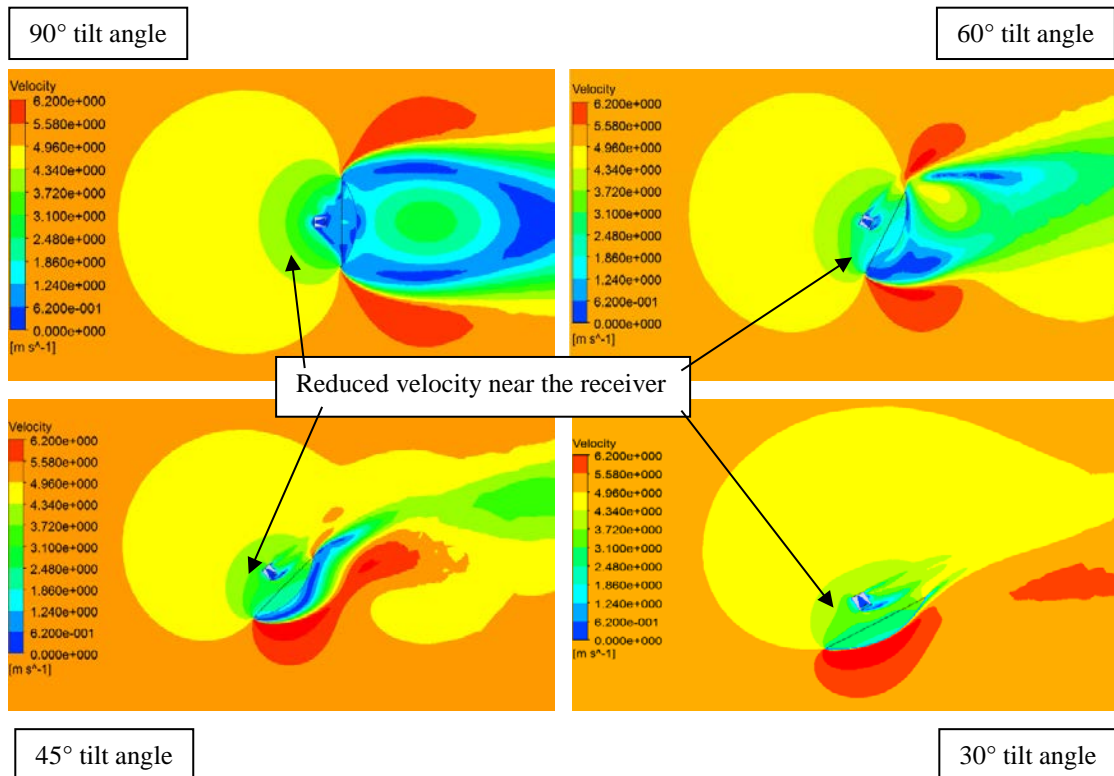


Figure 51: Effect of the dish on the velocities near the receiver at 5 m/s

Expanding on this point, Figure 52 shows the receiver temperature contours for a tilt angle of 45° and various wind speeds. It can be seen that, at 3 m/s, the air temperature inside the receiver was at a higher than 1 m/s and then decreased at higher wind velocities; this suggests a greater exchange of air from the ambient and higher heat loss from the receiver. In this range of tilt angles the dish acted as a blockage and slowed the air motion around the receiver. However as the angle was reduced further in the range of 30° to 0°, the blockage was less pronounced, and the flow over the dish became more uniform with no major flow separation (Figure 53). Under these conditions, the receiver location is such that the shape of the dish has less impact on the local flow around it, and so as the wind speed increases the magnitude of the convective heat losses also increases.

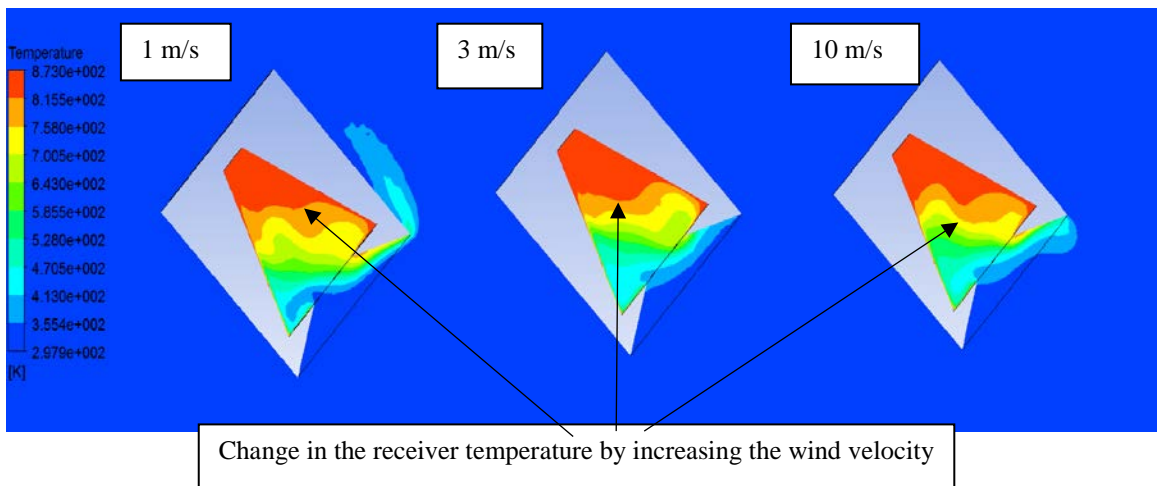


Figure 52: Temperature profile at 45° tilt angle at different wind speeds

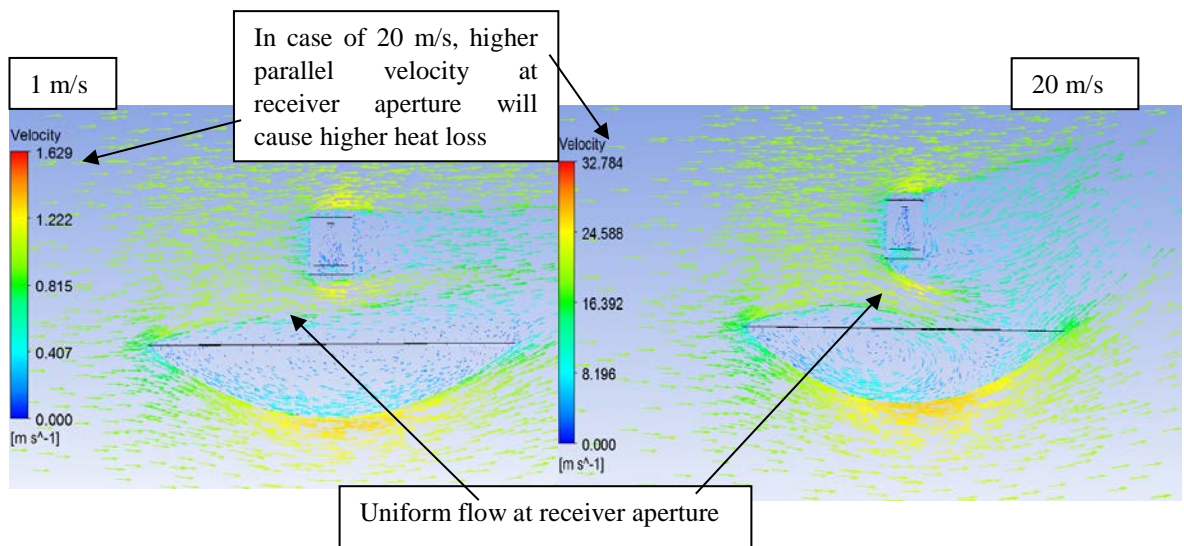


Figure 53: Velocity vectors at receiver aperture for 0° tilt angle

4.2.3 Wind flow from the back of the dish (negative incidence angles)

For the condition of wind impinging on the back surface of the dish ($\varphi = -90^\circ$), Figure 54 illustrates the heat losses. From this it should be noted that with a 0° tilt, the heat loss values were identical to those seen in parallel flow (Figure 49) because the dish had no effect on the air flow around the receiver.

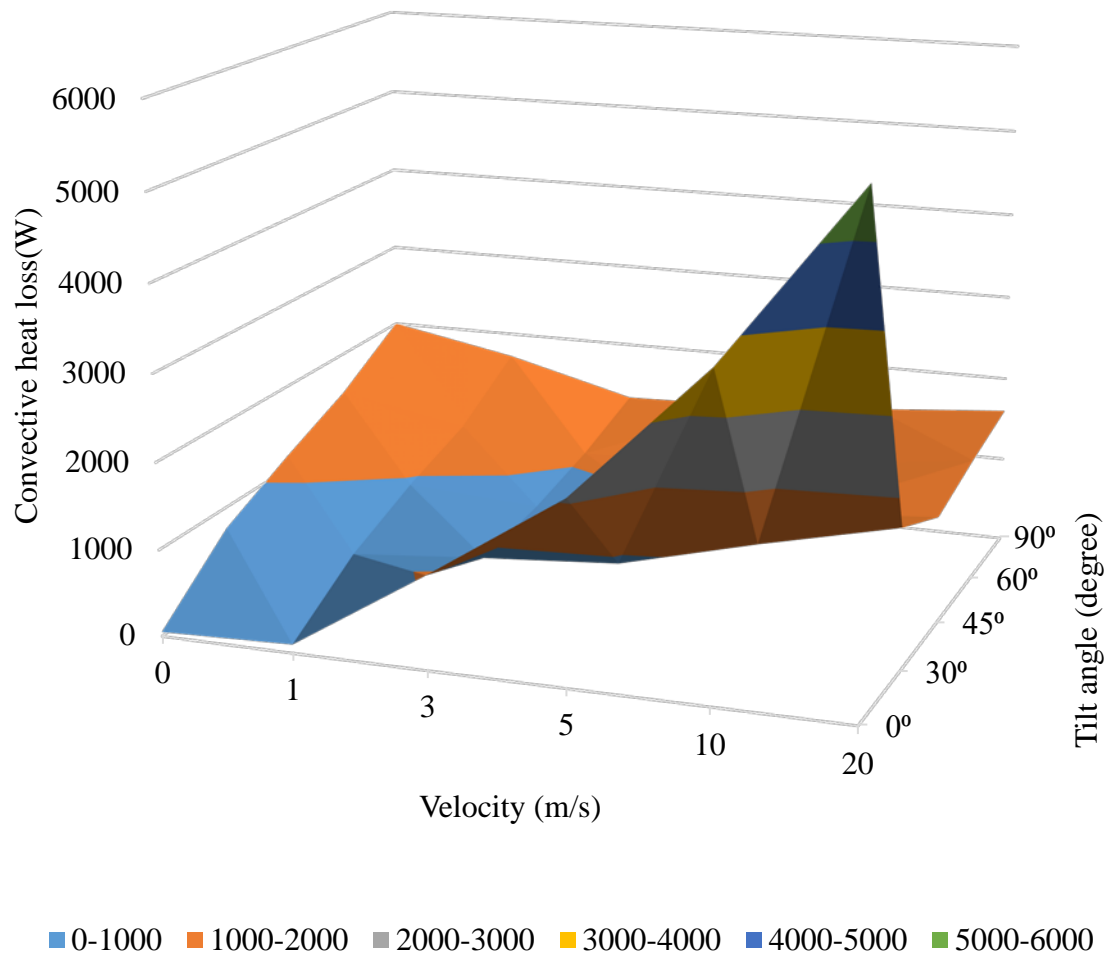


Figure 54: Flow impinging on the rear of the dish ($\phi = -90^\circ$)

However, when the wind does impinge on the dish's rear surface, the dish constitutes a bluff body, where the receiver is positioned in the wake of the dish as shown in Figure 55. Comparing these results to those in Figure 50, the heat loss trends were similar to those with the wind impinging on the front face. At low wind speeds the heat loss for all tilt angles converge towards the natural convection values. In both cases, the dish caused a stagnation zone around the receiver. It would seem that whether the receiver was in the wake, or the stagnation zone, the effect of wind speed on the magnitude of the convective heat loss was surprisingly similar.

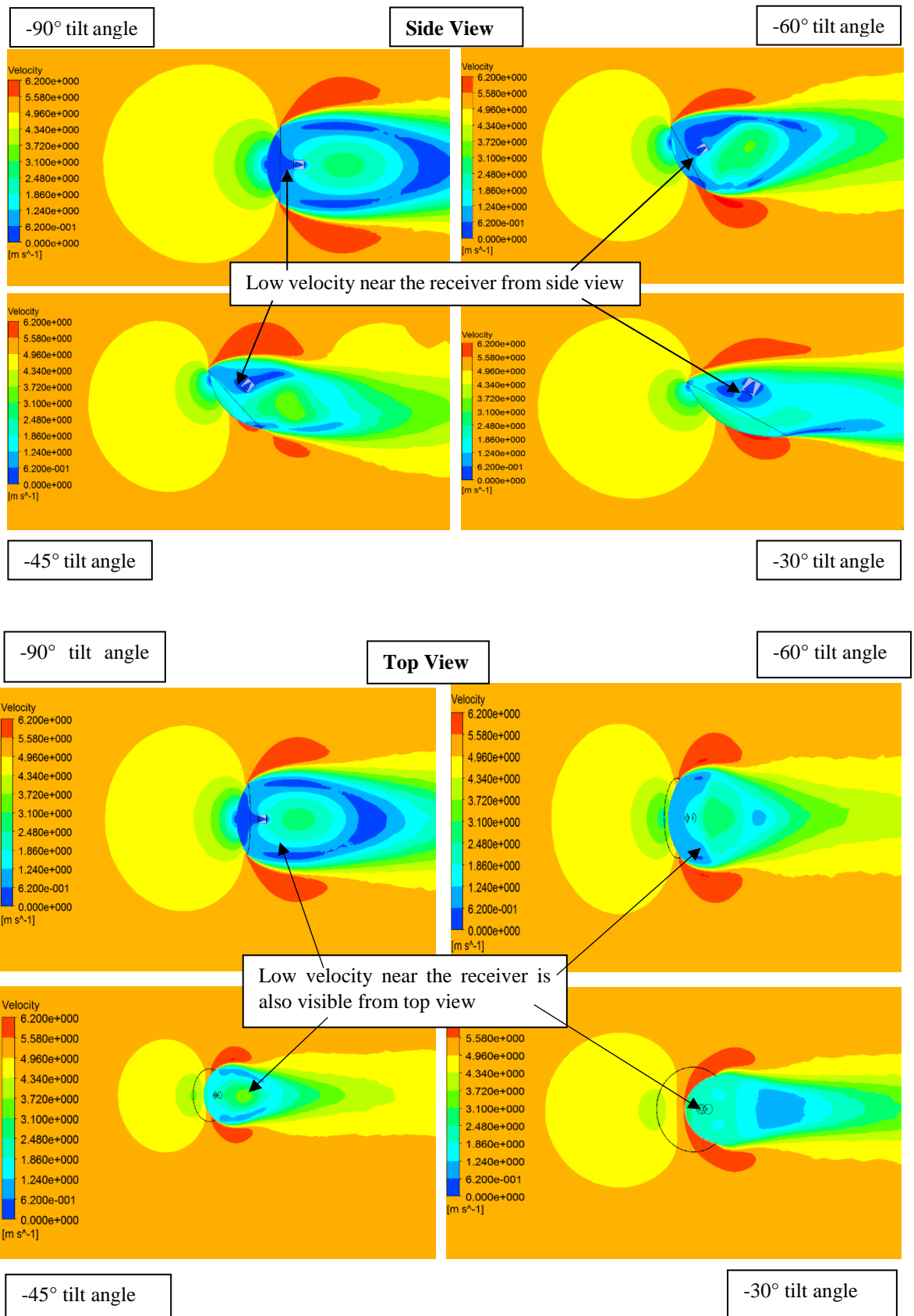


Figure 55: Effect of the dish on the velocities near the receiver at 5 m/s

4.3 Effect of tilt on heat loss

In order to better understand the effect of the tilt, the data can also be viewed with tilt as the independent variable. For any given wind speed and wind incidence angle, the effects of receiver tilt angles are shown in Figures 56-64.

From Figure 56 at a wind speed of 1 m/s, it is clear that the convective heat loss from the cavity receiver was less than that of natural convection for any tilt angle, as noted previously. These heat losses were observed to decrease as the tilt angle moved from $\theta=0^\circ$ (facing vertically downward) to $\theta=90^\circ$ (facing horizontally).

At 1 m/s, the heat losses were below those from natural convection (with no-wind condition as discussed in Section 3.1) at all operating conditions due to the suppression of hot air escaping from the cavity as shown in Figure 57. By changing the tilt orientation from 90° to 0° , there is a less scope for the air to sweep away the hot air, which affects the heat losses from the receiver (Figure 58).

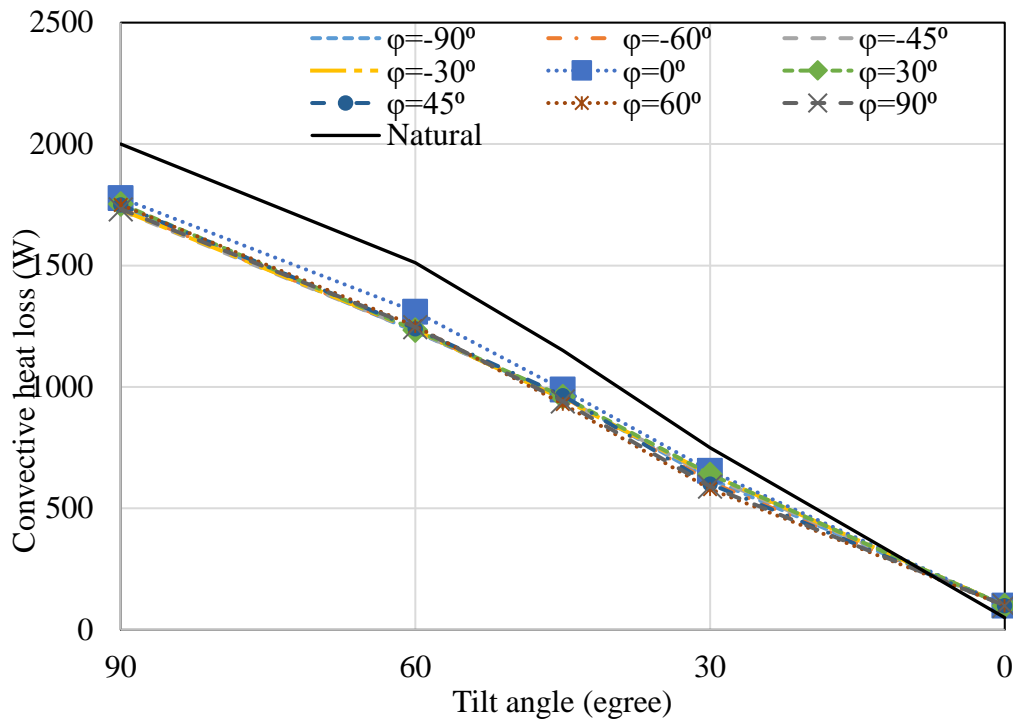


Figure 56: Convective heat loss as a function of tilt angle at $V=1$ m/s

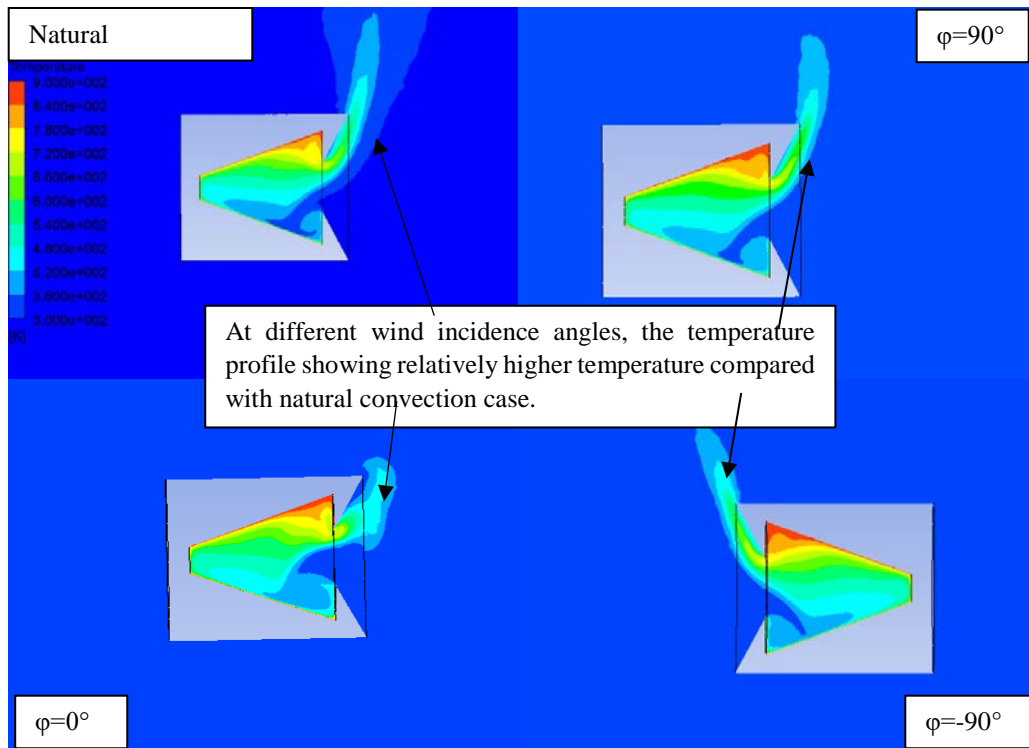


Figure 57: Temperature contours at different wind incidence angles with a wind velocity of 1 m/s at 90° tilt angle

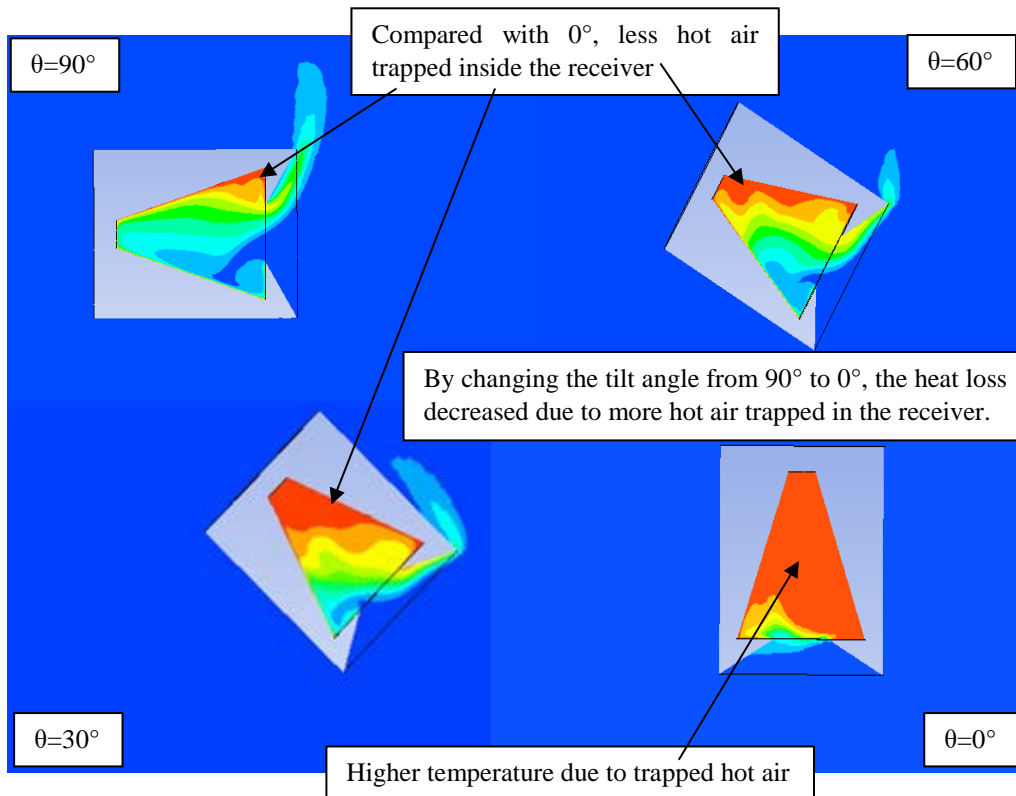


Figure 58: Temperature contours at different tilt angles with a wind velocity of 1 m/s at 0° wind incidence angle

Figure 59 shows that by increasing the velocity to 3 m/s, at a positive angle of incidence (ϕ), that the convective loss values decreased between 90° and 30° tilt angles but increased at 0° tilt angle for all wind angles except at $\phi=0^\circ$ (parallel to the aperture plane). For the case of flow parallel to aperture plane, the heat loss was at a maximum due to the negligible effect of the dish, as discussed in Section 5.2.1, while, for a negative ϕ , the dish structure provided a blockage to free stream (Figure 60), hence the heat loss was lower.

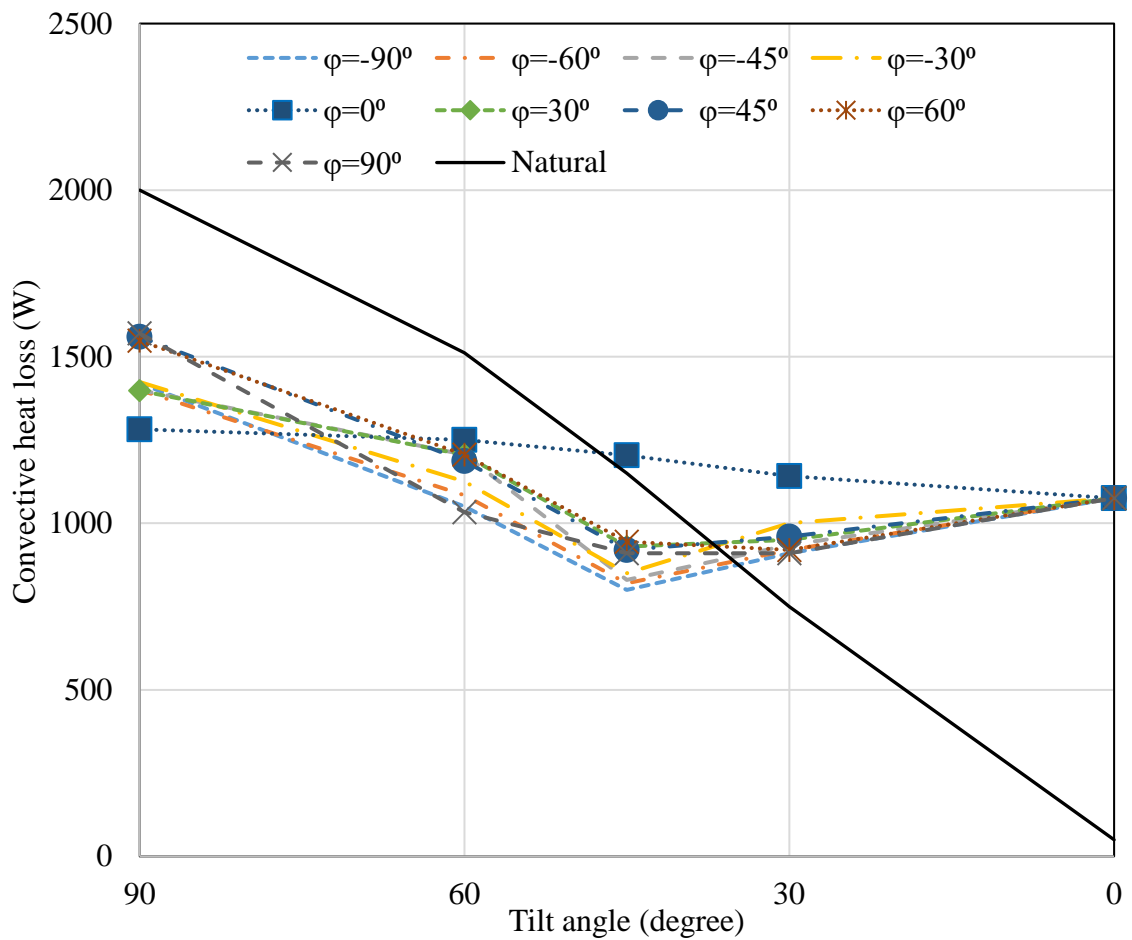


Figure 59: Convective heat loss as a function of tilt angle at $V=3$ m/s

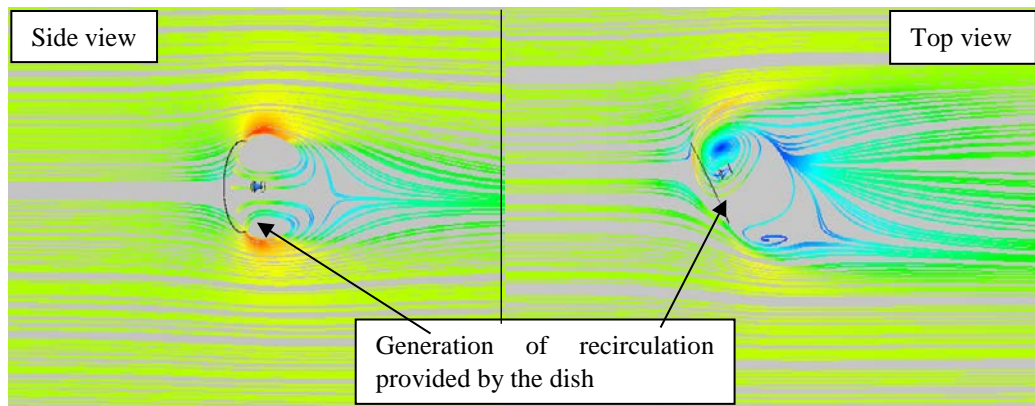


Figure 60: Streamlines showing the recirculation provided by the dish at $\phi=-60^\circ$

As with wind speeds of 1 m/s and 3 m/s, at 5 m/s and 10 m/s the convective heat loss decreased from the 90° to 30° tilt angle. However it is interesting to note that there was a drastic increase in heat loss at a zero degree tilt angle as shown in Figure 61 and Figure 62. This can be attributed to the fact that for this operating condition the wind is parallel to the receiver's aperture (Figure 63), which as has been seen previously, leads to a higher heat loss.

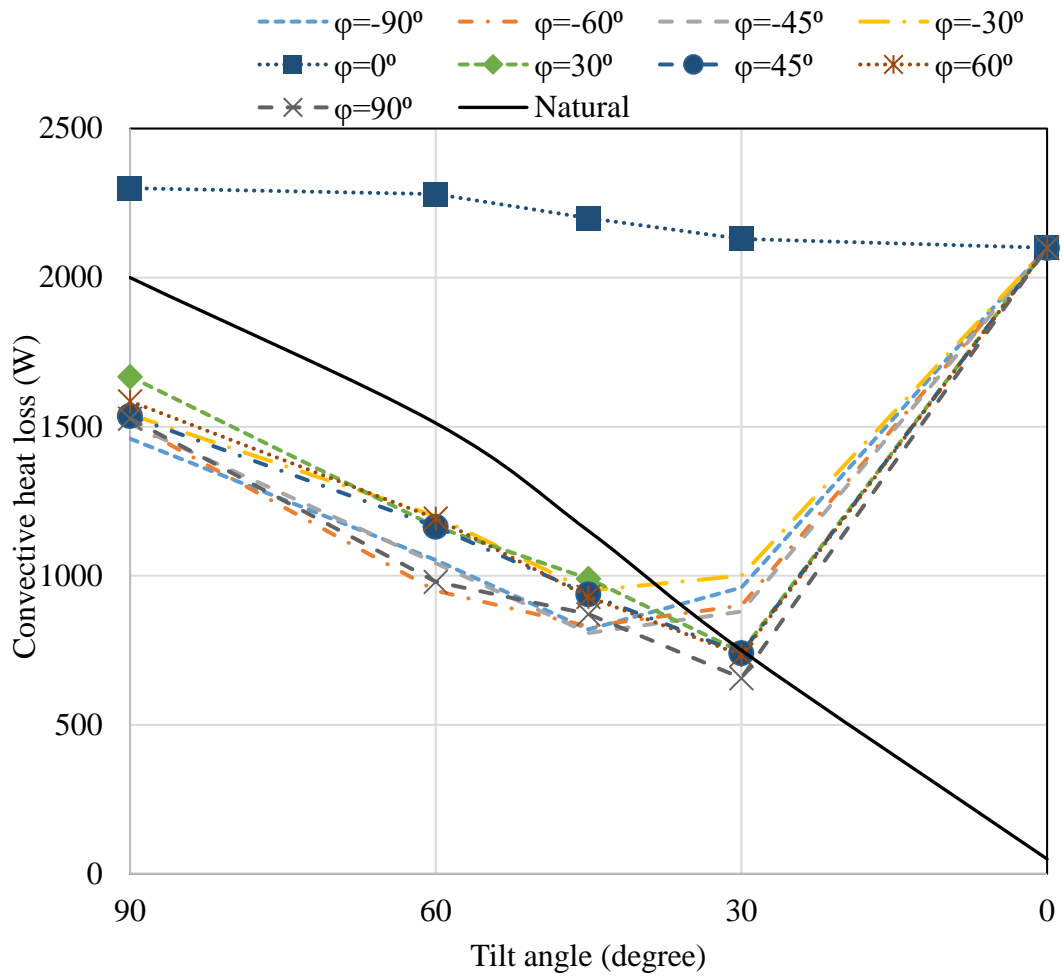


Figure 61: Convective heat loss as a function of tilt angle at $V=5$ m/s

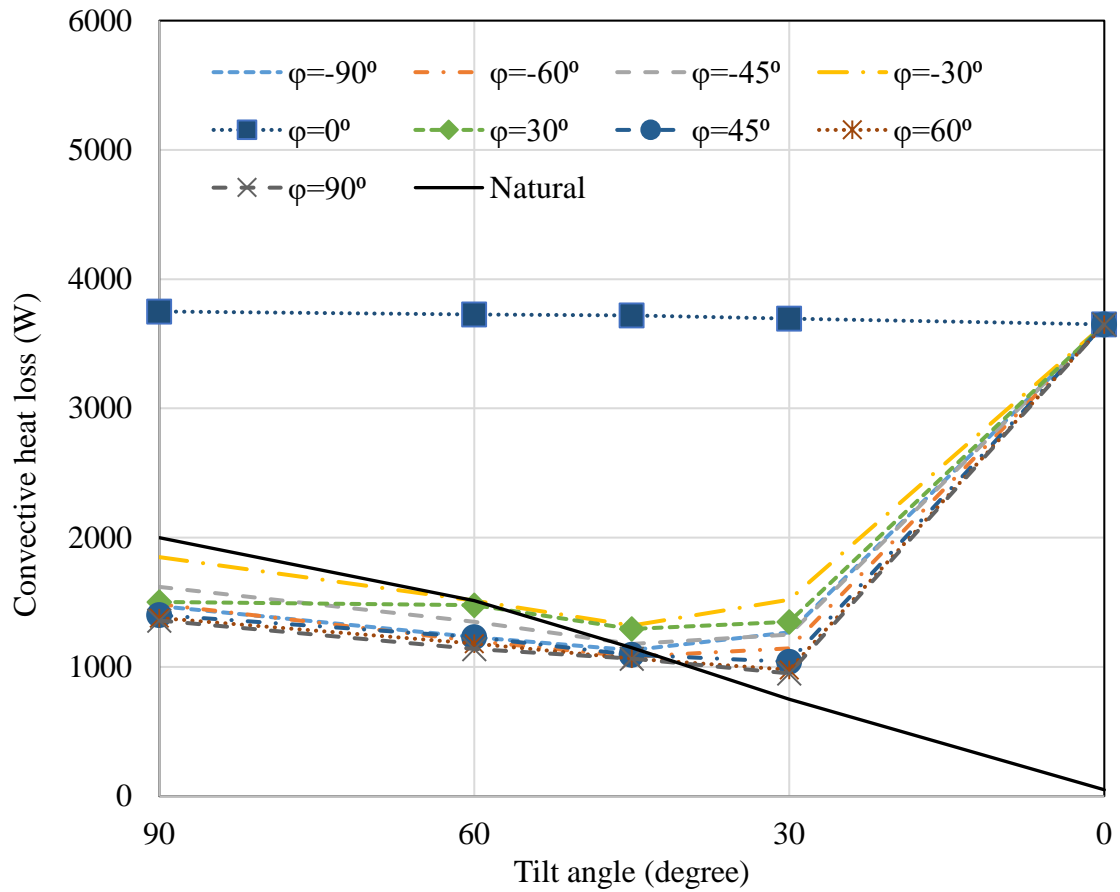


Figure 62: Convective heat loss as a function of tilt angle at $V=10$ m/s

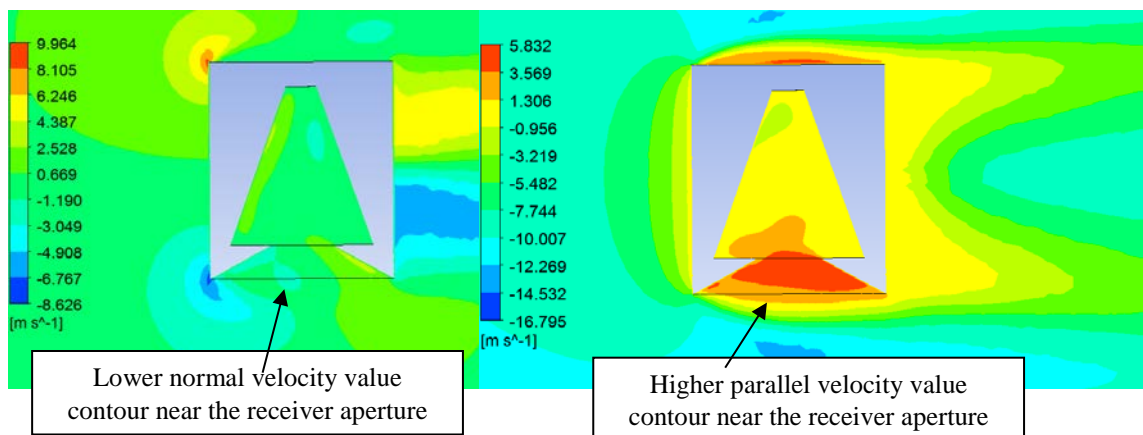


Figure 63: Normal and parallel velocity contour at receiver aperture at 10 m/s

Moving on from this, Figure 64 shows the heat loss from the receiver at 20 m/s. Heat losses were observed to be relatively less when the receiver was in the wake region of the dish. At this speed, the flow passes the dish at very high velocity resulting in a very low velocity zone near the receiver. Due to the creation of stagnation zone heat loss from the receiver increases (Figure 65).

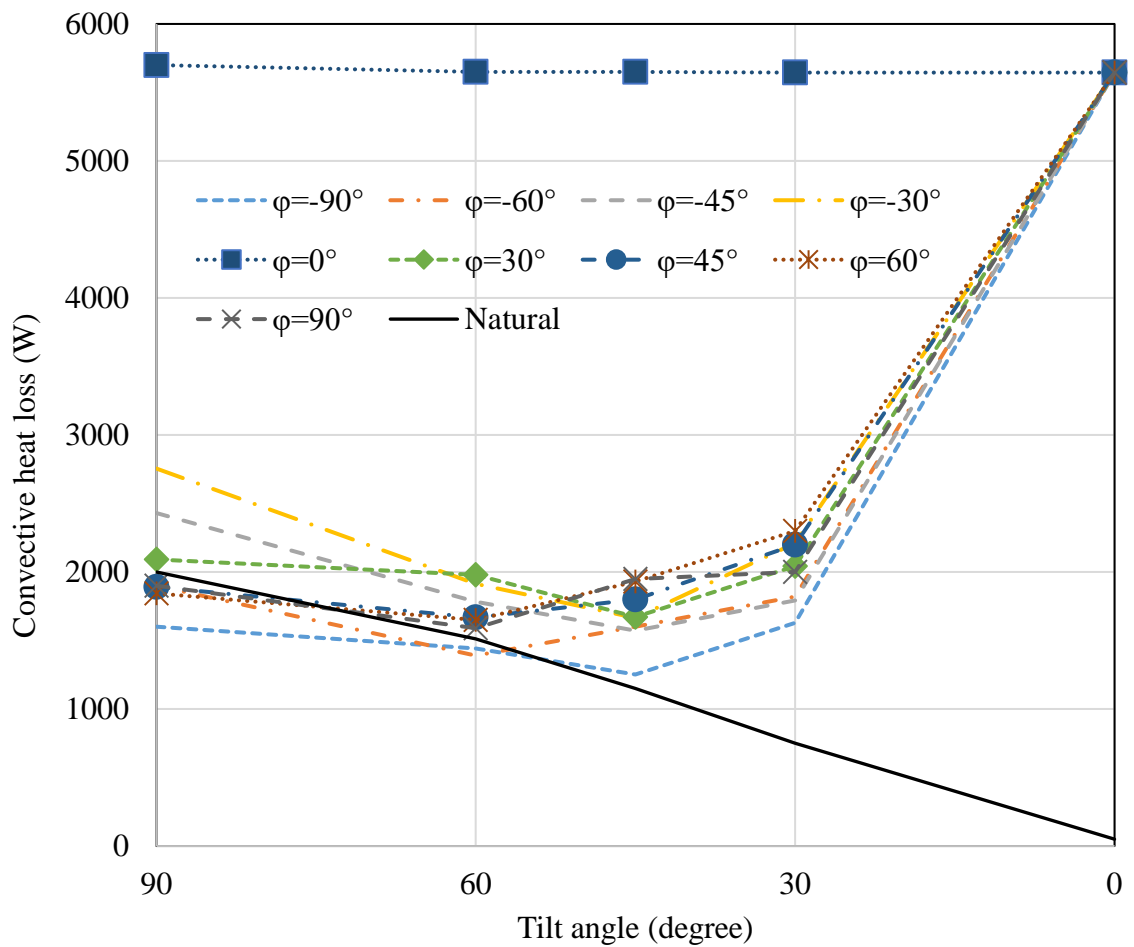


Figure 64: Convective heat loss as a function of tilt angle at $V=20$ m/s

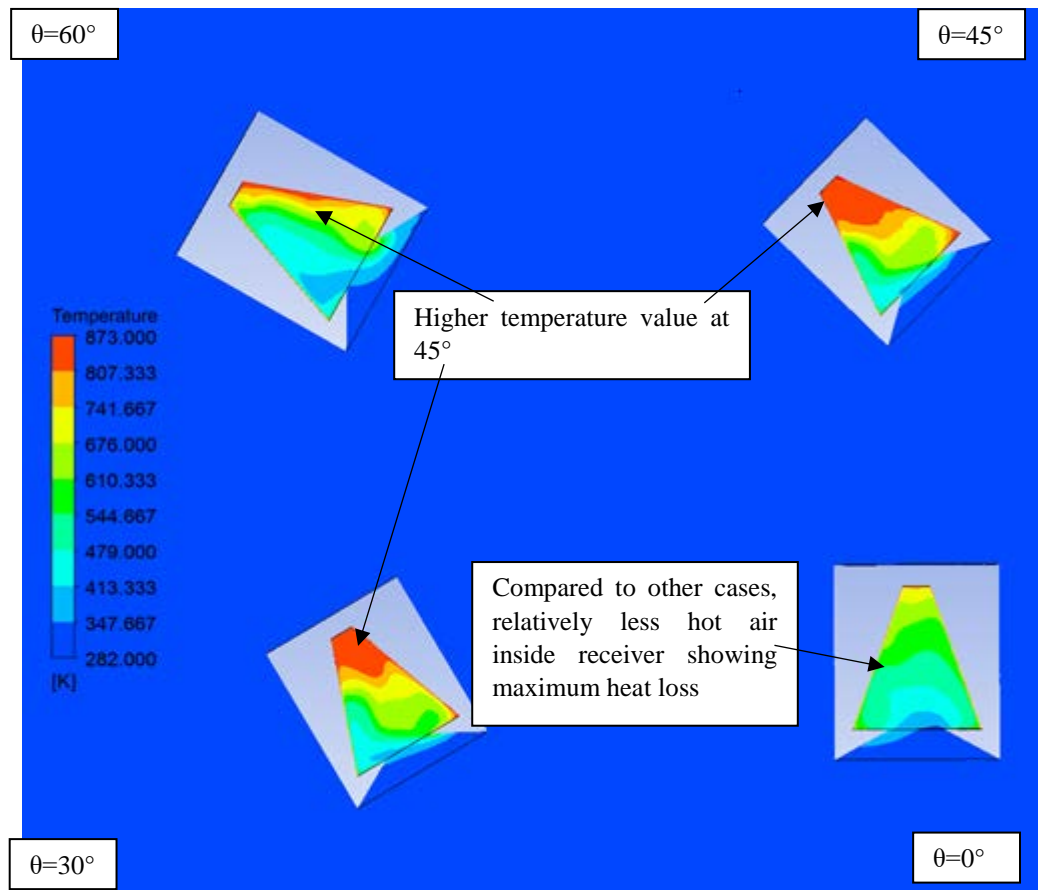


Figure 65: Temperature contours inside receiver at 20 m/s with positive wind incidence angle

From the above observations, it can be concluded that the dish structure affects the heat loss from the cavity receiver in most of the dish orientations except for tilt angles ranging from 30° to 0° . From 90° to 45° tilt angles, at low wind speeds (up to 3 m/s), the heat loss was almost identical for all wind incidence angles except for $\varphi = 90^\circ$ and $\varphi = -90^\circ$. From 3 m/s to 10 m/s, the heat loss was less than natural convection except when the flow was at $\varphi = 0^\circ$. In these two cases, the dish was at a position where it affected the free stream wind speed and subsequently the heat loss. In the range of 30° to 0° tilt angles, the dish did not disturb the flow very much for positive wind incidence angles. As a result the wind removed more heat from the receiver and the heat loss was greater than natural convection for wind speeds of 3 m/s or above.

4.4 Effect of wind incidence on heat loss

For a clearer understanding, the heat loss from the receiver is presented with wind incidence angle as the independent variable in this section.

As mentioned earlier in Section 5.3, the heat loss was less than that experienced by natural convection in most cases. This is due to suppression of the convective plume, which tries to escape from the receiver at very low velocity (Figure 57). For the complete range of wind incidence angles (-90° to 90°), the heat loss from the receiver was observed the same for all the tilt angles, at wind velocity of 1 m/s (Figure 66). To illustrate this, Figures 67-68 show the temperature and velocity contour at 1 m/s. From these, similar temperature profiles at different wind incidence angles were obtained, as well similar velocity vectors at the receiver. So it can be concluded that there is no impact of the dish on the convective heat loss from the receiver at very low wind velocities. However, when the flow is parallel to the aperture plan ($\varphi=0^\circ$), there is slightly higher heat loss from the receiver due to the wind velocity parallel to the receiver aperture.

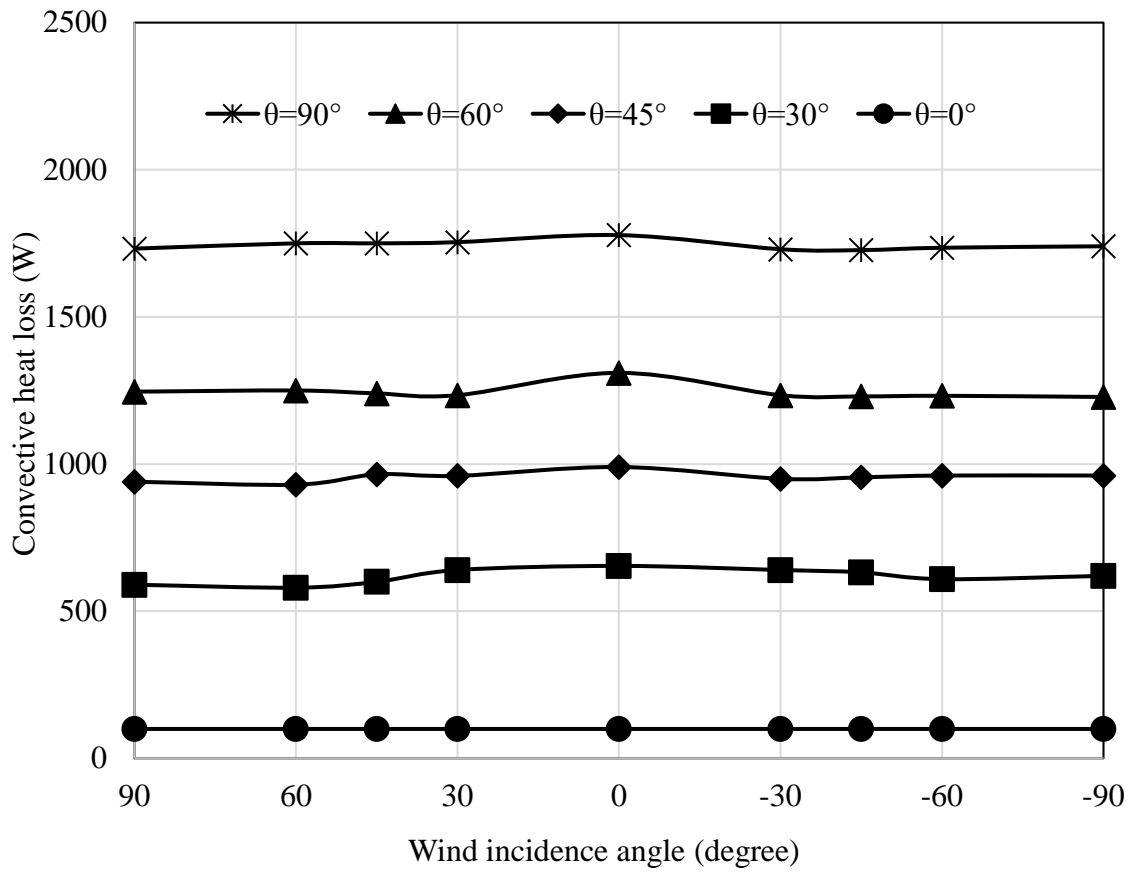


Figure 66: Convective heat loss as a function of wind incidence angle at $V=1\text{ m/s}$

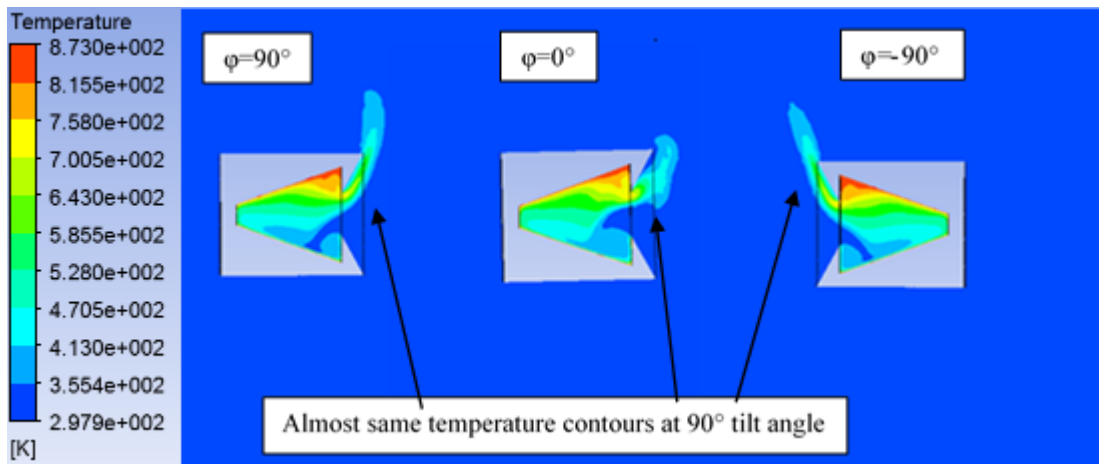


Figure 67: Temperature contours at receiver aperture with $V=1\text{ m/s}$

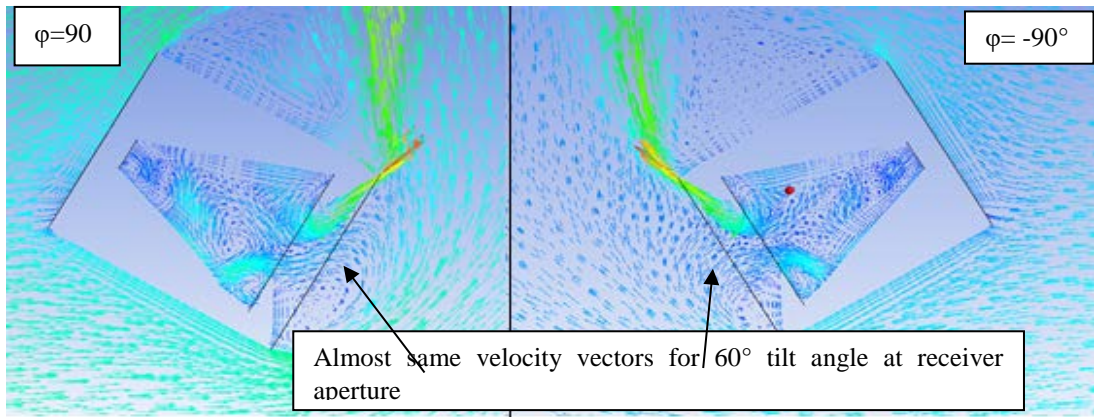


Figure 68: Velocity vector at receiver aperture with $V=1\text{ m/s}$

Compared with 1 m/s at 3 m/s, the heat loss shows a somewhat different behaviour at different tilt angles with changing wind incidence angles as shown in Figure 69. From this it can be seen that there is a small but noticeable impact of the dish on the convective heat loss. Also, it is clear that the heat loss from the receiver at 0° tilt angle is not affected by the dish structure irrespective of any wind incidence angle.

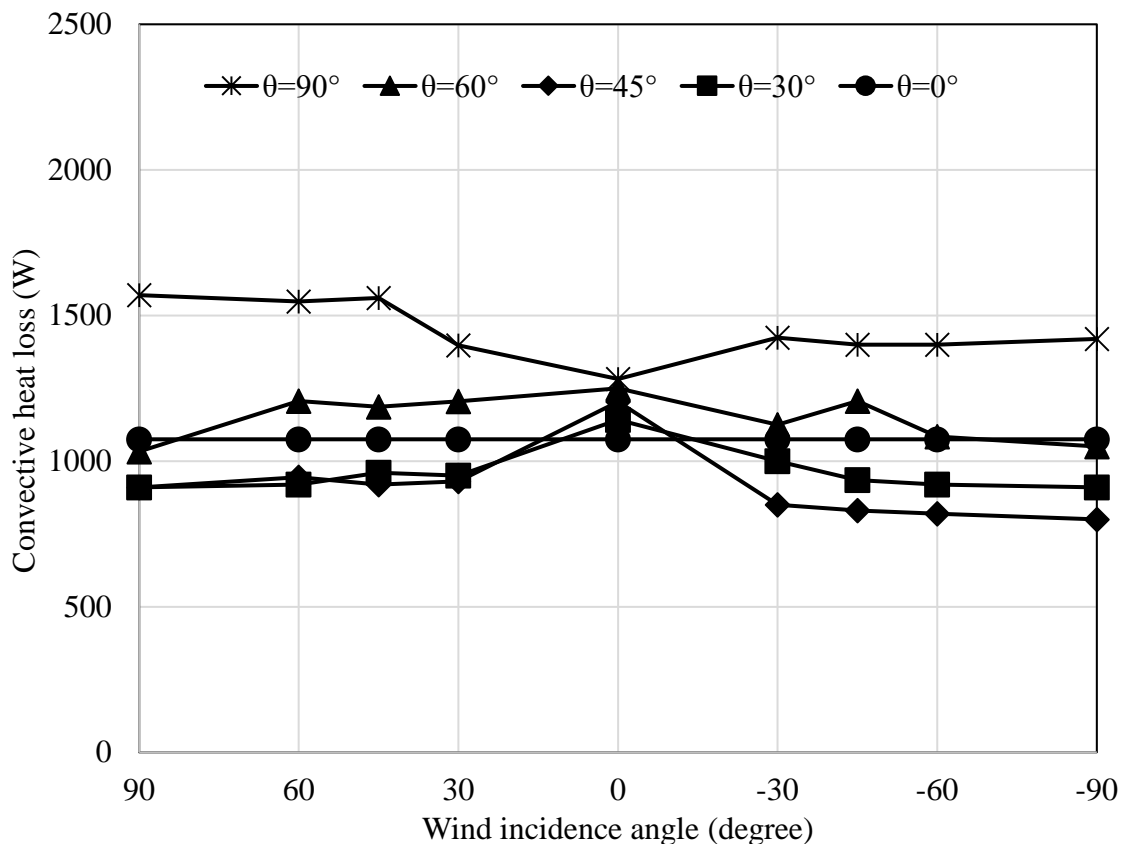
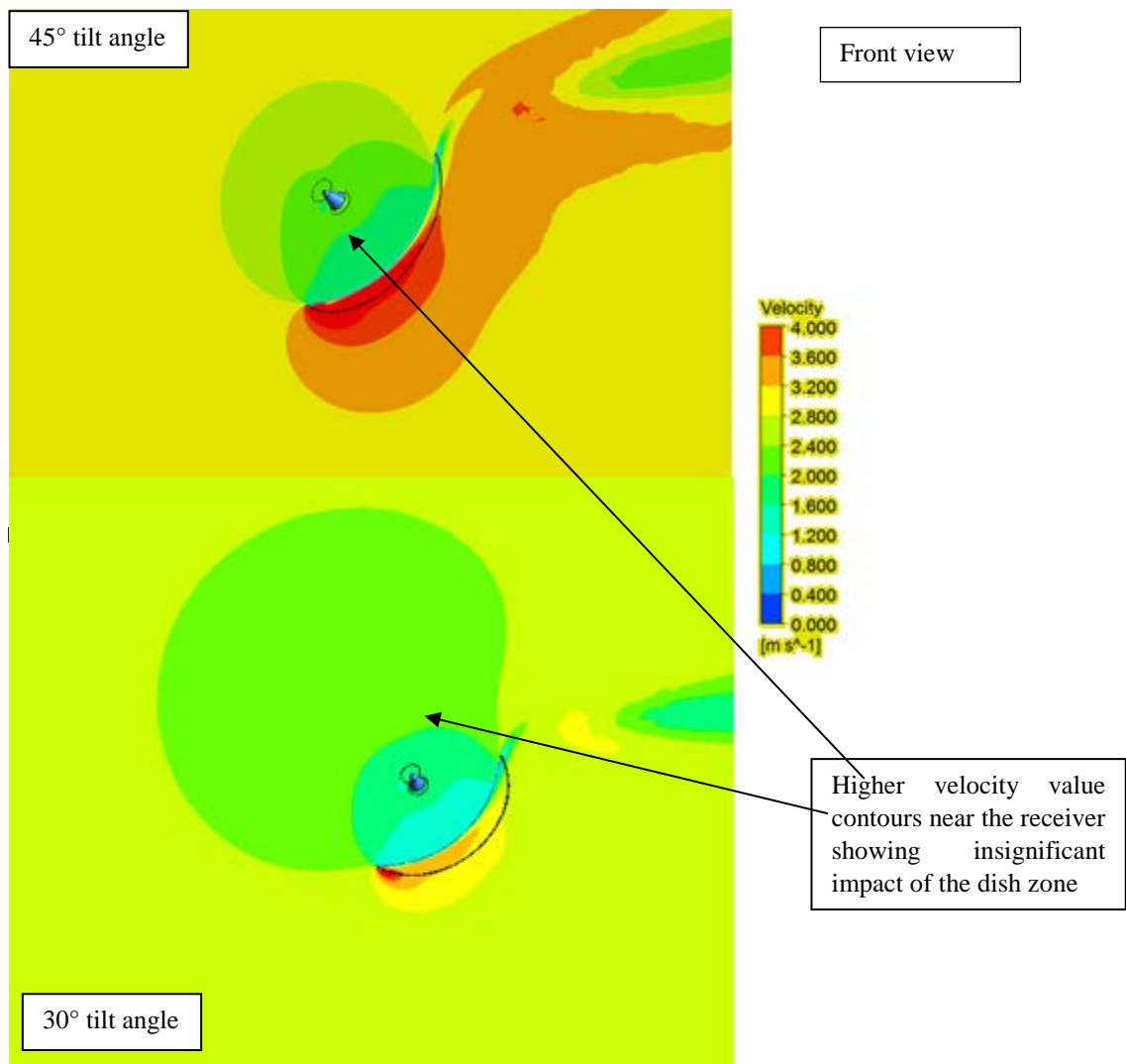
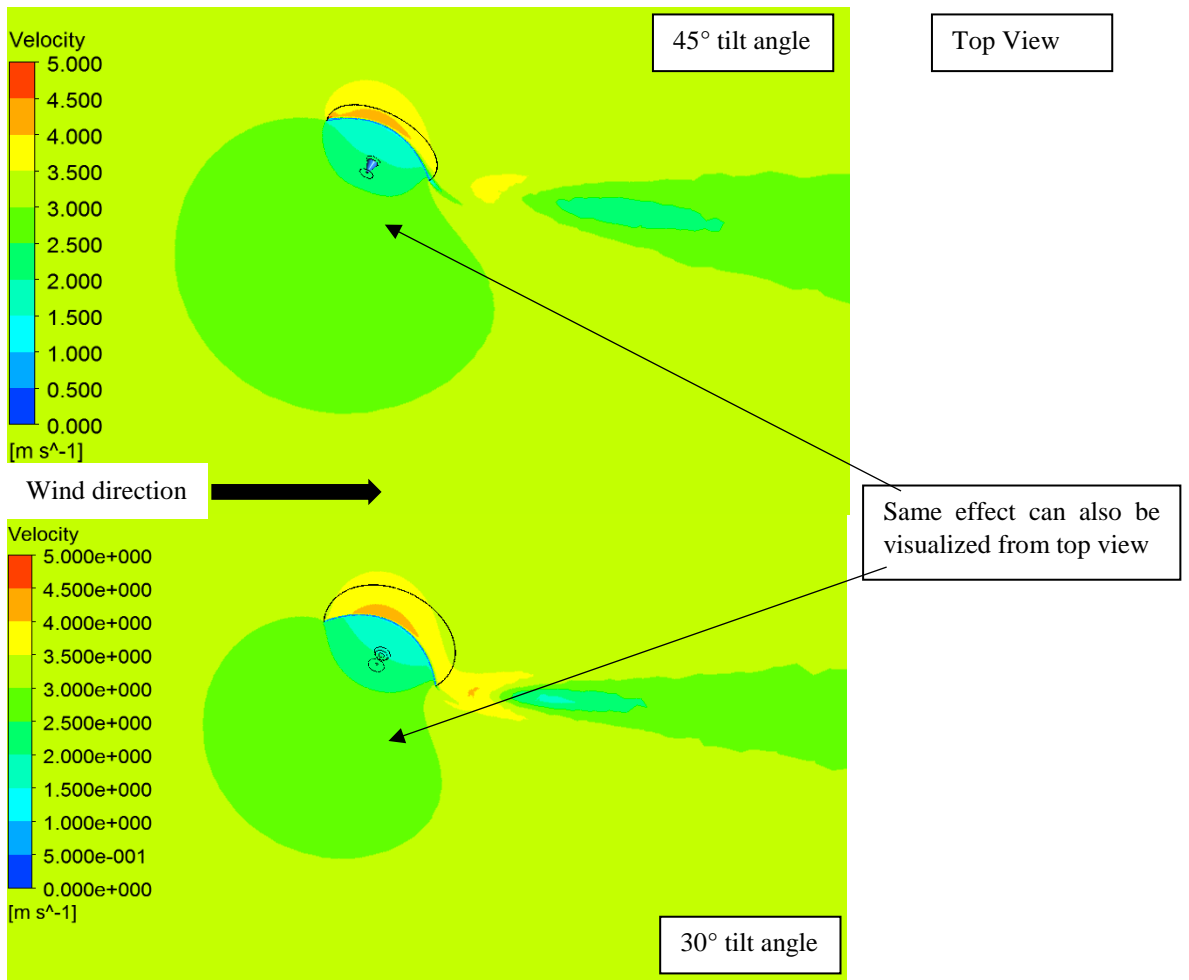


Figure 69: Convective heat loss as a function of wind incidence angle at $V=3\text{ m/s}$

For all tilt angles, except the 0° and 90° tilt angle, the maximum heat loss occurred when the flow was parallel to the receiver aperture plane ($\phi=0^\circ$). An increase in heat loss is visible for 30° and 45° tilt angle between the incidence angle ranges of $+30^\circ$ to -30° , as in this range, the flow is not significantly changed at the aperture plan of the receiver due to the presence of the dish (Figure 70). However, for the case of 0° tilt angle, the heat loss was same for all the wind incidence angles showing no impact of the dish on the heat loss. While for the case of 90° tilt angle at 0° wind incidence angle, due to random motion of air near the cavity inlet, the convective heat loss was found to decrease instead of an increase (Figure 71).



(a)



(b)

Figure 70: Velocity contours at 30° wind incidence angle with $V=3$ m/s

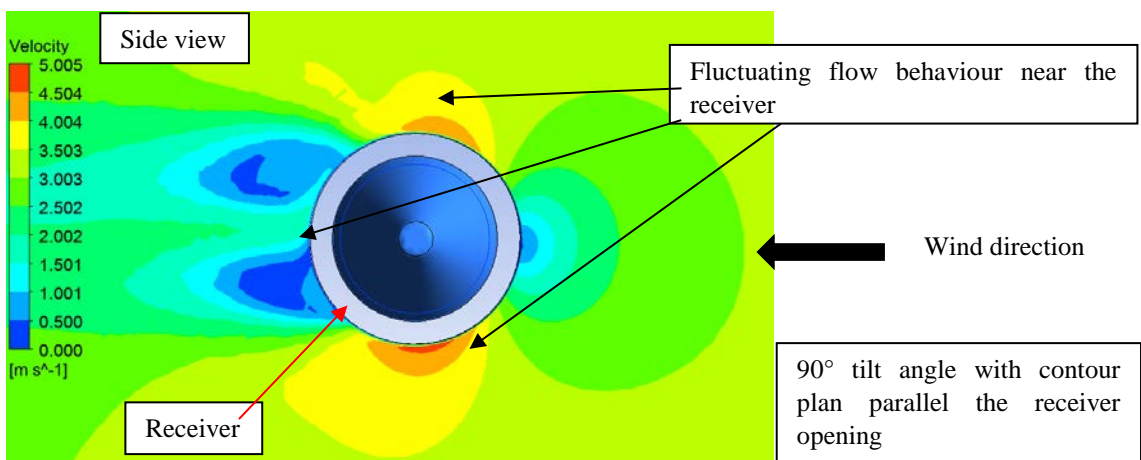


Figure 71: Velocity contour at 0° wind incidence angle with $V=3$ m/s

Continuing this theme, Figure 72 shows result for a wind velocity of 5 m/s. Compared with 3 m/s, the relatively smooth pattern indicates a dominance of forced convection over natural convection. From this, depending on the operating conditions, there is a velocity and operating orientations that cause a change between mixed and forced convection.

On inspection of Figure 72, for all positive wind incidence angles, the heat loss from the receiver decreased by reducing the tilt angle from 90° to 30° and then there was sharp increase at 0° tilt angle. As discussed earlier, at 0° tilt angle, air flow at the receiver was not disturbed by the dish and as expected, higher heat loss was observed at higher velocity due to direct exposure of the receiver to the free stream wind.

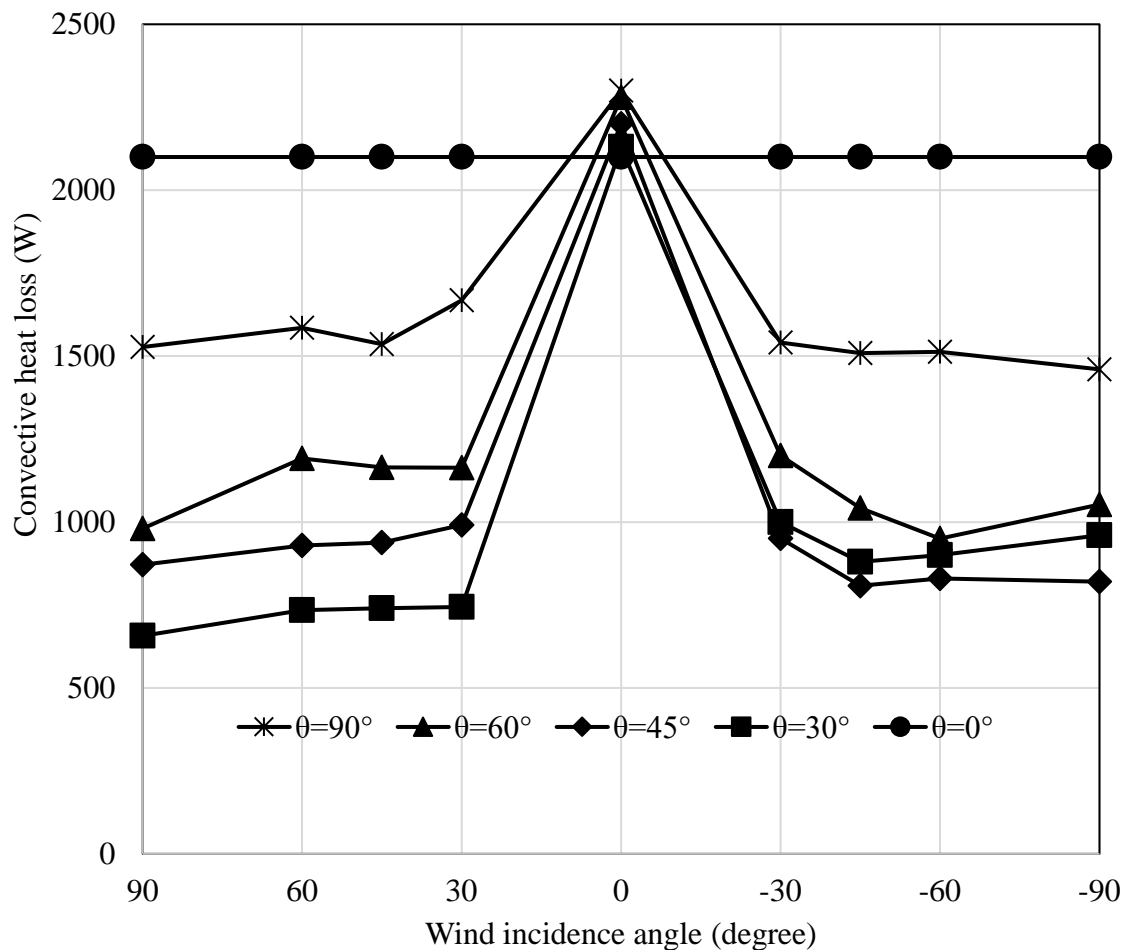


Figure 72: Convective heat loss as a function of wind incidence angle at $V=5\text{ m/s}$

However, for negative wind incidence angles, the receiver was located in the wake region of the dish. As a result the heat loss from the receiver was lower than that of positive wind incidence angle. The higher heat loss at 30° tilt angle was observed than 45° tilt angle for all negative wind incidence angles. The same phenomena is also observable at 3 m/s and above. During this orientation, the dish has provided a blockage and wind is not directly approaching toward the receiver (Figure 73), as a result more heat loss was observed at 45° and even at 60° tilt angles at higher speeds.

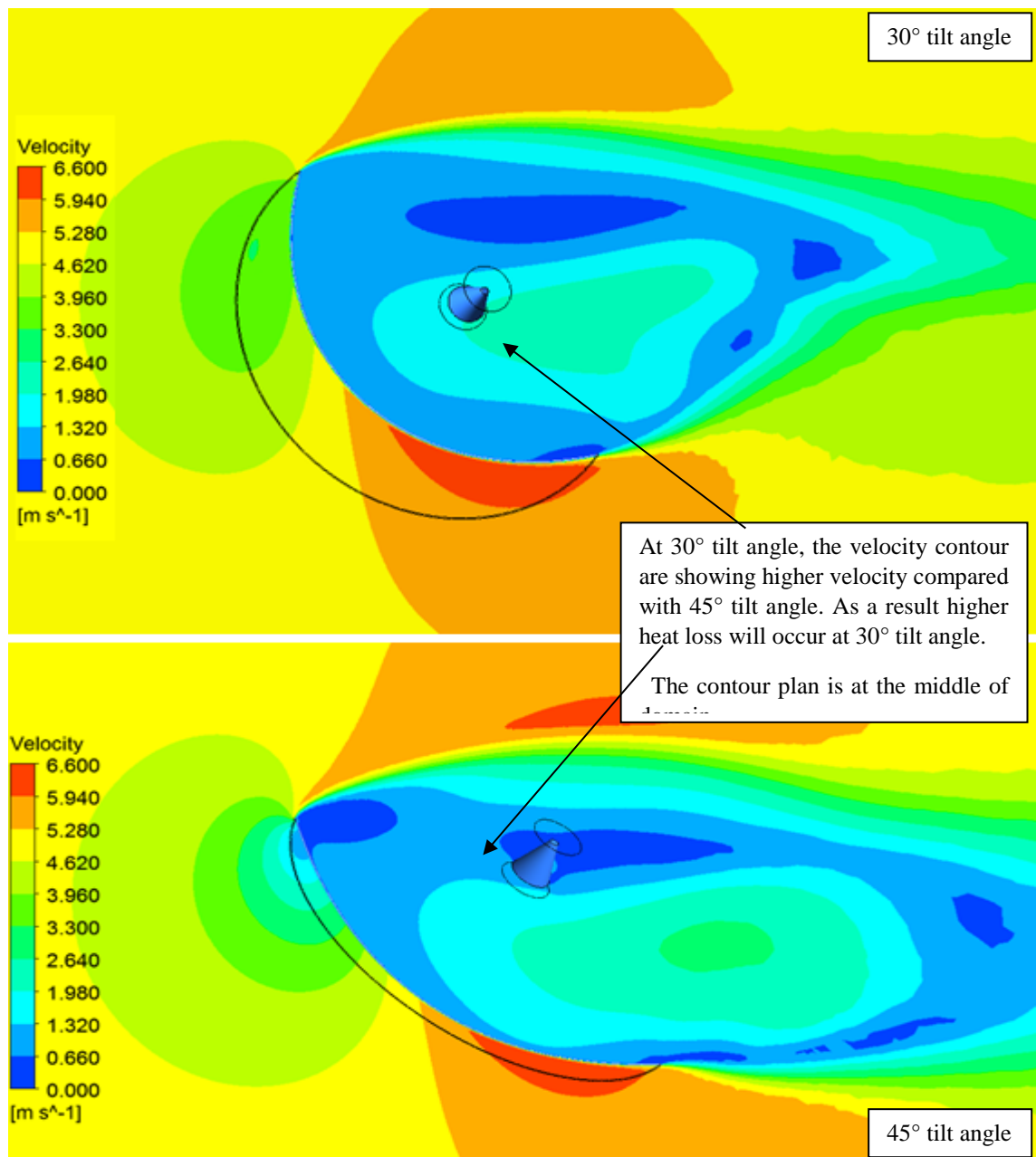


Figure 73: Top view of velocity contour at 45° wind incidence angle with $V= 5$ m/s

Finally, Figures 74-75 show the heat loss values for 10 m/s and 20 m/s respectively. As expected, the convective heat loss from the receiver was increased due to the dominance of the forced convection at this wind speed. With the higher wind velocities of 10 m/s and 20 m/s, the strong separation can be seen at the edges of the dish (Figure 76). At higher velocities, the heat loss from the receiver followed a similar pattern.

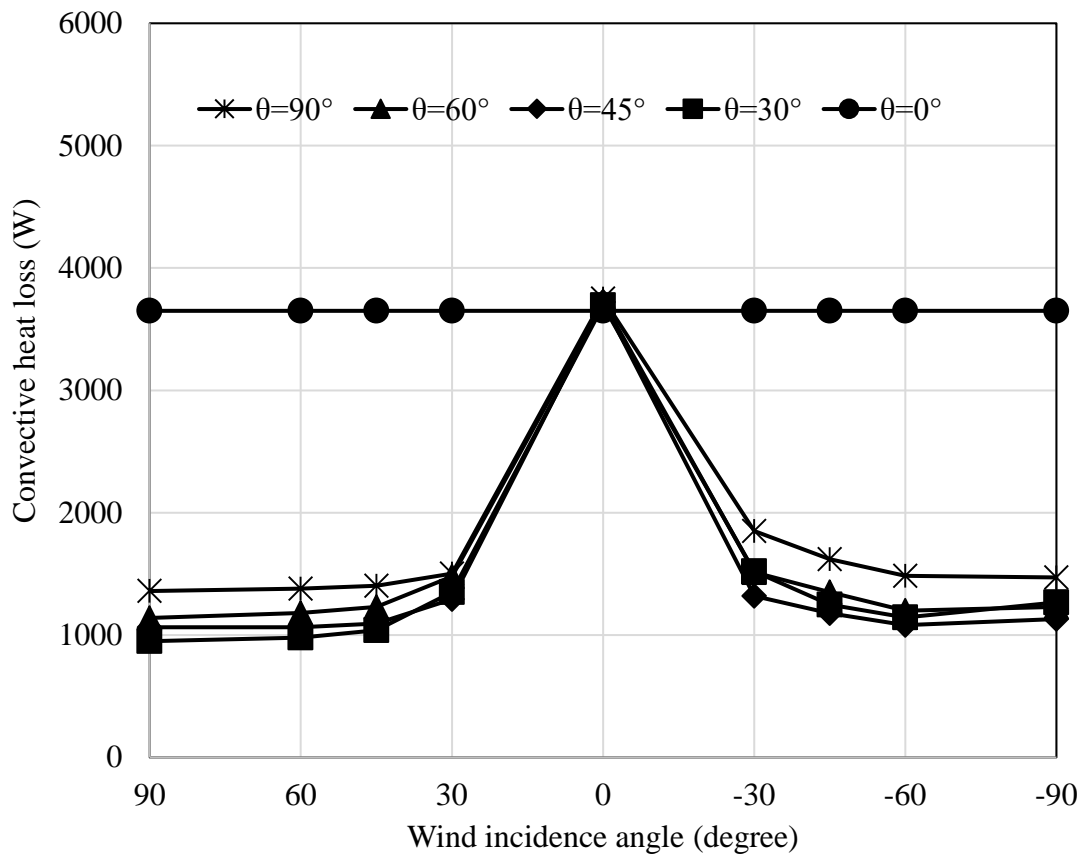


Figure 74: Convective heat loss as a function of wind incidence angle at $V=10$ m/s

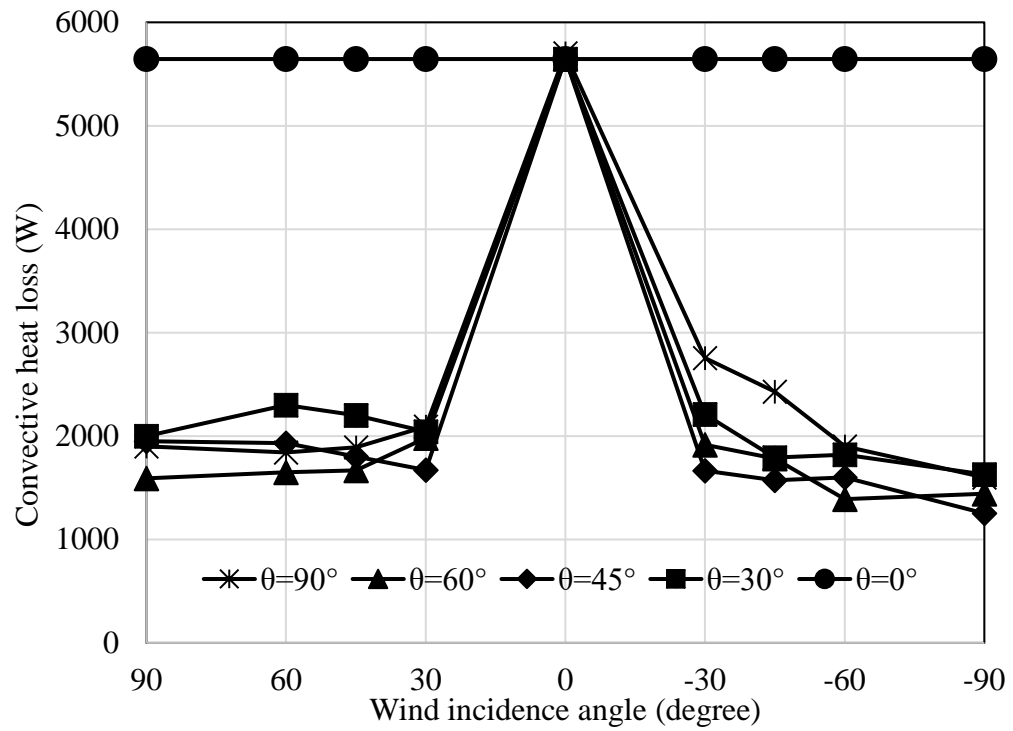


Figure 75: Convective heat loss as a function of wind incidence angle at $V=20$ m/s

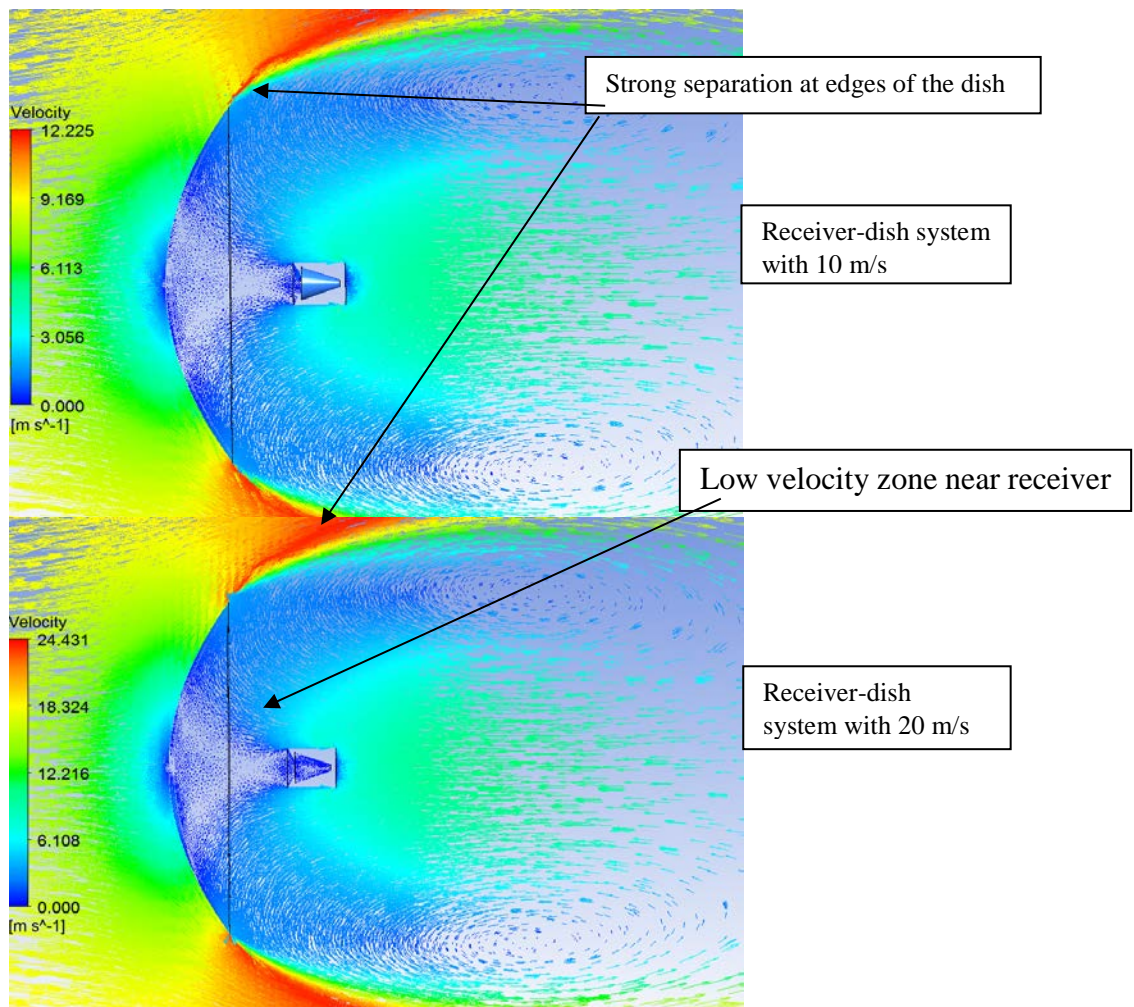


Figure 76: Velocity vectors for $\phi = -90^\circ$ tilt angle with the dish structure

The observations showed that the impact of the dish on the flow field is negligible for a range of wind incidence angles from $\varphi=30^\circ$ to $\varphi=-30^\circ$. Within this range, the cavity was in the occluded region of the dish structure and the reduction in local velocity was negligible. It was also observed that the wind incidence angle (φ) had the same outcome for the cavity facing vertically downward ($\theta=0^\circ$) at any given velocity, and in all cases the maximum convective heat loss occurred at $\theta=0^\circ$ inclination. The observations showed that convective heat loss is influenced by the orientation of the dish structure in the flow field, and in most cases, the dish shielded the cavity receiver from the flow. The dish had a negligible influence on heat loss for a range of tilt angles from $\theta=30^\circ$ to $\theta=-30^\circ$ and for a range of wind incidence angles $\varphi=30^\circ$ to $\varphi=-30^\circ$. Within these ranges, the flow field is more stream lined and the cavity receiver is well away from any disturbances in the local velocity field.

4.5 Heat loss correlation for coupled dish-receiver system

In the previous sections, convective heat loss from the receiver at different working conditions was discussed in detail. The work showed the effect of the dish on the convective heat loss and consequently on the performance of the parabolic dish system. However, there is a need to draw together the analysis performed in the previous chapters to develop a correlation for the heat loss from the cavity receiver based on the independent variables including free stream wind velocity, tilt and wind incidence angle.

The magnitude of convective heat transfer (Q) is generally expressed by Nusselt number (Nu). To determine the Nusselt number, previous studies suggested the generalized correlations with non-dimensional quantities for various geometrical configurations, driving forces and thermal fluid properties. Nusselt number (Nu) is commonly used as a dependent dimensionless parameter to determine the convective heat transfer coefficient (h).

Generally, the independent dimensionless parameters used in free convection studies are Prandtl Number (Pr), Grashof number (Gr) and tilt angle (θ). Sometimes, the natural convection is also defined using Rayleigh number ($Ra = Gr \cdot Pr$). The generalized forms of the relationship for free convection are given in Eq. 3 and Eq. 4 (Paitoonsurikarn, 2006):

$$Nu = CGr^mPr^n \quad (3)$$

Or

$$Nu = CRA^mPr^n \quad (4)$$

Where constants (C , m and n) are determined by either experimentally or analytically.

On the other hand, for the forced convection, Nusselt number is defined as a group of Reynolds and Prandtl number, as shown in Eq. 5.

$$Nu = CRe^mPr^n \quad (5)$$

Again the constant terms (C , m and n) are the determined by either experimentally or analytically.

For the combined convection, the Nusselt numbers are determined separately for free and forced convection and then combined by the expression given in Eq. 6 (Bergman et. al., 2011):

$$Nu^n = Nu_{forced}^n \pm Nu_{free}^n \quad (6)$$

In combined convection, the direction of external flow effects the magnitude of combined Nusselt number.

4.5.1 No-wind condition, heat transfer correlation

The correlations available for the no-wind condition, or natural convection heat loss are normally generalized using the Grashof or Rayleigh number and Prandtl number. In the proposed correlation, Nusselt number is defined as the function of the Grashof number (Gr) and the ratio of receiver wall temperature to ambient temperature ($\frac{T_w}{T_\infty}$). Keeping in mind that the parabolic dishes operate at high cavity temperatures between 500°C to 800°C (Stine, 1998), the correlation was established using the same temperature range.

By using non-linear regression technique (Oosterbaan, 1994, 2002), the dimensionless parameters were used to establish the Nusselt number correlation. The established correlation is given by Eq. 7:

$$Nu = 0.0027Gr^{0.54} \left(\frac{T_w}{T_\infty}\right)^{0.47} (2 + 1.8\cos^3\theta)^{-3.62} \quad (7)$$

Where T_w and T_∞ are cavity wall temperature and ambient air temperature in Kelvin. The cavity diameter was used as the characteristic length to determine the Grashof number, and the fluid properties were taken at the mean temperature. The proposed correlation coefficient is about 0.98 resulting a good comparison with the numerical simulation results.

4.5.2 Forced convection heat transfer correlation

In the previous studies, many models were carried out to determine the convective heat loss from the cavity receiver based on a particular geometry and under different operating/testing conditions without considering the impact of the dish. In the proposed correlation, the impact of dish structure on the convective heat loss was the main focus. The proposed correlation is integrating the wind velocity, incidence angle (φ), tilt angle

(θ), and variation of cavity wall temperature. As discussed earlier, the temperature range was selected between 500°C to 800°C.

A non-linear regression (Oosterbaan, 1994, 2002) was performed to establish the correlation between convection heat losses from the receiver. The steps to establish the correlations are given in Appendix C. The proposed correlation is based on the generalized form and introduces other functions for the two angles, as shown in Eq. 8:

$$Nu = CRe^m Pr^n f(\theta, \varphi) \quad (8)$$

Due to the presence of the dish in the flow, the mixed free and forced convection heat loss takes place at different tilt and wind incidence angles even at higher free stream velocities. Considering the intricate features of mixed heat convection, the proposed correlation was divided into following three segments depending on the flow behaviour near cavity receiver.

- i) At zero degree tilt angle, when cavity is positioned in the free stream flow, at any given wind incidence angle ($-90^\circ \leq \varphi \leq 90^\circ$) and wind velocity.
- ii) At zero degree wind incidence angle, when the flow is parallel to dish aperture, at given tilt angle ($0^\circ < \theta \leq 90^\circ$) and wind velocity.
- iii) At all wind incidence and tilt angles other than zero. In these regions the dish has an impact on the local flow velocity.

After careful consideration of all the important parameters, the final Nusselt number relationship was established and shown in Eq. 9:

$$Nu = a \left[\frac{(1.1 + 0.1 \cos \varphi)^b}{(1.1 + \cos \theta)^c} \right] Re^d Pr^e \quad (9)$$

The coefficients used in Nusselt correlations were found to shown in Table 2.

Case #	a	b	c	d	e
i	4.65×10^{-7}	0.27	0	1.33	0.333
ii	0.00174	0	0.872	0.722	0.333
iii	1.7	1.77	0.938	0.174	0.333

Table 2: Values of coefficients used in Nusselt correlation (Eq.9)

The characteristic length used in the Reynolds number was the diameter of the cavity receiver for zero degree tilt angle (case i), as there was no impact of the dish on the heat loss. While, for the remaining cases (ii and iii), diameter of the dish was used to define the Reynolds number. While the free stream velocity was used as the characteristic velocity. The fluid properties were taken at mean bulk temperature.

The Nusselt number correlation showed a relatively less strength of wind incidence angle to the tilt angle in the presence of the dish structure in the flow field. Figure 77 shows the correlation between the predicted and numerical results. It can be seen that most of the predicted data from the correlation lie between 25% of the numerical values obtained from numerical studies. Having data from validated CFD scheme, these correlations can be used with great confidence, within the temperature range mentioned, to predict the accurate performance of the parabolic dish systems.

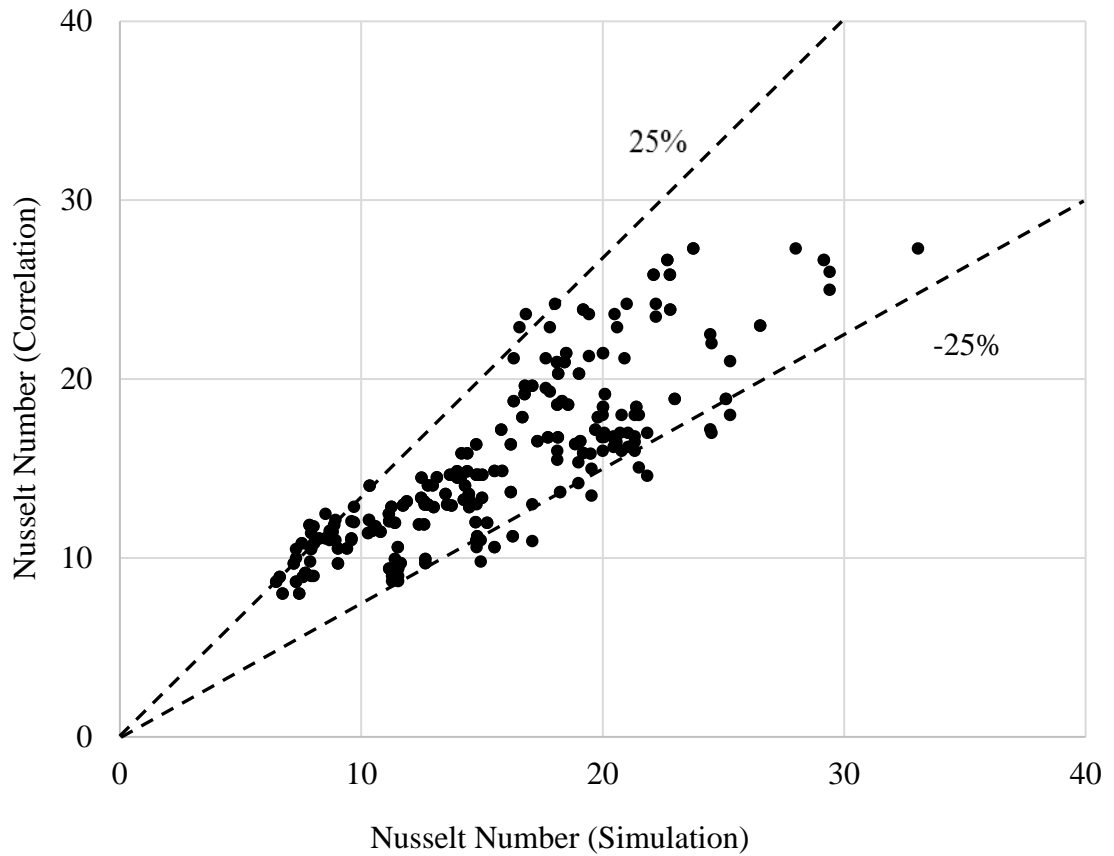


Figure 77: Comparison of Nusselt number obtained from correlation and numerical results

4.6 Chapter Summary

A comprehensive numerical study was performed to investigate the effect of the presence of the dish on convective heat losses from a cavity receiver in a coupled dish-cavity receiver system at different orientations.

Maximum heat loss occurred at a zero degree tilt angle during forced convection, irrespective of the wind incidence angle. From 0° to 30° tilt angles, the cavity is shifting its position such that the opening of cavity moves from free stream region to a flow region altered by the dish structure. As a result, the heat loss from the cavity at 30° tilt angle was observed lower compared with the 0° tilt angle.

In the case of flow parallel to the receiver's aperture plane ($\varphi=0^\circ$), heat losses were higher than in any other cases under the same operating conditions. This is because of higher

local velocity values at the aperture of the cavity receiver. For side-on flow, the variation was negligible irrespective of tilt angle. By changing the wind incidence angle to either 90° or -90° , the heat loss values were smaller than the side-on flow (parallel to the receiver's aperture plane) condition. Up to certain wind incidence angles, the dish structure provided a shield to receiver from the flow and the heat losses showed a decreasing trend. However, heat loss was observed to increase between $\phi = 30^\circ$ to $\phi = -30^\circ$, where the dish structure's impact on the flow field is negligible.

Based on the available data, two separate Nusselt number correlations were purposed for wind and no-wind regimes. The proposed correlation indicated the greater influence of tilt angle on the heat loss from the receiver in the presence of dish structure. The predicted Nusselt numbers from correlation were within acceptable range of numerical values.

This study concludes that dish structure has a significant impact on the convective heat losses from the cavity receiver, and presents a model and data that could now be used to correct output predictions for these systems.

Chapter 5: Conclusion and Recommendations

Historically, thermal decoupling of the cavity receiver from the dish simplifies the analysis of heat loss and is accurate where there is either no wind or certain wind incidence angles. However, outside of these situations the presence of the dish is expected to significantly affect the local air flow at the aperture of the receiver and hence the heat loss from the system.

This work used a computational (CFD) approach to investigate the effect of the dish structure on local flow behaviour near the cavity receiver and consequently on the convective heat loss from the receiver. The CFD was validated using experimental visualization of smoke around the dish. The numerical modelling of flow around the dish identified a significant disturbance in local air velocity in the cavity zone in the presence of the dish under most of the operating conditions, except where there was parallel flow to the aperture of the dish (tilt angle $\theta=0^\circ$). A comparison between heat losses with and without the presence of the dish for a particular case (wind impinging directly on the back side of the dish) revealed a 15% reduction in convective heat loss at a wind speed of 3m/s, which rose to a 40% reduction at 20 m/s. For the full experimental range of wind speeds and tilt angles, the convective heat loss was observed to be less than that from free convection (in a no-wind condition) up to a certain velocity.

The study demonstrated higher heat losses for side-on flow with a zero degree wind incidence angle than in any other case under the same operating conditions, due to higher local velocities at the open face of the cavity. At higher speeds, above 3 m/s, the heat losses from the cavity receiver at all tilt angles were the same, due to the insignificant effect of the dish on local flow velocities.

For all other wind incidence angles, the dish structure hindered free stream flow and altered local velocities near the cavity receiver. As a result considerably less heat loss

occurred from the cavity. A correlation describing the convective heat loss from the cavity was established to describe the influence of the dish structure.

The work presented in this study supports the assertion that the flow characteristics near the cavity receiver aperture depend strongly on the presence and orientation of the dish structure. This needs to be taken into account when analyzing the performance of parabolic dish systems to avoid an overly conservative and hence more expensive design.

5.1 Recommendations for future work

As mentioned in Chapter 1, all the researchers have investigated the convective heat losses from the cavity receiver by treating it as a separate entity decoupled from the dish. This study has demonstrated a great impact of the dish on the convective heat losses and a new dimension of research is now open for all. There is a great need to incorporate the dish in the flow system to get accurate models.

In addition to the investigation of the effect of the dish on local flow behaviour and heat loss from the cavity, some other important factors were partly discussed in the study and are worth investigating further in future work to improve parabolic dish systems. This study mainly focused on the influence of the dish on convective heat loss from the cavity, and showed a significant increase in heat loss for tilt angles between $\pm 30^\circ$ and 0° . A detailed numerical investigation is essential, using small incremental tilt angles between $\pm 30^\circ$ and 0° under different operating conditions, to identify the exact region in which the dish plays an important role in reducing the heat loss.

The size and positioning of the cavity can alter heat loss significantly, as discussed in Chapters 2 and 3. It is thus essential to investigate these effects in detail to improve the heat loss model for use in a range of real scenarios. Local flow behaviour was analysed for the geometry of a specific parabolic dish system, hence other geometries should also

be investigated. Also, the effect of the presence of the different dishes in parabolic dish system field is also need to be investigated.

Also, more work need to be done to explore the fundamental fluid dynamics and its impact on heat transfer. There is a need to better characterise the interactions of the shear layers separated from the dish and/or the receiver and the internal flow inside the receiver cavity, which may have significant implication to heat loss from the receiver. A comparison of wake size, separation location, wake shape, etc., would be added value to the future experimental work by showing either deviations or similarities with the numerical results.

The reduction of heat loss, observed at low wind velocities, needs further examination to get a clear picture of the interaction of the equally dominant buoyancy and wind-induced convective flow.

References

- ANSYS Inc., 2013, “CFX User Guide”, ANSYS, Canonsburg, USA.
- Behar, O., Khellaf, A., and Mohammedi, K., 2013, “A review of studies on central receiver solar thermal power plants”, *Renewable and Sustainable Energy Review*, Vol 23, pp. 12-39.
- Bergman, T. L., Incropera, F. P., Dewitt, D. P., and Lavine, A. S., 2011, “*Fundamentals of Heat and Mass Transfer*”, John Wiley and Sons, New York, USA.
- Christo, F., 2012, “Numerical modelling of wind and dust pattern around a full-scale paraboloidal solar dish”, *Renewable Energy*, Vol 32, pp.356-366.
- Clausing, A. M., 1981, “An Analysis of Convective Losses from Cavity Solar Central Receiver”, *Solar Energy*, Vol 27, pp. 295-300.
- Clausing, A. M., 1983, “Convection Losses from Cavity Solar Receivers-Comparisons between Analytical Predictions and Experimental Results”, *Journal of Solar Energy Engineering*, Vol 105, pp. 29-33.
- Clausing, A. M., Waldvogel, J. M., Lister, L. D., 1987, “Natural convection from isothermal cubical cavities with a variety of side-facing apertures”, *ASME Journal of Heat Transfer*, Vol 109, pp. 407-412
- Cui, F., He, Y., Cheng, Z., and Li, Y., 2013, “Study on combined heat loss of a dish receiver with quartz glass cover”, *Applied Energy*, Vol 112, pp. 690-696.
- Fang, J. B., Wei, J. J., Dong, X. W., and Wang, Y. S., 2011, “Thermal performance simulation of a solar cavity receiver under windy conditions”, *Solar Energy*, Vol 85, pp. 126-138.

Flesch, R., Stadler, H., Uhlig, R., Pitz-Paal, R., 2014, “Numerical analysis of the influence of inclination angle and wind on the heat losses of cavity receivers for solar thermal power towers”, *Solar Energy*, Vol 110, pp. 427–437.

Flesch, R., Stadler, H., Uhlig, R., Hoffschmidt, B., 2015, “On the influence of wind on cavity receivers for solar power towers: an experimental analysis”, *Applied Thermal Engineering*, Vol 87, pp. 724–735

Fluent, Inc., 2005, “*Fluent User Guide*”, Lebanon, USA.

Foster, R., Ghassemi, M., and Cota, A., 2010, “*Solar Energy: Renewable Energy and the Environment*”, Boca Raton: CRC Press, , New York, USA.

Goswami, D. Y., Kreith, F., and Kreider, J. F., 2000, “*Principles of solar engineering*”, (2nd edition), CRC Press, New York, USA.

Günther, M., and Shahbazfar, R., 2012, “Advanced CSP teaching materials”, Germany.

Hachicha, A., Rodríguez, I., Capdevila, R., and Oliva, A., 2013a, “Heat transfer analysis and numerical simulation of a parabolic trough solar collector”, *Applied Energy*, Vol 111, pp.581-592.

Hachicha, A. A., Rodríguez, I., Castro, J., and Oliva, A., 2013b, “Numerical simulation of wind flow around a parabolic trough solar collector”, *Applied Energy*, Vol 107, pp. 426-437.

Harris, J.A, Lenz, T.G., 1985, “Thermal performance of concentrator/cavity receiver system”, *Solar Energy*, Vol 34, pp. 135-142.

Holl, R. H., and de Meo, E. A., 1990, “*The Status of Solar Thermal Electric Technology*”, Springer, Boston, USA.

Holman, J. P., 1997, "*Heat transfer*", (8th edition), McGraw-Hill Companies, New York, USA.

Hosoya N., Peterka J.A, Gee R.C., and D., K., 2008, "*Wind tunnel tests of parabolic trough solar collectors*", *Technical Report NREL/SR-550-32282*, National Renewable Energy Laboratory, USA.

Jilte, R.D., Kedare, S. B., and Nayak, J. K., 2013, "Natural convection and radiation heat loss from open cavities of different shaped and sizes used in dish concentrator", *Mechanical Engineering Research*, Vol 3 (1), pp. 25-43.

Kaushika, N. D., 1993, "Viability aspects of paraboloidal dish solar collector systems" *Renewable Energy*, Vol 3, pp. 787-793.

Kaushika, N. D., and Reddy, K. S., 2000, "Performance of a low cost solar paraboloidal dish steam generating system", *Energy Conversion and Management*, Vol 41, pp. 713-726.

Khubeiz, J. M., Radziemska, E., and Lewandowski, W. M., 2002, "Natural convective heat transfer from an isothermal horizontal hemispherical cavity", *Applied Energy*, Vol 73, pp. 261-275.

Kim, K., Moujaes, S. F., and Kolb, G. J., 2010, "Experimental and simulation study of wind affecting particle flow in a solar receiver", *Solar Energy*, Vol 84, pp. 263-270.

Koenig, A. A., and Marvin, M., 1981, "*Convection heat loss sensitivity in open cavity solar receivers*", *Final report, DOE contract no. EG77-C-04-3985*, Department of Energy, USA.

Le Quere, P., Humphery, J. A., and Sherman, F. S., 1981a, "Numerical calculation of thermally driven two-dimensional unsteady laminar flow in cavities of rectangular cross section", *Numerical Heat Transfer, Part B*, Vol 4, pp. 249-283.

Le Quere, P., Penot, F., and Mirenyat, M., 1981b, “*Experimental study of heat loss through natural convection from an isothermal cubic open cavity*”, Sandia National Laboratories Report, SAND81-8014, USA.

Leibfried, U., and Ortjohann, J., 1995, “Convective Heat Loss from Upward and Downward-Facing Cavity Solar Receivers: Measurements and Calculations”, *ASME Journal of Solar Energy Engineering*, Vol 117, pp. 75-84.

Liovic, P., Kim, J. S., Hart, G., Stein, W., 2014, “Wind dependence of energy losses from a solar gas reformer”, *Applied Thermal Engineering*, Vol 63, pp. 333–346.

Lovegrove, K., Taumoefolau, T., Paitoonsurikarn, S., Siangsukone, P., Burgess, G., Luzzi, A., Johnston, G., Becker, O., Joe, W., and Major, G., 2003, “Paraboloidal dish solar concentrators for multi-megawatt power generation”, *Proceedings of the International Solar Energy Society (ISES) Solar World Conference*, Goteborg, Sweden.

Lupfert, E., Geyer, M., Schiel, W., Esteban, A., Osuna, R., and Zarza, E., 2001, “EUROTHROUGH design issues and prototype testing at PSA”, *Proceedings of Solar Forum 2001, Solar Energy: The Power to Choose*, Washington DC.

Ma, R. Y., 1993, “Wind effects on convective heat loss from a cavity receiver for a parabolic concentrating solar collector”, *Sandia National Laboratories Report*, SAND92-7293, USA.

Menter, F. R., 1993, "Zonal Two Equation $k-\omega$ Turbulence Models for Aerodynamic Flows", *Proceedings of the 23rd fluid dynamics, plasadynamics, and lasers conference*, *AIAA Paper*, Florida, USA.

Menter, F. R., 1994 "Two-Equation Eddy-Viscosity Turbulence Models for Engineering Applications", *AIAA Journal*, Vol. 32(8), pp. 1598-1605.

Naeeni, N., and Yaghoubi, M., 2007a, “Analysis of wind flow around a parabolic collector (1) fluid flow”, *Renewable Energy*, Vol 32(11), pp. 1898-1916.

Naeeni, N., and Yaghoubi, M., 2007b, “Analysis of wind flow around a parabolic collector (2) fluid flow”, *Renewable Energy*, Vol 32(11), 1259-1272.

Oosterbaan, R.J., 1994, “*Frequency and Regression Analysis of hydrological data*”, (2nd Revised edition), International Institute for Land Reclamation and Improvement, Wageningen, The Netherlands.

Oosterbaan, R.J., 2002, “*Drainage research in farmers' fields: analysis of data*”, International Institute for Land Reclamation and Improvement , Wageningen, The Netherlands.

Paetzold, J., Cochard, C., Fletcher, D., and Vassallo, A., 2014, “Wind flow around parabolic trough solar collectors- A parametric study for optimisation of wind forces and heat losses”, *Proceedings of Solar 2014: The 52nd Annual Conference of the Australian Solar Council*. Melbourne, Australia; 2014

Paetzold, J., Cochard, C., Fletcher, D., Vassallo, A., 2015, “Wind Engineering Analysis of Parabolic Trough Collectors to Optimise Wind Loads and Heat Loss”, *Energy Procedia*, Vol. 69, pp. 168-177

Paitoonsurikarn, S., and Lovegrove, K., 2002, “Numerical investigation of natural convection loss on cavity type solar receiver”, *Proceedings of the 40th Conference of the Australian and New Zealand Solar Energy Society (ANZSES)*, Newcastle, Australia.

Paitoonsurikarn, S., and Lovegrove., K., 2003, “On the study of convection loss from open cavity receiver in solar paraboloidal dish applications”, *Proceedings of the 41st Conference of the Australian and New Zealand Solar Energy Society (ANZSES)*, Melbourne, Australia.

Paitoonsurikarn, S., Taumoefolau, T., and Lovegrove, K., 2004, “Estimation of convection heat loss from paraboloidal dish cavity receivers”, *Proceedings of the 42nd Conference of the Australian and New Zealand Solar Energy Society (ANZSES)*. Perth, Australia.

Paitoonsurikarn, S., 2006, “*Study of a Dissociation Reactor for an Ammonia-Based Solar Thermal System*”, PhD Thesis, Australian National University, Australia.

Paitoonsurikarn, S., and Lovegrove, K., 2006a, “A new Correlation for predicting the free convection loss from solar dish concentrating receivers”, *Proceedings of the 44th Conference of the Australian and New Zealand Solar Energy Society (ANZSES)*, Canberra, Australia.

Paitoonsurikarn S., and Lovegrove K., 2006b, “Effect of paraboloidal dish structure on the wind near a cavity receiver”, *Proceedings of the 44th Conference of the Australian and New Zealand Solar Energy Society (ANZSES)*. Canberra, Australia.

Philibert, C., 2011, “*Solar Energy Perspectives*”, International Energy Agency (IEA), OECD Publication, France.

Philibert, C., 2014, “*Technology Roadmap: Solar Thermal Electricity*”, International Energy Agency (IEA), OECD Publication, France.

Prakash, M., Kedare, S. B., and Nayak, J. K., 2009, “Investigation on heat losses from a solar cavity receiver”, *Solar Energy*, Vol 83, pp. 157-170.

Price, H., Lufert, E., and Kearney, D., 2002, “Advances in Parabolic Trough Solar Power”, *ASME Journal of Solar Energy Engineering*, Vol 124(2), pp.109–125.

Reddy, K. S., and Sendhil Kumar, N., 2008, “Combined laminar natural convection and surface radiation heat transfer in a modified cavity receiver of solar parabolic dish”, *International Journal of Thermal Science*, Vol 47, pp. 1647-1657.

Reddy, K., and Sendhil Kumar, N., 2009, "Convection and surface radiation heat losses from modified cavity receiver of solar parabolic dish collector with two stage concentration", *Heat and Mass Transfer*, Vol. 45, pp. 363-373.

Reddy, K.S., Srihari, V. T., and Veershetty G., 2015, "Combined heat loss analysis of solar parabolic dish – modified cavity receiver for superheated steam generation", *Solar Energy*, Vol 121, pp. 78-93.

Reddy, K. S., Veershetty, G., and Srihari, V. T., 2016, "Effect of wind speed and direction on convective heat losses from solar parabolic dish modified cavity receiver", *Solar Energy*, Vol 131, pp.183-198.

Robert, F., Hannes, S., Ralf, U., and Bernhard, H., 2015, "On the influence of wind on cavity receivers for solar power towers: An experimental analysis", *Applied Thermal Engineering*, Vol 87, pp. 724-735.

Kumar, S. N., and Reddy, K. S., 2007, "Numerical Investigation of natural convection heat loss in modified cavity receiver for fuzzy focal solar dish concentrator", *Solar Energy*, Vol 81, pp. 846-855.

Samane, J., Garcia-Barberena, Zaversky, F., 2015, "Modeling solar cavity receivers: a review and comparison of natural convection heat loss correlations", *Energy Procedia*, Vol 69, pp.543-552.

Siebers, D. L., and Kraabel, J. S., 1984, "*Estimating convective energy losses from solar central receivers*", *Sandia National Laboratories Report, SAND 84-8717, USA.*

Steinfeld, A., 2005, "Solar thermochemical production of hydrogen-a review" *Solar Energy*, Vol 78, pp. 603-615.

Stine, W.B., 1998, "*Stirling engines*", CRC Press, New York, USA.

Stine, W. B., and Diver, R. B., 1994, “*A Compendium of Solar Dish/Stirling Technology*”, Technical Report, Albuquerque, Livermore: Sandia National Laboratories, USA.

Stine, W. B., and McDonald, C. G., 1989, “Cavity Receiver Heat Loss Measurements”, *Proceedings of the International Solar Energy Society Solar World Congress*, Kobe, Japan

Tan, T., Chen, Y., Chen, Z., and Siegel, N., 2009, “Wind effect on performance of solid particle solar receivers with and without the protection of an aero-window”, *Solar Energy*, Vol 83, pp. 1815-1827.

Taumoefolau, T., 2004, “*Experimental investigation of convection loss from a model solar-concentrator cavity receiver*”, Masters Thesis, Australian National University, Canberra, Australia.

Taumoefolau, T., and Lovegrove, K., 2002, “An experimental study of natural convection heat loss from a solar concentrator cavity receiver at varying orientation”, *Proceedings of the 40th Conference of the Australian and New Zealand Solar Energy Society (ANZSES)*, Newcastle, Australia.

Taumoefolau, T., Paitoonsurikarn, S., Hughes, G., and Lovegrove, K., 2004, “Experimental investigation of natural convection heat loss from a model solar concentrator cavity receiver”, *Journal of Solar Engineering*, Vol 126, pp.801-807.

Trinder, M., and Jabbal, M., 2013, “Development of a smoke visualisation system for wind tunnel laboratory experiments”, *International Journal of Mechanical Engineering Education*, Vol 41(1), pp.27-43.

Tyner, C. E., Kolb, G. J., Geyer, M., & Romero, M., 2001, “Concentrating solar power in 2001 an IEA/Solar PACES summary of present status and future prospectus”,

presented at the meeting of the Solar PACES, Retrieved from www.solarpaces.org (Last cited: 25-04-2016)

Vikram, T.S. and Reddy, K.S., 2014, “Estimation of heat losses from modified cavity mono-tube boiler receiver of solar parabolic dish for steam generation”, *Energy Procedia*, Vol.57, pp. 371–380.

Vikram, T.S., Reddy, K.S., 2015, “Investigation of convective and radiative heat losses from modified cavity based solar dish steam generator using ANN”, *International Journal of Thermal Sciences*, Vol. 87, pp. 19–30

Wagner, G. L., 1996, “*Solar concentrator wind loading*”, Masters Thesis, Texas Tech University, USA.

Wang, M., and Siddiqui, K., 2010, “The impact of geothermal parameters on the thermal performance of a solar receiver of dish-type concentrated solar energy system”, *Renewable Energy*, Vol 35, pp. 2501-2513.

Wu, S.,Y., Xiao, L., Cao, Y., and Li, Y. R.,2010, “Convection heat loss from cavity receiver in parabolic dish solar thermal power system: A review”, *Solar Energy*, Vol. 84, pp. 1342-1355.

Wu, S. Y., Guan, J. Y., Xiao, L., Shen, Z. G., and Li, D. L., 2013, “Effect of wind direction on heat loss of a fully open cylindrical cavity with only the bottom wall heated”, *2nd IET Renewable Power Generation Conference (RPG 2013)*, Beijing, 2013, pp. 1-4

Wu, S. Y., Guo, F. H., and Xiao, L., 2014, “Numerical investigation on combined natural convection and radiation heat losses in one side open cylindrical cavity with constant heat flux.”, *International Journal of Heat and Mass Transfer*, Vol. 71, pp. 573-584.

Wu, S. Y., Shen, Z., G., and Xiao, L., 2015, "Experimental investigation and uncertainty analysis on combined heat losses characteristics of a cylindrical cavity with only bottom wall heated at constant heat flux", *Heat Transfer Engineering*, Vol. 36, pp. 539-552.

Xiao, L., Wu, S. Y., and Li, Y. R., 2012, "Numerical study on combined free-forced convection heat loss of solar cavity receiver under wind environment", *International Journal of Thermal Sciences*, Vol. 60, pp. 182-194.

Yasuaki, S., Fujimura, K., Kunugi, T., and Akino, N., 1994, "Natural convection in a hemispherical enclosure heated from below", *International Journal of Heat and Mass Transfer*, Vol 37, 1605-1617.

Yeh, K. C., Hughes, G., and Lovegrove, K., 2005, "Modelling the convective flow in solar thermal receiver", *Proceedings of the 43rd Conference of the Australian and New Zealand Solar Energy Society (ANZSES)*, Dunedin, New Zealand.

Appendix A: Mesh sensitivity analysis and domain selection

In order to get good results from the numerical simulation, after defining the turbulence model and boundary conditions, mesh sensitivity analysis was performed to investigate the effect of grid sizes on the numerical results. Mesh sensitivity test is an index to determine that how the mesh quality influence the numerical output. To investigate mesh sensitivity, different grid sizes were tested to check their effects on the drag force coefficient experienced by the dish structure. The following steps were followed to get a good mesh size:

- Creating the initial mesh with a reasonable elements and investigating the output
- By recreating the denser mesh, especially near to the main area of interest, and re-investigating the output.
- Comparing the output with previous one. If results matches, Use that mesh size.
- Otherwise, keep increasing the mesh density and repeating the steps until the results converge.

Figure 78 shows the variation of drag coefficient experienced by the dish structure at different grid sizes. Small mesh elements were used near the dish-cavity region to predict the flow behaviour accurately, while the far regions were meshed with larger grid sizes. Figure 79 shows the mesh size in the cavity area and around the coupled dish system. After performing mesh independence tests with different grid sizes, high-quality mesh was chosen with grid size of approximately 4.7 million elements, being used to perform a steady state simulation of the flow around the dish in a virtual wind tunnel. Regions further from the dish were meshed with larger grid sizes to improve computational speed.

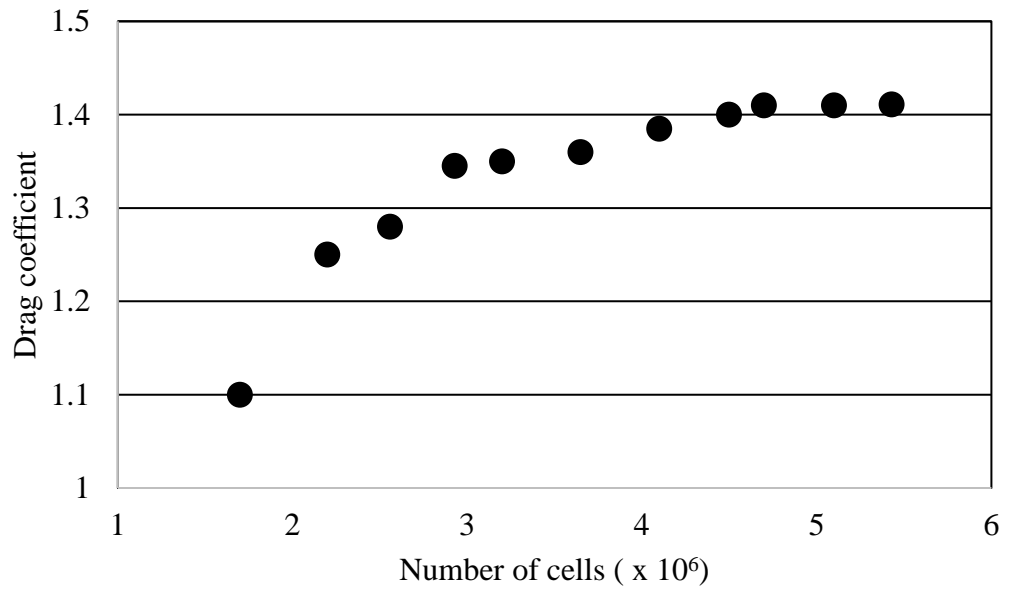


Figure 78: Grid independency test

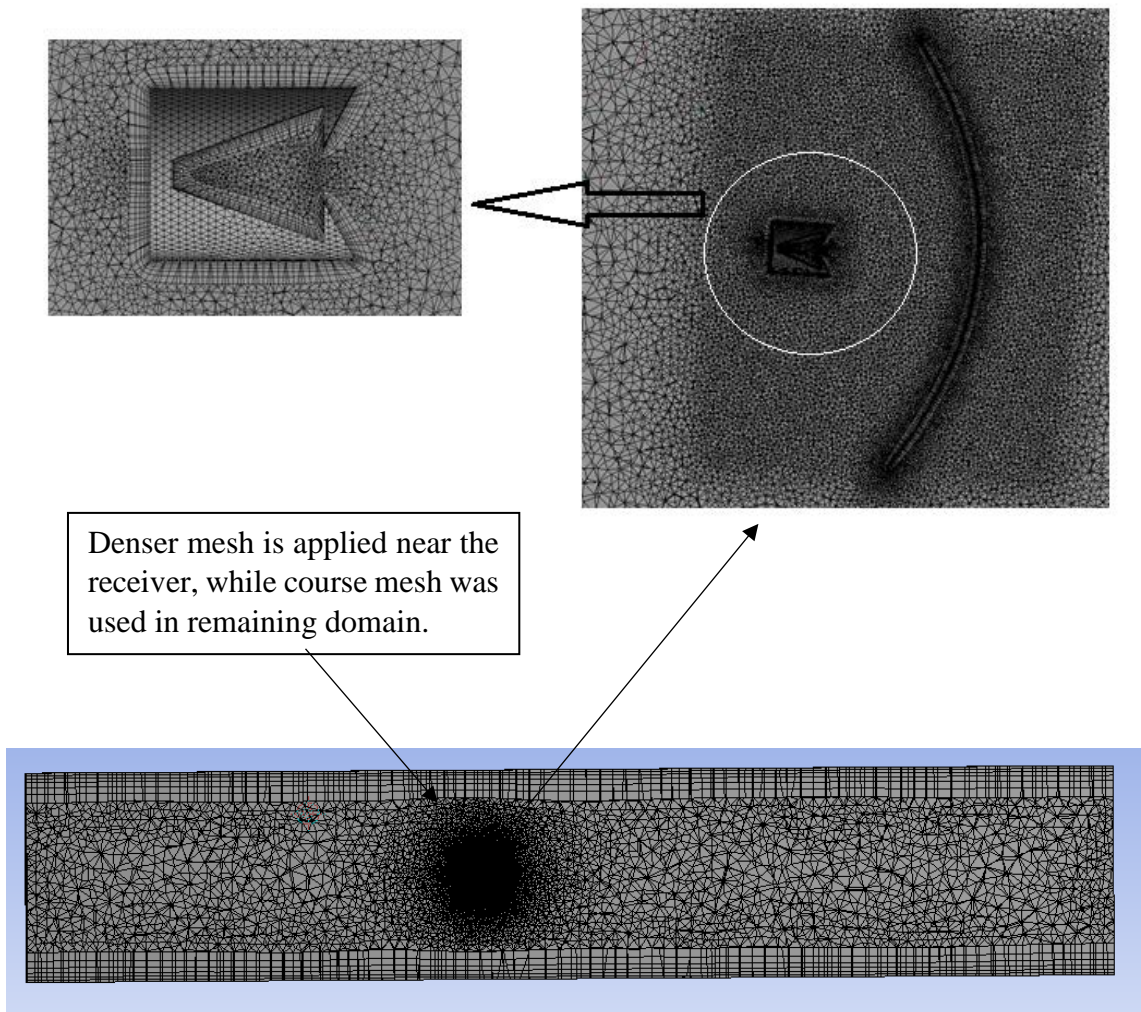


Figure 79: Mesh around the dish and receiver

To model the open environment in which the system operates, computational domains of various widths (10m, 20m, 25m, 30m, 35m and 40m) were examined. The domain was extended to 75m upstream and 105m downstream. These values were selected as a reference from the study conducted by Paitoonsurikarn (2016). With different widths, the Drag force coefficient was checked to select a good domain size to investigate the flow behaviour. Figure 80 shows the drag coefficient experienced by the dish structure against the domain size. The change in the drag coefficient becomes insignificant beyond 25m. After getting the constant drag coefficient, the domain was selected with 15D upstream to get a fully developed flow, 21D downstream to capture all the affected parameters and 6D in the lateral direction to avoid any shear effects of the walls on the flow field near dish, where D is the aperture diameter (Figure 81).

In order to avoid any instability in the convective heat transfer, full span domain was modelled. Also, the dish and receiver occupies 0.005% of the total computational domain's volume in order to modelling the external flow with minimal effect of proximity of pressure boundaries to the dish.

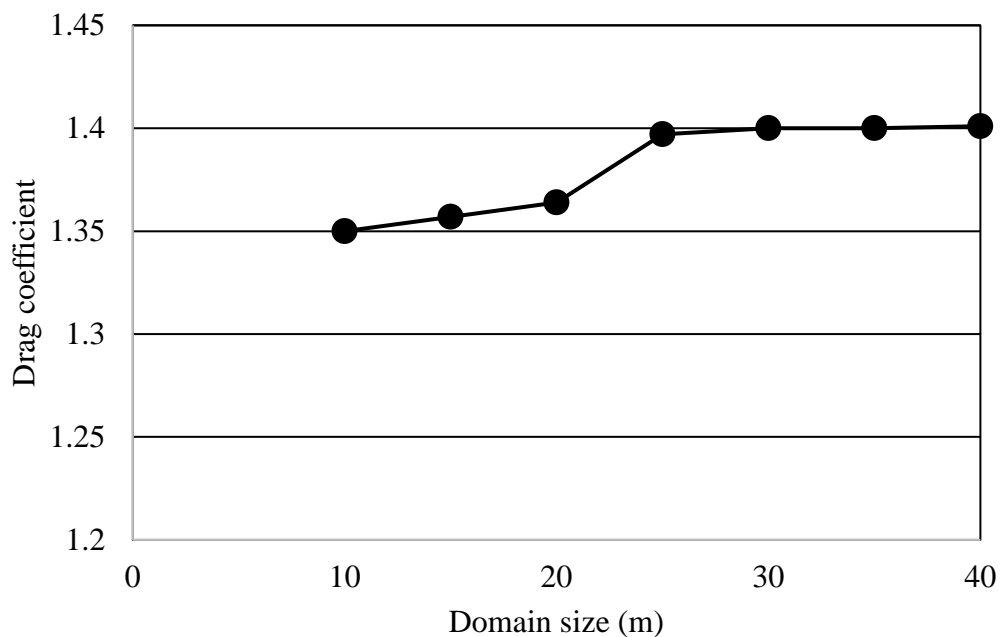


Figure 80: Variation of drag force v/s domain size

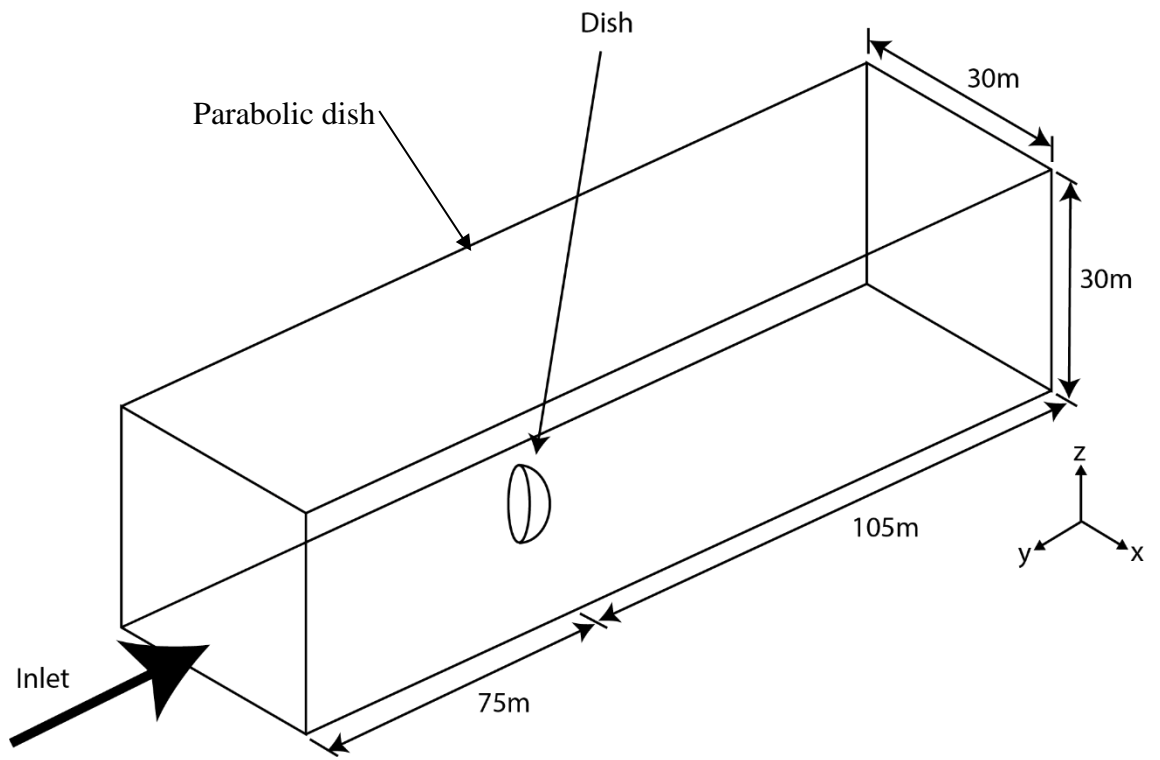


Figure 81: Simulation domain around dish cavity system

Appendix B: Wind tunnel testing results

In order to assess the homogeneity of flow in the wind tunnel, the velocities were measured at different locations by changing the volume flow rate (Table 3). The velocity profiles were examined with fully open, 75% open and 50% open valve. During the investigation, interrupted flow was produced at fully open situation, while for the remaining cases, the air flow displayed a homogenous behaviour (Figures 82-84).

		Divisions along width of test section (mm)						Max (m/s)	Min (m/s)	Greatest difference (m/s)	Average (m/s)
		90	170	250	330	410					
		Divisions along the high of test section (mm)									
Divisions along the high of test section (mm)	Fully open	80	9.4	10.8	10.1	11.1	9.4	12.5	9.4	3.1	10.644
		140	10.1	11.8	9.8	11.8	9.4				
		200	10.2	12	9.6	11.9	9.8				
		260	10	12.1	9.7	12.4	9.7				
		320	10.1	12.5	10.1	12	10.3				
	Open 75%	80	9	8.9	8.7	8.6	8.5	10.1	8.5	1.6	9.336
		140	9.3	9.3	9	9.2	9.1				
		200	9.7	9.5	9.9	9.3	9.5				
		260	9.5	9.6	9.5	9.7	9.4				
		320	9.6	9.5	10.1	9.3	9.7				
	Open 50%	80	7.5	7.5	7.6	7.3	7.4	8.6	7.3	1.3	8.08
		140	8.1	8.1	7.9	8	8				
		200	8.3	8.2	8.2	8.6	8.1				
		260	8.4	8.2	8.6	8.4	8				
		320	8.4	8.1	8.5	8.6	8				

Table 3: Wind velocity data in empty tunnel

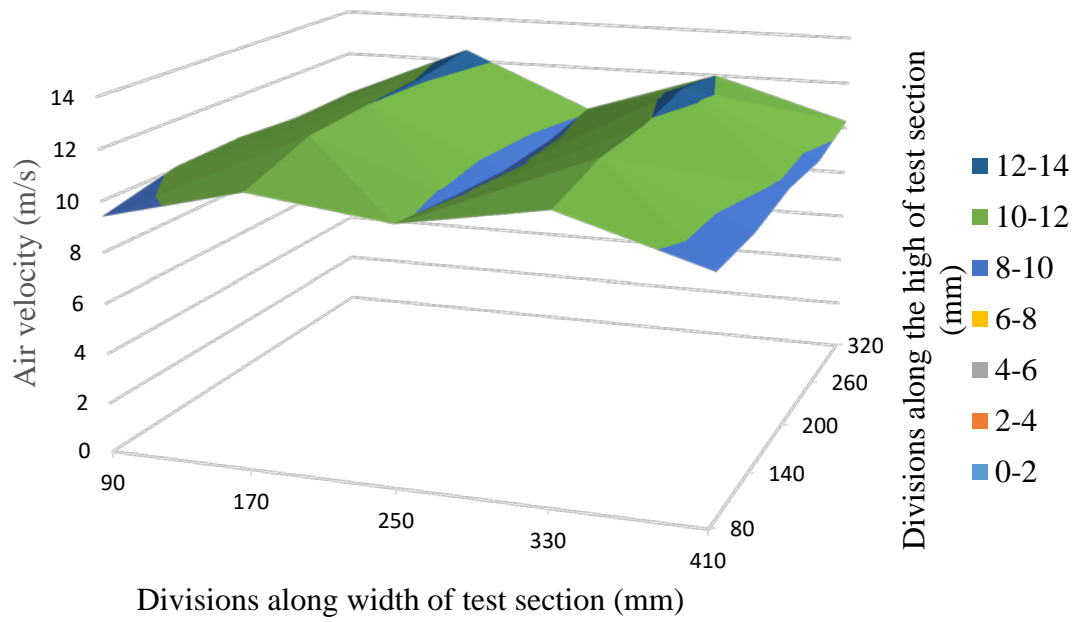


Figure 82: Surface plot of velocity profile with 100% open fan

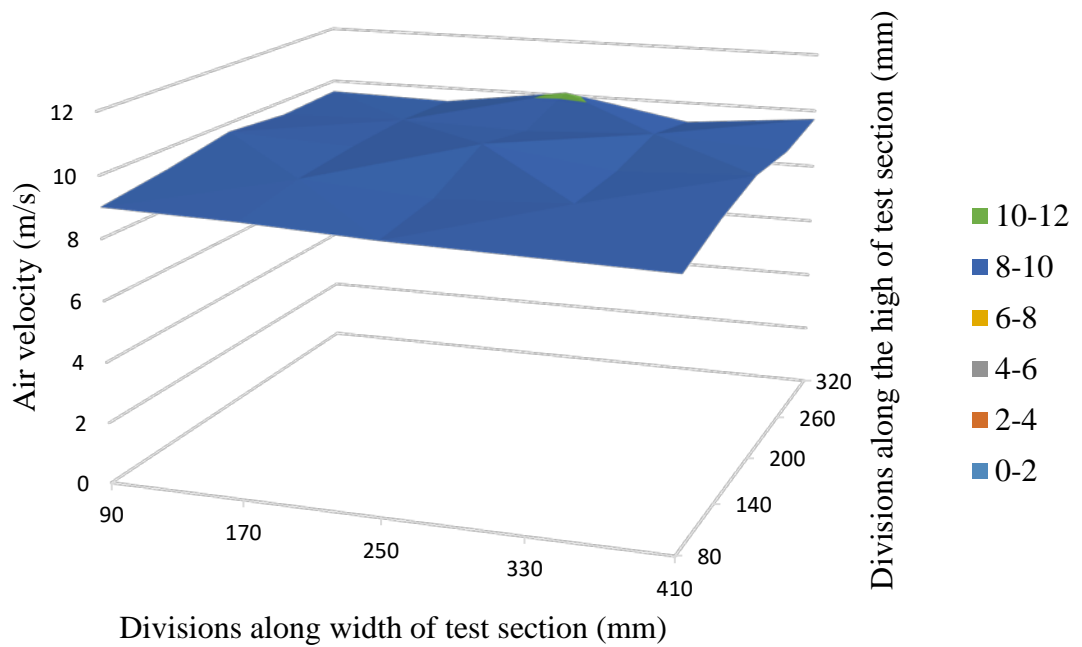


Figure 83: Surface plot of velocity profile with 75% open fan

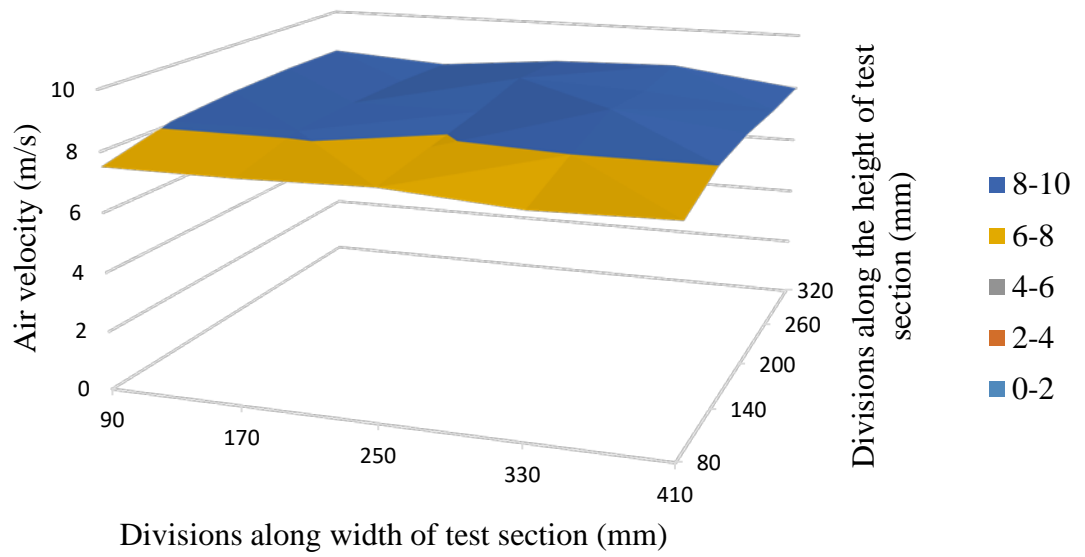


Figure 84: Surface plot of velocity profile with 50% open fan

Appendix C: Step to establish the Nusselt number correlation

The following steps were performed in developing the correlation:

1. The general correlation model used in literature is given by:

$$Nu = CRe^m Pr^n$$

2. To indicate the effects of dish, a function comprises of the key angles was induced in above:

$$Nu = CRe^m Pr^n f(\theta, \psi)$$

3. Now, the function was developed based to ensure the proper curve fitting. For the purpose, method based on hit-and-trials was utilized to determine the constants (A,B,C and D):

$$f(\theta, \psi) = \left[\frac{(A + B \cos \psi)^b}{(D + E \cos \theta)^c} \right]$$

4. Hence, the correlation model resulted in:

$$Nu = a \left[\frac{(1.1 + 0.1 \cos \psi)^b}{(1.1 + \cos \theta)^c} \right] Re^d Pr^e$$

5. This is a log-log form. Therefore, to determine its coefficients and exponents, lets take log on both sides and expand:

$$\ln Nu = \ln a + b \ln(1.1 + 0.1 \cos \psi) - c \ln(1.1 + \cos \theta) + d \ln Re + e \ln Pr$$

6. Following transformations are used to convert the equation in to the linear model:

$$\langle Y \rangle = \ln Nu$$

$$\langle A \rangle = \ln a$$

$$\langle X_1 \rangle = \ln(1.1 + 0.1 \cos \psi)$$

$$\langle X_2 \rangle = -\ln(1.1 + \cos \theta)$$

$$\langle X_3 \rangle = \ln Re$$

$$\langle X_4 \rangle = \ln Pr$$

And the linear model would be:

$$\langle Y \rangle = \langle A \rangle + b \langle X_1 \rangle + c \langle X_2 \rangle + d \langle X_3 \rangle + e \langle X_4 \rangle$$

7. For each case, the value of $\langle Y \rangle$, $\langle X_1 \rangle$, $\langle X_2 \rangle$, $\langle X_3 \rangle$ and $\langle X_4 \rangle$ was determined for the whole set of experiments.
8. The least-square curve fitting method was then utilized to obtain the coefficients, found as:

Case #	a	b	c	d	e
i	4.65×10^{-7}	0.27	0	1.33	0.333
ii	0.00174	0	0.872	0.722	0.333
iii	1.7	1.77	0.938	0.174	0.333

Table 4: Values of coefficients used in Nusselt correlation (Eq.9)

9. The reverse of the transformations shown in step-6 were used to develop the final correlation for each case.
10. The R^2 value for each case was determined to ensure the accuracy of curve fitting, which were more than 90% in all the cases.